

Skolkovo Institute of Science and Technology

EXPERIMENTAL INVESTIGATIONS OF THERMAL PROPERTIES OF  
UNCONVENTIONAL HYDROCARBON RESERVOIRS AT FORMATION  
TEMPERATURES

*Doctoral Thesis*

by

ANASTASIA GABOVA

DOCTORAL PROGRAM IN PETROLEUM ENGINEERING

Supervisor  
Professor Yuri Popov

Co-supervisor  
Dr. Evgeny Chekhonin

I hereby declare that the work presented in this thesis was carried out by myself at Skolkovo Institute of Science and Technology, Moscow, except where due acknowledgment is made and has not been submitted for any other degree.

Candidate (Anastasia Gabova)

Supervisor (Prof. Yuri Popov)

Co-supervisor (Dr. Evgeny Chekhonin)

## Abstract

Experimental data on thermal properties (thermal conductivity, coefficient of linear thermal expansion (CLTE), volumetric heat capacity (VHC)) of rocks at elevated temperatures is necessary for heat flow density determination, enhanced oil recovery methods, basin and petroleum system modeling, wellbore stability analysis, designing radioactive waste repositories, etc. Such information is especially actual for organic-rich shales that exhibit significant thermal anisotropy and heterogeneity and were not studied comprehensively previously. Nowadays, there is a lack of experimental data on thermal properties of organic-rich rocks at elevated temperatures and results are not reliable. A new sophisticated technique was developed to carry out thermal conductivity measurements of organic-rich rocks from various unconventional formations in a temperature range of 30-300 °C. Divided-bar and optical scanning methods were combined in the thermal conductivity measurements in order to account for thermal anisotropy and heterogeneity of the rocks and improve the quality of the experimental data. This approach enabled us to reveal and overcome systematic errors in previous measurements of oil shale samples using the divided-bar method and to develop an approach for the correction of measurement results. It allowed us to account for the thermal contact resistance, non-parallelism of rock samples surfaces, and changes in rock samples structure during heating the samples. The CLTE of shale samples was studied with a quartz dilatometer specially adapted for the measurements on standard core plugs. Strong correlations between the CLTE, thermal conductivity, and total organic carbon were established. Detailed profiles of CLTE along studied wells were obtained for the first time due to the application of the optical scanning technique and established correlations between the thermal conductivity and CLTE. These profiles fit well with total organic carbon obtained with pyrolysis. CLTE anisotropy was assessed for organic-rich shale samples together with thermal conductivity anisotropy. The new methodology for determining volumetric heat capacity at elevated temperatures for unconventional reservoir rocks allowed us to obtain new equations which relate thermal conductivity to temperature. New developed methodology of thermal conductivity measurements on rock cuttings at elevated temperatures provides measurements for unconventional reservoir rocks. It allowed us to obtain new equations which relate the thermal conductivity of the matrix to temperature. 114 rock samples from seven oil fields were totally studied with the techniques developed and enhanced to establish the behavior of the thermal properties at elevated temperatures within the temperature range of 25-300 °C.

## Publications

### *Peer-Reviewed Articles in International Scientific Journals*

1. Popov Y., Spasennykh M., Shakirov A., Chekhonin E., Romushkevich R., Savelev E., **Gabova A.**, Zagranovskaya D., Valiullin R., Yuarullin R., Golovanova I., Sal'manova R. Advanced determination of heat flow density on an example of a west Russian oil field. *Geosciences*. 2021, 11(8): 346. <https://doi.org/10.3390/geosciences11080346>
2. **Gabova A.**, Chekhonin E., Popov Yu., Savelev E., Romushkevich R., Popov E., Kozlova E. Experimental investigation of thermal expansion of organic-rich shales. *International Journal of Rock Mechanics and Mining Sciences*. 2020, 132, 104398. DOI:10.1016/j.ijrmms.2020.104398
3. **Gabova A.**, Popov Y., Savelev E., Romushkevich R., Chekhonin E., Plotnikov V., Emelyanov D., Akhmadishin A. Experimental investigation of the effect of temperature on thermal conductivity of organic-rich shales. *Journal of Petroleum Science and Engineering*. 2020, 193, 107438. <https://doi.org/10.1016/j.petrol.2020.107438>
4. Chekhonin E., Popov E., Popov Y., **Gabova A.**, Romushkevich R., Spasennykh M., Zagranovskaya D. High-Resolution evaluation of elastic properties and anisotropy of unconventional reservoir rocks via thermal core logging. *Rock Mechanics and Rock Engineering*. 2018, 51(1): 2747–2759. DOI:10.1007/s00603-018-1496-z
5. Popov Y., Popov E., Chekhonin E., **Gabova A.**, Romushkevich R., Spasennykh M., Zagranovskaya D. Investigations of Bazhenov formation using thermal core logging technique. *Oil Industry*. 2017, (03): 22–27. DOI:10.24887/0028-2448-2017-3-22-27

### *Patent*

Gabova A., Goncharov A., Popov Y., Chekhonin E., Spasennykh M., 2020. Approach for determining the thermal conductivity of particles of solid materials at elevated temperatures. Russian patent, №220.017.FB7B.

### *Extended abstracts in conference proceedings*

1. Popov E., Goncharov A., Popov Y., Spasennykh M., Chekhonin E., Shakirov A., **Gabova A.** Advanced techniques for determining thermal properties on rock samples and cuttings and indirect estimating for atmospheric and formation conditions. *IOP Conference Series: Earth and Environmental Science*. Scopus, 2019.

2. **Gabova A.**, Chekhonin E., Popov E., Savelev E., Kozlova E., Popov Y., Karpov I. Experimental investigations of thermal expansion coefficient of Bazhenov formation rocks. *Proceedings of ISRM European Rock Mechanics Symposium EUROCK 2018*. Scopus, 2018
3. Popov Y., Spasennykh M., Valiullin R., Yarullin R., Ramazanov A., Zagranovskaya D., Zakharova O., Golovanova I., Chekhonin E., Savelev E., **Gabova A.**, Popov E., Shakirov A. First experience of maintenance of basin modeling with up-to-date complex of experimental geothermic investigations. *Proceedings of 19th Scientific-Practical Conference on prospecting and development of oil and gas fields «Geomodel-2018»*, 4 p. Scopus, 2018.
4. Popov Y., Chekhonin E., Romushkevich R., Popov E., Savelev E., **Gabova A.**, Emelyanov D., Ahmadshin A., Smyshlyaeva M., Grischenko M. The modern role of thermal petrophysics in prospecting, exploration and development of HC deposits by example of Em-Egovskoye oilfield. *Proceedings of 19th Scientific-Practical Conference on prospecting and development of oil and gas fields «Geomodel-2018»*, 4 p. Scopus, 2018.
5. Popov Y., Popov E., Chekhonin E., **Gabova A.**, Savelev E. New role of thermal petrophysical technologies at exploration, prospecting and development of oil-gas fields. *Proceedings of 5th International Conference on prospecting and development of oil and gas fields «GeoBaikal 2018»*, 4 p. Scopus, 2018.
6. **Gabova A.**, Chekhonin E., Popov E., Savelev E., Kozlova E., Popov Y., Karpov I. Investigation of coefficient of linear thermal expansion of Bazhenov formation rocks. *In: Proceedings of 19th Scientific-Practical Conference on prospecting and development of oil and gas fields «Geomodel-2017»*, 4 p. Scopus, 2017.
7. Popov E., **Gabova A.**, Chekhonin E., Romushkevich R., Savelev E. Bazhenov formation characterization with rock thermal property profiling technique. *79th EAGE Conference & Exhibition 2017, Paris, June 12-15, 2017*. Scopus.
8. Popov E., Popov Y., **Gabova A.**, Chekhonin E., Romushkevich R., Spasennykh M., Stenin V., Kozlova E., Deliya S., Shayakhmetov T., Drandusov K. Results of combined investigations of Domanic formation with continuous thermal core profiling. *In: Proceedings of 19th Scientific-Practical Conference on prospecting and development of oil and gas fields «Geomodel-2017»*, 4 p. Scopus, 2017.
9. Popov E., Romushkevich R., **Gabova A.**, Popov Y., Savelev E., Romanov Y., Spiridonov D. Thermal Properties of Bazhen Formation Rocks of Surgut and Nizhnevartovsk Arches of Western-Siberian Plate from Continuous Core Profiling. *In: Proceedings of 19th Scientific-Practical Conference on prospecting and development of oil and gas fields «Geomodel-2017»*, 4 p. Scopus, 2017.

10. Popov Y., Popov E., Chekhonin E., **Gabova A.**, Romushkevich R., Spasennykh M. Thermal core logging as new method of investigations of Bazhenov formation at exploration, prospecting and development of hydrocarbon fields. *Conference "New GIS-technologies for oil-gas companies"*. Ufa, 14-16 November, 2017.
11. Popov Y., Popov E., Romushkevich R., Chekhonin E., **Gabova A.**, Spasennykh M., Zagranovskaya D., Karpov I., Ovcharenko Y. Interrelations of Bazhenov shale properties and their significance at exploration, prospecting and development of hydrocarbon fields. *Conference "Shale science: Problems of prospecting and development"*, Moscow, 10-11 April, 2017.
12. Popov Y., Romushkevich R., **Gabova A.**, Chekhonin E., Popov Yu., Spasennykh M., Zagranovskaya D., Belenkaya I., Karpov I. Development of database on Bazhenov formation thermal properties for hydrodynamic and basin and petroleum system modeling. *In: Proceedings of 18th Scientific-Practical Conference on prospecting and development of oil and gas fields «Geomodel-2016»*, 4 p. Scopus, 2016.
13. Popov Y., Popov E., Chekhonin E., Romushkevich R., Spasennykh M., Bogdanovich N., Kozlova E., **Gabova A.**, Zhukov V., Zagranovskaya D., Karpov I., Belenkaya I., Ovcharenko Y., Alekseev A., Kalmykov G., Gutman I., Oksenoyd E. Thermal core logging as new technique of Bazhenov formation investigations for prospecting, exploration and recovery of hydrocarbons. *In: Proceedings of 18th Scientific-Practical Conference on prospecting and development of oil and gas fields «Geomodel-2016»*, 4 p. Scopus, 2016.
14. Popov E., **Gabova A.**, Karpov I., Zagranovskaya D., Romushkevich R., Spasennykh M., Chekhonin E., Popov Y. Correlations between thermal core logging, gamma logging and gamma spectrometry data. *In: Proceedings of 18th Scientific-Practical Conference on prospecting and development of oil and gas fields «Geomodel-2016»*, 4 p. Scopus, 2016.
15. Spasennykh M., Popov E., Chekhonin E., Romushkevich R., Zagranovskaya J., Belenkaya I., Zhukov V., Karpov I., Saveliev E., **Gabova A.** Thermal properties of Bazhen formation sediments from thermal core logging. *Proceedings volume of EGU General Assembly*, Vienna, Austria, April 19-22, 2016. Scopus.

## Acknowledgments

I would like to express my gratitude to the people which helped and supported me during my Ph.D. study and research.

First of all, I want to say many thanks to my supervisor, Professor Yuri Popov, for being a supportive mentor and advisor. Especially thanks for practice in experimental research, writing publications, scientific discussions, and for the opportunity to be a part of a world-leading team of thermal petrophysics.

Also, I thank my co-supervisor Dr. Evgeny Chekhonin for constant support in my research, for giving useful recommendations and advice, and for very efficient discussions.

Many thanks to Raisa Romushkevich for her support and advice in the geological part of my research.

I am very grateful to Dr. Elena Kozlova for her support and constant help with pyrolysis experiments.

I would like to say thanks to the laboratory team that helped to conduct experiments for my research. Thanks to Dr. Evgeny Popov who helped with equipment adjustment and samples preparation for my research and also for constant advice and support. Thanks to Egor Savelev, Dr. Alexander Goncharov, Dmitry Ostrizhny, Sergey Pohilenko, Valentin Solomatin for help in the experimental part of my research.

Many thanks to Professor Mikhail Spasennykh for the opportunity to conduct research in the center for Hydrocarbon Recovery, for constant help and support.

Also, I would like to mention the help of the Educational Office of the Skolkovo Institute of Science and Technology in my Ph.D. study and say many thanks to all team members.

Many thanks to all my colleagues from the Center for Hydrocarbon Recovery for a friendly and positive atmosphere during my Ph.D. study and research.

## Table of contents

Abstract.....	iii
Publications .....	iv
Acknowledgments .....	vii
Table of contents .....	viii
List of figures.....	x
List of tables .....	xv
Symbols .....	xvii
Abbreviations.....	xix
Chapter 1. Introduction.....	1
1.1 The necessity of experimental data on thermal properties at elevated temperatures for the solution of actual problems in oil&gas science and industry .....	1
1.2 Statement of the problem.....	7
1.3 Outline of the Thesis.....	8
Chapter 2. Literature review and the current state of the problem .....	9
2.1 Thermal conductivity dependence of unconventional reservoirs at elevated temperatures – current state of the art .....	9
2.2 Coefficient of linear thermal expansion at elevated temperatures – current state of the art .....	15
2.3 Volumetric heat capacity at elevated temperatures – current state of the art .....	18
2.4 Thermal conductivity measurements on rock cuttings and unconsolidated rocks at elevated temperatures – current state of the art .....	19
2.5 Summary .....	20
Chapter 3. Experimental .....	23
3.1 Enhancement of experimental basis for thermal conductivity measurements at elevated temperatures.....	23
3.1.1 Method of measuring thermal conductivity at elevated temperatures.....	23
3.1.1.1 Thermal conductivity measurements procedure using a DTC-300 instrument.....	23
3.1.1.2 Metrological study of DTC-300 instrument .....	24
3.1.2 New measuring methodology for thermal conductivity by combining DTC-300 results with those of TCS .....	26
3.1.3 Modification of DTC-300 results .....	30
3.1.3.1 Accounting for rocks flatness deviation .....	30
3.1.3.2 Variations in rock sample diameters .....	31
3.2 The technique of measurements of thermal conductivity of rock cuttings and non-consolidated rocks at elevated temperatures.....	33
3.2.1 Materials and methods.....	33
3.2.2 Theoretical approach .....	34

3.3	Enhancement of experimental basis for CLTE measurements at elevated temperatures on core samples.....	37
3.3.1	Experimental basis of CLTE measurements .....	37
3.3.2	Integration of dilatometer and Thermal Conductivity Scanner .....	40
3.3.2.1	Influence of rock anisotropy.....	40
3.4	The technique of measurements of volumetric heat capacity of rocks at elevated temperatures.....	42
3.4.1	Measurements of specific heat capacity at elevated temperatures .....	42
3.4.2	Integration of differential scanning calorimeter and dilatometer for measuring volumetric heat capacity at elevated temperatures.....	43
Chapter 4.	Experimental results.....	45
4.1	Unconventional reservoir rocks under study .....	45
4.2	Thermal conductivity at elevated temperatures .....	46
4.2.1	Rock collection for studying thermal conductivity at elevated temperatures .....	46
4.2.2	Results of measurements .....	48
4.2.3	Changes in thermal conductivity of unconventional reservoir rocks during heating and cooling .....	66
4.2.4	Analysis of thermal conductivity with temperature characteristic of unconventional reservoir rocks in comparison with other sedimentary rocks.....	67
4.3	CLTE investigations for unconventional reservoir rocks .....	68
4.3.1	Rock collections for studying CLTE .....	68
4.3.2	CLTE and thermal conductivity measurements at room temperature.....	70
4.3.3	CLTE anisotropy at room temperature.....	72
4.3.4	Integrated analysis and core state control.....	74
4.3.5	CLTE measurements at elevated temperatures .....	77
4.4	Volumetric heat capacity of unconventional reservoir rocks at elevated temperatures ....	80
4.4.1	Rock collection for studying volumetric heat capacity at elevated temperatures ...	80
4.4.2	Results of measurements for unconventional reservoir rocks .....	81
4.4.3	Equations that relate volumetric heat capacity to temperature for unconventional reservoir rocks .....	91
4.4.4	Analysis of volumetric heat capacity with temperature characteristic of unconventional reservoir rocks in comparison with other sedimentary rocks .....	92
4.5	Experimental investigations of thermal conductivity on rock cuttings and non-consolidated rocks at elevated temperatures.....	92
Chapter 5.	Conclusion .....	97
5.1	Summary.....	97
5.2	Conclusions and recommendations .....	98
Bibliography	.....	101

## List of figures

<b>Figure 1.</b> DTC-300 instrument for measuring thermal conductivity of rock samples at elevated temperatures.....	23
<b>Figure 2.</b> The precision of thermal conductivity measurements with DTC-300 instrument with temperature estimated from experiments on standard samples. ....	26
<b>Figure 3.</b> Influence of difference in rock sample flatness on the relative difference between effective thermal conductivity measured with DTC-300 and TCS instruments at room temperature. $R$ is the correlation coefficient, $RMSE$ is the root mean square error. ....	31
<b>Figure 4.</b> Thermal conductivity of marble samples with different diameters with the temperature. ....	32
<b>Figure 5.</b> The dependence of thermal conductivity of marble samples on samples diameter. ....	32
<b>Figure 6.</b> Corrected thermal conductivity values of marble samples with different diameters at elevated temperatures. ....	33
<b>Figure 7.</b> Main (a) and auxiliary equipment (b, c) used in the study; a - Quartz dilatometer with an installed core sample, b - Thermal Conductivity Scanner, c - HAWK pyrolysis instrument...	41
<b>Figure 8.</b> Differential scanning calorimeter NETZSCH - DSC 214 Polyma. ....	43
<b>Figure 9.</b> Thermal conductivity decrease for rock samples from the Bazhenov and Abalak formations in the 30-300 °C temperature range. Different colors refer to different rock samples: ♦ – 1AB, ▲ – 2AB, ● – 5AB, ■ – 3BF, ■ – 4BF, ● – 5BF. Thermal conductivity values at initial temperature $T_0 = 30$ °C are shown in Table 11.....	50
<b>Figure 10.</b> Curves drawn on a scatter diagram of average percentage of thermal conductivity decrease with temperature for rock samples from different formations: ♦ – Abalak formation, ● – Bazhenov formation, ■ – sample 3BF from the Bazhenov formation, - – correction for the Bazhenov formation, - – correction for the Abalak formation, - – correction for sample 3BF from the Bazhenov formation. Thermal conductivity values at initial temperature $T_0 = 30$ °C are shown in Table 11.....	51
<b>Figure 11.</b> Changes in thermal conductivity for rock samples of the Golchikh and Abalak formations of oil field 2 with increasing temperature. Black dotted line - curve obtained by averaging thermal conductivity overall rock samples of the Golchih formation; brown dotted line - curve obtained by averaging thermal conductivity overall rock samples of the Abalak formation. ....	53
<b>Figure 12.</b> Relative change in thermal conductivity for rock samples from the Golchih and Abalak formations of oil field 2 with increasing temperature. Black dotted line - curve obtained by	

averaging the relative change in thermal conductivity for all rock samples of the Golchih formation; brown dotted line - curve obtained by averaging the relative change in thermal conductivity for all rock samples of the Abalak formation. Thermal conductivity values at initial temperature  $T_0 = 30\text{ }^\circ\text{C}$  are shown in Table 12.....53

**Figure 13.** Changes in thermal conductivity for rock samples of Bazhenov formations of oil field 3 with increasing temperature.....55

**Figure 14.** Relative change in thermal conductivity for rock samples from the Bazhenov formation of oil field 3 with increasing temperature. Black dotted line - curve obtained by averaging the relative change in thermal conductivity for all rock samples of the Bazhenov formation. Thermal conductivity values at initial temperature  $T_0 = 30\text{ }^\circ\text{C}$  are shown in Table 14. ....55

**Figure 15.** Changes in thermal conductivity for rock samples of Bazhenov formations of oil field 4 with increasing temperature.....56

**Figure 16.** Relative change in thermal conductivity for rock samples from the Bazhenov formation of oil field 4 with increasing temperature. Black dotted line - curve obtained by averaging the relative change in thermal conductivity for all rock samples of the Bazhenov formation.....57

**Figure 17.** Curves drawn on the thermal conductivity-temperature scatter diagram for Mendym samples (■ – 1Md, ● – 2Md, ▲ – 3Md, ◆ – 4Md, ■ – 5Md, ● – 6Md, ● – 7Md, ● – 8Md, ▲ – 9Md, ● – 10Md) in the 30-300 °C temperature range. Thermal conductivity values at initial temperature  $T_0 = 30\text{ }^\circ\text{C}$  are shown in Table 15.....59

**Figure 18.** Curves lines drawn on the thermal conductivity-temperature scatter diagram for Domanic samples (■ – 1Dm, ● – 2Dm, ▲ – 3Dm, ● – 4Dm, ● – 5Dm, ● – 6Dm, ◆ – 7Dm) in the 30-300 °C temperature range. Thermal conductivity values at initial temperature  $T_0 = 30\text{ }^\circ\text{C}$  are shown in Table 15.....60

**Figure 19.** Curves lines drawn on the thermal conductivity-temperature scatter diagram for Sargaev samples (◆ – 1S, ■ – 2S, ▲ – 3S, ● – 4S) in the 30-300 °C temperature range. Thermal conductivity values at initial temperature  $T_0 = 30\text{ }^\circ\text{C}$  are shown in Table 15. ....60

**Figure 20.** The curve drawn on the thermal conductivity-temperature scatter diagram for the Timan sample (Tm) in the 30-300 °C temperature range. Thermal conductivity values at initial temperature  $T_0 = 30\text{ }^\circ\text{C}$  are shown in Table 15.....61

**Figure 21.** Curves drawn on the average thermal conductivity- temperature scatter diagram for lithotypes from different formations in the 30-300 °C temperature range. Different colors are related to different lithotypes: ● – dolomites (Mendym), ▲ – limestones (Mendym), ◆ – limestones (Domanic), ● – limestones (Sargaev), ▲ – sandstone (Timan), ■ – argillites (Domanic), ■ – clayey

limestones (Mendym), ◆ – clayey limestones (Sargaev). Thermal conductivity values at initial temperature $T_0 = 30\text{ }^\circ\text{C}$ are shown in Table 15.....	61
<b>Figure 22.</b> Curves drawn on the average thermal conductivity- temperature scatter diagram for different lithotypes from different formations (● – clayey limestones, ▲ – dolomites and sandstones, ■ – limestones and argillites, - – clayey limestones with correction, - – dolomites and sandstones with correction, - – limestones and argillites with correction) in the 30-300 °C temperature range. Thermal conductivity values at initial temperature $T_0 = 30\text{ }^\circ\text{C}$ are shown in Table 15.....	62
<b>Figure 23.</b> A Bazhenov sample before heating (a) and after heating to 300 °C (b).....	63
<b>Figure 24.</b> A synthetic sample of kerogen.....	65
<b>Figure 25.</b> Thermal conductivity of kerogen sample at elevated temperatures measured with DTC-300 instrument. Bars values correspond to precision determined in <i>Chapter 3.1.1.2</i> .....	65
<b>Figure 26.</b> Thermal conductivity values of Golchih and Abalak formations rocks measured with the DTC-300 instrument during heating and cooling. Different symbols relate to different rock samples. ....	66
<b>Figure 27.</b> Relative change in thermal conductivity for unconventional and other sedimentary rock samples with increasing temperature.....	68
<b>Figure 28.</b> Results of CLTE (measurement unit is $10^{-6}\text{ K}^{-1}$ , the data are shown by red lines and numbers) and thermal conductivity (measurement unit is $\text{W}/(\text{m}\cdot\text{K})$ , black line and numbers) measurements of BF core plugs at different directions to the bedding plane (a, c, e, g, i, k). The results of solving the optimization problem by the ellipse parameters method (blue lines) and the CLTE measurement results (red markers) are shown in corresponding figures b, d, f, h, j, l.....	74
<b>Figure 29.</b> Correlation TC vs CLTE for core plugs from BF from 3 oil fields. ....	75
<b>Figure 30.</b> Correlations density vs CLTE (parallel to bedding at temperature range 25-50 °C) (a), density vs TOC (b), and density vs TC (c) for core plugs from BF from 3 oil fields. Dark blue points relate to samples from well 1; light blue points relate to samples from wells 4, 5.....	75
<b>Figure 31.</b> Detailed profile of CLTE and pyrolysis data (red markers) for BF rocks from well 4 (c), well 5 (b) and well 1 (a). ....	76
<b>Figure 32.</b> Correlation CLTE vs TOC for BF rocks from 3 wells.....	77
<b>Figure 33.</b> CLTE variations (parallel to the bedding plane) with a temperature increase for core plugs from the BF (a) and the AF (b) (well 1). Bars values correspond to the precision of CLTE measurements ( <i>Chapter 3.3.1</i> ).....	78
<b>Figure 34.</b> CLTE values change with temperature for core plugs from the BF (wells 4, 5). Bars values correspond to the precision of CLTE measurements ( <i>Chapter 3.3.1</i> ).....	78

<b>Figure 35.</b> CLTE variations (parallel to the bedding plane) with a temperature increase for core plugs from the BF (well 3). Bars values correspond to the precision of CLTE measurements (Chapter 3.3.1). .....	79
<b>Figure 36.</b> CLTE variations (parallel to the bedding plane) with a temperature increase for core plugs from the GF and AB (well 2). Bars values correspond to the precision of CLTE measurements (Chapter 3.3.1). .....	79
<b>Figure 37.</b> Variations of CLTE with a relative change of core plug mass after measurements at 300 °C for BF rocks (Samples №4, 5, 6, 7, 8, 10, 12-13, 15-23). .....	80
<b>Figure 38.</b> Photo of sample №1 before (a) and after (b) high-temperature measurements with a zoomed area of bitumen exudation (c). .....	80
<b>Figure 39.</b> The dependence of the density on temperature, calculated by the formula (15), for a sample from the studied collection of rocks, which has the maximum CLTE ( $\alpha = 15.9 \cdot 10^{-6} \text{ K}^{-1}$ ). .....	85
<b>Figure 40.</b> The dependence of the volumetric heat capacity on temperature for Bazhenov formation rock samples from oil field 1. ....	86
<b>Figure 41.</b> The dependence of the volumetric heat capacity on temperature for Abalak formation rock samples from oil field 1. ....	86
<b>Figure 42.</b> The ratio of volumetric heat capacity at elevated temperatures to initial volumetric heat capacity ( $T_0 = 25 \text{ °C}$ ) for Bazhenov formation rocks. ....	87
<b>Figure 43.</b> The ratio of volumetric heat capacity at elevated temperatures to initial volumetric heat capacity ( $T_0 = 25 \text{ °C}$ ) for Abalak formation rocks. ....	87
<b>Figure 44.</b> Experimental data on the change in the specific heat capacity of rock samples from the Golchih and Abalak formations (Oil field 2) with temperature increasing. The black dotted line is the curve obtained by averaging the specific heat capacity for all samples. ....	88
<b>Figure 45.</b> Dependence of density on temperature for rock samples of the Golchih and Abalak formations (Oil field 2). ....	89
<b>Figure 46.</b> The dependence of the volumetric heat capacity of the matrix for all rock samples of the Golchih and Abalak formations (Oil field 2) on temperature. The dashed line is the curve obtained by averaging the volumetric heat capacity of the matrix over all samples. ....	89
<b>Figure 47.</b> Experimental data on the change in the specific heat capacity of rock samples of the Bazhenov formation with an increase in temperature. The black dotted line is the curve obtained by averaging the specific heat capacity for all samples. ....	90

**Figure 48.** The dependence of the volumetric heat capacity, averaged over all rock samples of the Bazhenov formation (Oil field 4), on temperature. The dashed line is the curve obtained by averaging the volumetric heat capacity of all samples. ....91

**Figure 49.** The volumetric heat capacity increasing relatively to initial volumetric heat capacity ( $T_0 = 25\text{ }^\circ\text{C}$ ) for Bazhenov formation and other sedimentary rocks. ....92

**Figure 50.** The results of determining the dependences of the thermal conductivity of the matrix on temperature from the results of measuring the thermal properties on rock cuttings. The equations show the average decreasing of thermal conductivity for the corresponding lithotype. ....95

**Figure 51.** Comparison of the results of determining the dependences of the thermal conductivity of the matrix on temperature (according to the results of measurements on rock cuttings) with the results of determining the dependences of the thermal conductivity of rocks on temperature (according to the results of measurements on standard samples). The dashed lines represent the dependences obtained from the results of measurements on rock cuttings, the solid lines represent the dependences obtained from the results of measurements on standard rock samples. ....96

## List of tables

<b>Table 1.</b> Effective thermal conductivity of shales and experimental conditions of high-temperature measurements for different shale formations obtained from the literature. ....	14
<b>Table 2.</b> Summary of published CLTE studies of shales.....	17
<b>Table 3.</b> Summary of published specific heat capacity studies of shales.....	19
<b>Table 4.</b> Results of accuracy estimation using standard reference samples on DTC-300 instrument at room temperature.....	25
<b>Table 5.</b> Main technical characteristics of the calorimeter DSC NETZSCH 214 Polyma.....	43
<b>Table 6.</b> Number of unconventional reservoir rocks for studying thermal conductivity, CLTE, and VHC at elevated temperatures. ....	45
<b>Table 7.</b> The collection of studied rocks from Oil field 1. ....	46
<b>Table 8.</b> The collection of studied rocks from Oil field 3. ....	47
<b>Table 9.</b> The collection of studied rocks from Oil field 5. ....	47
<b>Table 10.</b> Results of thermal property measurements of rock samples from Bazhenov and Abalak formations at room temperature with a TCS before measurements at elevated temperatures. ....	49
<b>Table 11.</b> TCS measurements of thermal properties of Bazhenov and Abalak samples at room temperature after heating to 300 °C and subsequent cooling. ....	51
<b>Table 12.</b> Results of thermal property measurements of rock samples from Golchih and Abalak formations at room temperature with a TCS before measurements at elevated temperatures. ....	52
<b>Table 13.</b> TCS measurements of thermal properties of Golchih and Abalak formations samples at room temperature (after heating to 300 °C and subsequent cooling). ....	54
<b>Table 14.</b> TCS measurements of thermal conductivity of Bazhenov formation samples at room temperature (after heating to 300 °C and subsequent cooling).....	54
<b>Table 15.</b> TCS measurements of thermal properties of Mendym, Domanic, Sargaev, and Timan samples at room temperature before measurements at high temperatures. ....	58
<b>Table 16.</b> TCS measurements of thermal properties of Mendym, Domanic, Sargaev, and Timan samples at room temperature (after heating to 300 °C and subsequent cooling).....	63
<b>Table 17.</b> Equations which relate average thermal conductivity to temperature in the 30-300 °C temperature range for studied lithotypes from different formations. ....	64
<b>Table 18.</b> Changes in thermal properties of unconventional reservoir rocks from 5 oil fields after heating. ....	67
<b>Table 19.</b> Characteristics of studied rock samples from oil field 1. ....	69

<b>Table 20.</b> Results of CLTE, CLTE anisotropy coefficient, density, TOC and thermal properties measurements .....	71
<b>Table 21.</b> Characteristics of studied rock samples from oil field 1.....	81
<b>Table 22.</b> The results of measurements of the specific heat capacity of sample №1.....	82
<b>Table 23.</b> The results of measurements of the specific heat capacity of sample №3.....	82
<b>Table 24.</b> The results of measurements of the specific heat capacity of sample №4.....	83
<b>Table 25.</b> The results of measurements of the specific heat capacity of sample №5.....	83
<b>Table 26.</b> The results of measurements of the specific heat capacity of sample №6.....	83
<b>Table 27.</b> The results of measurements of the specific heat capacity of sample №7.....	83
<b>Table 28.</b> The results of measurements of the specific heat capacity of sample №8.....	84
<b>Table 29.</b> The results of measurements of the specific heat capacity of sample №9.....	84
<b>Table 30.</b> The results of measurements of the specific heat capacity of sample №10.....	84
<b>Table 31.</b> The results of measurements of the specific heat capacity of sample №11.....	84
<b>Table 32.</b> Equations of VHC vs temperature for studied unconventional reservoir rocks.....	91
<b>Table 33.</b> The results of determining the thermal conductivity of the matrix (at 25, 50, and 75 °C) and the volumetric heat capacity of the matrix (at 25 °C) based on the results of measurements on rock-cuttings.....	93
<b>Table 34.</b> Correlation equations of the temperature dependence of measured thermal conductivities of rock cuttings.....	97

## Symbols

$\lambda$	thermal conductivity (W/(m·K))
$\lambda_{\text{average}}$	average of the thermal conductivity component with the recorded thermal conductivity profile of the rock sample (W/(m·K))
$\lambda_{\text{max}}$	maximum of the thermal conductivity component with the recorded thermal conductivity profile of the rock sample (W/(m·K))
$\lambda_{\text{min}}$	minimum of the thermal conductivity component with the recorded thermal conductivity profile of the rock sample (W/(m·K))
$\lambda_{\text{apparent}}$	apparent thermal conductivity (W/(m·K))
$\lambda_{\perp}$	thermal conductivity component perpendicular to the bedding plane (W/(m·K))
$\lambda_{\parallel}$	thermal conductivity component parallel to the bedding plane (W/(m·K))
$\lambda_{\text{TCS}}$	thermal conductivity measured with the TCS (W/(m·K))
$\lambda_{\text{DTC-300}}$	thermal conductivity measured with the DTC-300 instrument (W/(m·K))
$\lambda_{\text{A}}$	thermal conductivity of air (W/(m·K))
$\lambda_{\text{B}}$	thermal conductivity of material-filler (W/(m·K))
$\lambda_{\text{mixture}}$	thermal conductivity of solid sample mixture (W/(m·K))
$\lambda_{\text{M}}$	thermal conductivity of rock cuttings (W/(m·K))
K	thermal anisotropy coefficient
$\beta_1$	thermal heterogeneity factor obtained from scanning the sample along core axis
$\beta_2$	thermal heterogeneity factor obtained from scanning the sample perpendicular to core axis
A	accuracy (%)
P	precision (%)
U	uncertainty (%)
R	determination coefficient
h	thickness of sample (mm)
D	diameter of sample (mm)
C	volumetric heat capacity (MJ/(m <sup>3</sup> ·K))
$C_p$	specific heat capacity (J/(kg·K))
$C_M$	volumetric heat capacity of rock cuttings (MJ/(m <sup>3</sup> ·K))
$C_A$	volumetric heat capacity of air (MJ/(m <sup>3</sup> ·K))

$C_B$	volumetric heat capacity of material-filler (MJ/(m <sup>3</sup> ·K))
$C_{\text{mixture}}$	volumetric heat capacity of solid sample mixture (MJ/(m <sup>3</sup> ·K))
$C_a$	heat capacity of air (J/(kg·K))
$\rho_a$	density of air (g/(cm <sup>3</sup> ))
$V_M$	volume fraction of rock cuttings
$V_A$	volume fraction of air
$V_B$	volume fraction of material-filler in the solid sample mixture
$\alpha$	coefficient of linear thermal expansion (K <sup>-1</sup> )
$\rho$	density (g/(cm <sup>3</sup> ))
$T_i$	initial temperature (K)
$T_f$	final temperature (K)
$l_0$	initial length of the sample at the temperature $T_i$ (mm)
$\alpha_{q.s.}$	correction for expansion of dilatometer the quartz system at the temperature range $T_i - T_f$
$\alpha_q$	average CLTE value of quartz glass standard sample in particular temperature range according to certificate (K <sup>-1</sup> )

## Abbreviations

CLTE	coefficient of linear thermal expansion
VHC	volumetric heat capacity
TCS	thermal conductivity scanner
EOR	enhanced oil recovery
DSC	differential scanning calorimeter
DTA	differential thermal analysis
STD	standard deviation
RMSE	root mean square error
TOC	total organic carbon

## Chapter 1. Introduction

### 1.1 The necessity of experimental data on thermal properties at elevated temperatures for the solution of actual problems in oil&gas science and industry

Experimental data on the thermal properties of hydrocarbon reservoirs and surrounding formations at elevated temperatures are important for a variety of purposes: determining heat flow density, designing and optimizing thermal methods of enhanced oil recovery (EOR), basin and petroleum system modeling, exploitation of geothermal reservoirs and design of radioactive waste disposal. However, there is an acute shortage of such data at present, particularly for unconventional reservoir rocks. Modeling of sedimentary basins and petroleum systems using any basin simulator requires data on the deep heat flow and thermal rock properties (thermal conductivity, specific heat or volume) and reservoir properties at elevated temperatures (Hantschel and Kauerauf, 2009). However, the experimental work of recent years established the serious problems to obtain baseline data on thermal properties of rocks and heat flow, reducing the reliability of basin modeling.

Nowadays equipment (e.g., thermal conductivity scanner) is already developed for thermal properties measurements on cores at room temperatures. The optical scanning method and instruments were developed for contact-free, non-destructive measurements of effective thermal conductivity and thermal diffusivity of rocks and minerals. This technology allowed us to provide economical, fast, detailed, and reliable data of effective thermal conductivity, thermal diffusivity, and volumetric heat capacity measured on thousands of cores from many scientific boreholes (Popov et al., 2016b). However, there are disadvantages of methodologies of thermal properties measurements at elevated temperatures, including thermal conductivity, coefficient of linear thermal expansion, and volumetric heat capacity.

A number of researchers have reported the results of experimental investigation of effective thermal conductivity of various rocks and minerals at high temperatures and pressures (Abdulagatova et al., 2009; Vosteen and Schellschmidt, 2003; Clauser, 2006; Miklashevskiy et al., 2006; Ramazanov and Magdiev, 2014). Experiments to investigate the simultaneous influence of high temperature and high pressure are extremely hard to arrange, so an “additive” approach is normally used where the dependencies “thermal conductivity vs temperature” and “thermal conductivity vs pressure” are studied separately (Seipold, 1998; Clauser and Huenges, 1995). The studies have shown that thermal conductivity is most dependent on temperature (Clauser, 2006; Vosteen and Schellschmidt, 2003). Experimental data on thermal conductivity of hydrocarbon

reservoirs and surrounding formations at elevated temperatures are important for determining heat flow density (Sekiguchi, 1984), modeling basin and petroleum systems (Hantschel and Kauerauf, 2009), and developing and improving thermal methods of EOR, such as steam-assisted-gravity-drainage (Irani and Cokar, 2016). Data on thermal conductivity of rocks are also necessary for calculating heat losses from underground steam and hot water pipes including those used in thermal EOR, and for exploitation of geothermal reservoirs (Somerton, 1992; Clauser, 2006; Khan and Maqsood, 2007). Heat transfer calculations have also become increasingly important in the analysis of in-situ combustion and underground nuclear explosions (Somerton and Boozer, 1960).

Estimation of thermal conductivity of rocks with increasing temperature is also important for the design of radioactive waste disposal where heat generation induces thermal stresses that influence the stability of disposal (Gilliam and Morgan, 1987; Durham and Abey, 1981; Garitte et al., 2014). The effective thermal conductivity of rock samples decreases at elevated temperatures mainly due to corresponding changes in the thermal conductivity of the rock-forming minerals. Changes in mineral composition, pore structure, and propagation of microcracks prompted by heating of the rock sample often cause an additional reduction of thermal conductivity. The complexity of the heat transfer mechanism in rocks makes it difficult to correctly calculate the effective thermal conductivity of porous materials from theoretical modeling of the effective thermal conductivity of rocks (Clauser, 2006; Sun et al., 2016). This makes it important to use representative experimental data concerning thermal properties in simulations, as uncertainties about thermal conductivity have a significant impact on modeling results (Popov et al., 2013).

Extensive studies of the thermal properties of various types of rocks have been carried out. But the results obtained by different measurement techniques often contain systematic errors due to poor contact with the studied rock sample (Merriman et al., 2017). Methods of thermal core logging exist, which allowed (Kukkonen and Suppala, 1999) to measure the effective thermal conductivity of rocks in-situ, but they are not widely used due to significant duration of the required measurements, insufficient radius of influence, and difficulties in analyzing the influence of borehole fluid (Miklashevsky et al., 2006; Novikov et al., 2008).

Laser-flash measurements, which provide absolute values, give lattice thermal diffusivity near room temperature for hard minerals that is 20% higher than methods involving multiple contacts, and 10% higher than single-contact methods. Contact methods underestimate lattice thermal diffusivity near 298 K due to loss of heat at interfaces. As temperature increases, data obtained using contact methods are increasingly contaminated with a spurious radiative transfer, sometimes even at 298 K (Hofmeister et al., 2007).

Real rocks are a complex composition of various crystalline and amorphous bodies, far from ideal forms, with different dependencies of thermal resistance on temperature, and with different nature of the combination of these dissimilar elements. Therefore, the nature of the dependence of effective thermal conductivity of rocks on temperature can vary greatly depending on all the above factors.

The study of the temperature dependence of effective thermal conductivity of rock samples was carried out by (Tarelko, 2011). The results obtained confirm the general conclusion about a decrease in the thermal conductivity coefficient with increasing temperature and about a high degree of variability from sample to sample.

The results of the study of the temperature dependence of effective thermal conductivity for sedimentary rocks of the Volga-Ural province are given in the monograph (Lipaev, 2013). It was shown that for these rocks the effective thermal conductivity decreases with temperature, as follows from general physical concepts. Similar results were obtained in the experimental work (Vosteen and Schellschmidt, 2003) for the rocks of the Alpine region. The combination of different minerals in the rock skeleton can lead, however, to very different thermal conductivity dependences on temperature. For the collection of samples (sandstones, limestones, siltstones, dolomites) studied in (Abdulagatov et al., 2006), the effective thermal conductivity is practically independent of temperature.

The monograph (Babaev et al., 1987) presents the results of experiments on measuring the effective thermal conductivity of sedimentary rocks, in which an increase in thermal conductivity with increasing temperature is observed. However, there are no data on the composition of rocks, which could explain this type of dependence.

In general, according to numerous data, unconventional reservoir formations have a very complex mineral composition, different and rather complex textures. Physical parameters of such rocks, necessary for the numerical simulations can hardly be estimated by analogy, or determined by calculation, based on the parameters of the rocks included in the composition components. To obtain the initial data, systematic laboratory petrophysical research should be obtained (Yudin et al., 2015). Shale rocks are more sensitive to temperature increase than other rocks due to their specific physical and mechanical properties. The organic matter is pyrolyzed at high temperatures, which increases the porosity and propagation of cracks in rock samples (Wang et al., 2018). The effective thermal conductivity of shales is influenced by many factors, including composition, porosity, temperature, and pressure (Gillian and Morgan, 1987; Ilozobhie et al., 2016). As mentioned above, the experimental procedure for effective thermal conductivity measurements, which give simultaneous consideration to temperature and pressure, is very complicated and only

a few such experiments have been carried out (Abdulgatova et al., 2009; Durham and Abey, 1981; Horai and Susaki, 1989; Miklashevsky et al., 2006; Smith, 1978; Prats and O'Brien, 1975; DuBow et al., 1980). It is also difficult to ensure reliable metrology in such experiments.

Information about the coefficient of linear thermal expansion (CLTE) of rock samples is necessary for the estimation of the thermal stress of rock mass that is caused by the thermal expansion of rocks. Knowledge of CLTE allows us to predict how rocks will behave under thermal stress (Siratovich et al., 2015) and to establish depth intervals with possible borehole wall collapse for prevention of rock drilling equipment damage (Wong and Brace, 1979). CLTE estimation is important in designing repositories for radioactive wastes for safety control as well (Heard and Page, 1982; Gens et al., 2007) as the long-term influence of high temperatures can change mechanical characteristics of shales (Smith, 1978). Another application of the thermal expansion data is related to caprock integrity assessment for thermal EOR methods (Chekhonin et al., 2012).

A lot of factors can influence the thermal expansion of rocks: temperature, pressure, mineralogical composition, crystal orientation, texture, porosity, pore fluid properties, and microfracturing (Siegesmund, 2000; Huotari and Kukkonen, 2004). One of the reasons for rocks damage is different thermal expansion of rock components (minerals, pore fluids). As thermal expansion coefficients are anisotropic and different for rock-forming minerals, it results in stress accumulation at grain boundaries of different minerals. The minerals with the largest thermal expansion have the strongest influence on the strain of the studied rock sample as a whole (Harvey, 1967; Somerton, 1992; Pitts, 2017). Exceeding breaking points at the contact of mineral grains can lead to rocks disruption. The thermal expansion causes cracks propagation between mineral grains that increases porosity and leads to changes in elastic moduli of rocks and rock stresses (Wong and Brace, 1979; Bauer and Handin, 1983; Cooper and Simmons, 1977).

Phase change reactions in minerals that occurred due to high temperatures can cause induced thermal stresses (Somerton, 1992). As coefficients of linear and volumetric strain are often given for constant volume and pressure systems, thermal cycling cracking during thermal expansion at atmospheric pressure occurs (Wong and Brace, 1979; Cooper and Simmons, 1977).

In general, the published data on rock thermal expansion are not numerous and involve a narrow range of minerals and rocks. Previously published CLTE data often do not provide the necessary quality of CLTE measurements for oil-rich shales. Particularly, the CLTE measurements with different orientations of principal axes of CLTE were previously performed only on several shale samples drilled from full-size core samples that cannot allow accounting for the influence of essential heterogeneity of organic-rich shales on the quality of rock anisotropy characterization (Wong and Brace, 1979). At the same time, accounting for significant heterogeneity and

anisotropy of oil-rich shales is important for studying correlations of CLTE with other physical properties of rocks to provide all measurements on the same rock sample that allows us to exclude heterogeneity

Very often, CLTE anisotropy is not considered in previous publications at all (Popov et al., 2008). However, high anisotropy of shales and unstable CLTE behavior with temperature can influence the thermal stress of rocks and stability of formation (Grebowicz, 2014).

In most publications, experimental data on CLTE is given as average values within wide temperature ranges (50 °C and more), while results of differential CLTE measurements with a heating interval of 20-250 °C were not published previously, although detailed information on CLTE vs temperature variations for different temperature ranges is necessary for rock stress modeling (Yanchenko, 2009).

Volumetric heat capacity (VHC) as one of the thermal properties of rocks and other materials determines the dynamics of the thermal regime of a heating or cooling medium. The VHC is related to the thermal conductivity and the thermal diffusivity by the ratio  $C = \lambda/a$ . The VHC is related to the specific heat  $c$  and the density of the medium by the ratio  $C = C_p \cdot \rho$ . VHC is one of the initial parameters, data on which are required when calculating the characteristics of dynamic heat transfer processes in rock massifs. In geological and geophysical work, such calculations are necessary, for example, in the development of thermal methods for the production of high-viscosity oils, modeling the thermal evolution of sedimentary basins and oil and gas systems, studying paleoclimatic processes, and in many other cases.

In the practice of geological and geophysical work, another common approach is to determine the VHC from data on thermal conductivity and thermal diffusivity of rocks, obtained independently from the results of measurements of these properties on different instruments and different rock samples.

In the absence of experimental data, the approximate value of the heat capacity can be obtained by calculation. The VHC can be calculated using the formula  $C = f_m \cdot c_m \cdot \rho_m + f_o \cdot c_o \cdot \rho_o + f_w \cdot c_w \cdot \rho_w$ , where  $f$  is the volume fraction of a substance,  $c$  is the specific heat capacity of a substance,  $m$  is a mineral substance,  $o$  is an organic matter,  $w$  - water (Hillel, 1980). However, the results obtained in this way in most cases cannot be assessed as accurate because it is not always possible to accurately determine the volume fraction of the substance contained in the rock. The presented simple analytical and empirical formulas for calculating the specific heat capacity of rocks can be used only as a first approximation for qualitative estimates of its value.

The results of an experimental study of the temperature dependences of the specific heat capacity for minerals with different average atomic weights are presented in (Petrinin and Popov,

2011). For almost all minerals in the temperature range characteristic of thermal gas treatment, there is a temperature dependence of the heat capacity. The same conclusion can be drawn from the data on the temperature dependence of the heat capacity of a number of sedimentary rocks given in the monograph (Babaev et al., 1987). The monograph (Dyakonov and Yakovlev, 1969) notes that in the temperature range 0-200 °C, the increase in heat capacity with increasing temperature is approximately 1.5-2% for every 10 °C.

To describe the dependence of the heat capacity of rocks on temperature, approximate formulas are often used, for example, a linear dependence (Dmitriev and Goncharov, 1990):

$$C = C_{20} + n \cdot 10^{-1}(T - 20),$$

where the parameter  $n$  is determined from the experiment.

As stated, this approximation is valid for temperatures in the range 0 - 500 °C (Dmitriev and Goncharov, 1990).

More precise is the three-term formula (Birch et al., 1949):

$$C_p = a + b \cdot T - c \cdot T^{-2},$$

The same expression is used to calculate the true heat capacities from the measured value of the average heat capacity over a certain temperature interval (Birch et al., 1949). The values of the parameters  $a$ ,  $b$ ,  $c$  of this dependence for more than 100 minerals are given in the reference book (Birch et al., 1949).

A number of works use formulas with a larger number of terms, for example (Findikakis et al., 2004):

$$C_p = k_0 + k_1 \cdot T^{-0.5} + k_2 \cdot T^{-2} + k_3 \cdot T^{-3}$$

or

$$C_p = A_1 + A_2 \cdot T + A_3 \cdot T^{-2} + A_4 \cdot T^{-0.5} + A_5 \cdot T^2,$$

as well as simplified versions of these equations.

In particular, for each of the minerals studied in (Findikakis et al., 2004) used their own equations to describe the temperature dependence of the specific heat.

The work (Kurbanov, 2007) investigated the thermophysical properties of rocks in the temperature range 20-300 °C and the pressure range 0.1-150 MPa. The work was carried out on an extensive collection of sedimentary rock samples from the Eastern Ciscaucasia, which was distinguished by a wide range of petrophysical characteristics, composition, and structure of the samples. Petrographic analyzes of the samples were performed both before and after the study. As a result, it was found that up to 500 °C, in the first approximation, the heat capacity of the studied rocks linearly increased with increasing temperature.

## 1.2 Statement of the problem

Preliminary studies that have already been performed provide a basis for the measurements of thermal properties of core samples at reservoir temperatures. Nevertheless, nowadays there are problems that relate to:

- number of experimental data on effective thermal conductivity, CLTE with temperature is not representative for unconventional reservoir rocks;
- experimental data on VHC is absent for unconventional reservoir rocks;
- measurement techniques often contain systematic errors;
- the absence of metrological analysis;
- lack of anisotropy analysis for effective thermal conductivity and CLTE of unconventional reservoir rocks;
- lack of correlation analysis of CLTE with other physical properties;
- absence of measurements of thermal conductivity of non-consolidated rocks at elevated temperatures;
- thermal properties of unconventional reservoir rocks at elevated temperatures cannot be estimated analytically due to complex mineral composition and texture.

The disadvantages of methods for measuring thermal properties of unconventional reservoir rocks at elevated temperatures and nowadays problems mentioned above encouraged to:

- develop new methodologies for determining thermal properties of unconventional reservoir rocks at elevated temperatures;
- get representative data on thermal properties of unconventional reservoir rocks at elevated temperatures;
- provide metrological analysis of measurements;
- provide anisotropy analysis of CLTE for unconventional reservoir rocks;
- provide correlation analysis for thermal conductivity and CLTE;
- provide measurements of thermal conductivity of particles of solid material at elevated temperatures.

New methodologies should be used on the basis of reliable and contact-free measurement techniques as unconventional reservoir rocks are enough fragile due to numerous fractures. One of the equipment that can provide such measurements is the Thermal Conductivity Scanner (TCS) (Popov et al., 2016). The combination of TCS with equipment for measurements of thermal properties at elevated temperatures gives the possibility to exclude nowadays disadvantages and

problems. Lack of anisotropy analysis is also can be excluded by combination with TCS, as it allows us to measure core samples in different directions to the core axis. It also helps to compare effective thermal conductivity and CLTE anisotropy for unconventional reservoir rocks that was not provided before. Also, it gives the possibility to find a new correlation of effective thermal conductivity with other properties such as CLTE. It also can be the basis for measurements of the thermal conductivity of rock particles of solid material at elevated temperatures.

### **1.3 Outline of the Thesis**

For obtaining goals mentioned above it is necessary to carry out the following steps:

- to develop a new approach to the measurement of rock thermal properties at elevated temperatures for unconventional reservoir rocks and non-consolidated rocks;
- to apply the approach to organic-rich rocks from unconventional reservoirs and improve the quality of thermal conductivity measurements;
- to determine the degree of CLTE anisotropy and range of CLTE values for unconventional reservoir rocks;
- to compare directions of CLTE anisotropy main axes with the direction of the main axes of thermal conductivity tensor;
- to analyze new correlations between CLTE, thermal conductivity, TOC, and density for unconventional reservoir rocks;
- to analyze temperature behavior of CLTE of unconventional reservoir rocks;
- to develop a new methodology of VHC measurements and establish new equations which relate VHC to temperature for unconventional reservoir rocks.

## Chapter 2. Literature review and the current state of the problem

### 2.1 Thermal conductivity dependence of unconventional reservoirs at elevated temperatures –current state of the art

Nowadays, the following techniques are used for thermal conductivity measurements at elevated temperatures.

- Divided-bar technique. The sample in the form of a disk is measured between two disks from a reference material with constant heat, the temperature drop is constant (Pasquale et al., 2015). After obtaining the stable state effective thermal conductivity of the sample is determined by comparison of temperature drop along with its height with the temperature drop in the reference sample (Popov et al., 1999). This method is required much time for measurements, but it provides thermal anisotropy of rock samples.
- Line heat source method. For instruments based on this method thin sonde with the heating element and temperature sensor is used (Popov et al., 1999; Barry-Macaulay et al., 2013; Sass et al., 1984). In contrast with steady-state methods, there is no necessity in thermal equilibrium, as a result, measurements are provided faster. Thermal conductivity value is determined from the theoretical model that determines the value of temperature response on thermal impulse. Sonde is placed into a rock sample or on its surface. However, this method can only provide data regarding heat diffusion in material for its calculations and cannot test anisotropic materials.
- Guarded hot plate method. This method determines thermal resistance, effective thermal conductivity, and heat flux density through the studied sample. For this, the electric power supplied to the heater of the hot engine is measured (Hammerschmidt et al., 2002). The disadvantages of this method are long measurement and the contact resistance between the thermocouple and the specimen surface causes a major source of error.
- Laser flash method. This method determines thermal diffusivity. During measurements, the sample's surface is heated by a short laser impulse. Induced temperature change is registered on the other side of the sample. Thermal conductivity is determined if the specific heat capacity and the density of material are given (Merriman et al., 2013). Such a method doesn't provide direct thermal conductivity measurements, density and specific heat capacity are necessary.

The investigation of thermal properties of shales at high temperatures has recently acquired new importance (Grebowicz, 2014) but experimental data on such properties remain scant (Jha et

al., 2016). The effective thermal conductivity of four rock samples from the Green River oil field at high temperatures (40-400 °C) and high pressure was studied by DuBow et al. (1976) using the comparative method. The thermal comparator technique compares the ability of the test sample to transport heat with that of reference material to conduct the same amount of heat. It was observed that the effect of pressure on thermal conductivity only becomes significant at high temperatures (above 300-400 °C). In contrast to other studies, the experimental data showed that the effective thermal conductivity of shales remains steady or increases with increasing temperature. This is because, when oil shales approach retorting temperatures (when they are heated to 200-400 °C) the role of solid-fluid and fluid-fluid heat transfer mechanisms increases and, at relatively low porosities, may predominate over thermal transfer properties. Analysis of shale anisotropy has only rarely been carried out (Popov et al., 2017; Yu et al., 2015; Wang et al., 2018). Unfortunately, even in these rare investigations, thermal anisotropy was estimated from a comparison of measurement results obtained for different rock samples, which fails to exclude the influence of rock heterogeneity on the anisotropy estimation. The heterogeneity of the studied rock samples and their changes as a result of heating was not taken into account in the above-mentioned experiments.

Sokolova et al. (1986) studied effective thermal conductivity of three samples of bituminous argillites from Bazhenov formation (West Siberia, Russia) with a dynamic calorimeter using an IT- $\lambda$ -400 instrument and observed abnormally low thermal conductivity (1.1-1.3 W/(m·K)) within a temperature range of 25-200 °C. A very weak reduction of thermal conductivity of shale rocks with temperature (10% at 100 °C) was observed in comparison with other sedimentary rock samples. Unfortunately, the orientation of the studied rock samples relative to the heat flow direction was not recorded and analysis of rock heterogeneity and anisotropy was not carried out, although the high thermal heterogeneity and anisotropy of shale rocks are generally acknowledged (Popov et al., 2016a; Popov et al., 2017).

Another calculation of effective thermal conductivity, both parallel and perpendicular to the bedding plane, for two anisotropic shales (at the Liaoning Fushun open-cast mine in China), was provided by Wang et al. (2018) using thermal diffusivity measured with Netzsch LFA laser thermal conductivity analyzer at temperatures ranging from room temperature to 600 °C and known parameters of density and specific heat capacity. The authors concluded that the main reason for the change in the thermal characteristics of the shales and their anisotropy were thermal cracks caused by the temperature increase. Numerous cracks appear parallel to bedding when the temperature increases up to 400 °C that leads to increasing the anisotropy coefficient of both thermal conductivity and some other physical parameters. However, as in the other experiments

mentioned above, the number of studied rock samples dealt with by Wang et al. (2018) is not representative and the procedure of core sampling is not described.

Yu et al. (2015) calculated effective thermal conductivity of six oil shale samples (Fushun, China) parallel and perpendicular to bedding using thermal diffusivity measured with Netzsch LFA laser thermal conductivity analyzer in a temperature range of 25-300 °C and known parameters of density and specific heat capacity. The authors found a weak decrease of thermal conductivity with temperature (about 10% at 100 °C) and a high value of the rock thermal anisotropy coefficient (1.8), which remained unchanged with temperature. The variations of the effective thermal conductivity component parallel to bedding with temperature are 1.35-1.85 W/(m·K) and variations perpendicular to bedding are 0.75-1.00 W/(m·K). The organic content of the studied rock samples was not analyzed and the core sampling procedure was not described.

Jha et al. (2016) measured the effective thermal conductivity of Jhiri shale (India) using the single guarded hot parallel plate method (ASTM C177-13, 2013). Heating to 200 °C causes a marked reduction of effective thermal conductivity (by 32%), possibly due to the evaporation of moisture from the pores. Effective thermal conductivity changes by 10% at temperature range 200-400 °C that can be related to pore volume increasing of the studied rock sample. At high temperatures (400-700 °C) effective thermal conductivity changes only by (2-3%) due to, probably, ductile behavior of rock samples at such high temperatures. No information is provided about the orientation of the rock samples, their anisotropy, heterogeneity, and organic content.

Gilliam and Morgan (1987) studied effective thermal conductivity variations within a temperature range of 25-200 °C using the comparative method for Devonian, Pierre, and Green River formations and established a conductivity range of 0.68-1.09 W/(m·K). The authors noted that variables, which ought to be considered, are temperature, pressure, rock composition, and anisotropy of thermal conductivity in the rocks (not all of these were considered in the studies).

Key findings of the previous publications are summarized in *Table 1* to (1) show ranges of effective thermal conductivity variations of shales in different temperature intervals, and (2) to present information about the experimental procedures used for different shale formations. It can be seen that samples from different shale formations have a broad range of effective thermal conductivity (0.25-4.36 W/(m·K)). Specific thermal conductivity behavior of shales at high temperatures can be seen, including a weak decrease of effective thermal conductivity (2-10%) at 100 °C in comparison with other sedimentary rock samples (about 10-15%, according to Popov et al. (2013)). The publications show that effective thermal conductivity of shales at high temperatures depends on many factors, including orientation of the core sample relative to the

direction of heat flow, temperature range, organic content in core samples, and the environment in which experiments are performed (air, nitrogen, argon, etc.).

Orientation of the shale samples relative to the direction of heat flow in measurements using the divided-bar technique (Popov et al., 2016b) has a major impact on effective thermal conductivity values since most of the shale samples have a high degree of anisotropy. Effective thermal conductivity measured parallel to bedding is normally 30-50% higher than effective thermal conductivity measured perpendicular to bedding (Gilliam and Morgan, 1987; Nottenburg et al., 1978; Rajeshwar and DuBow, 1980; Popov et al., 2016a).

Different effective thermal conductivity values of shales in different temperature ranges can be explained by the specific nature of the decomposition of organic matter at high temperatures (Rajeshwar and DuBow, 1980). A slight decrease of effective thermal conductivity with temperature is observed in most shales (Rajeshwar and DuBow, 1980; Sokolova et al., 1986; Nottenburg et al., 1978; Gilliam and Morgan, 1987). However, in some shales, effective thermal conductivity behavior is essentially related to a particular temperature range. At 25-200 °C free and bound water loss is observed (Wang et al., 2018), at 200-400 °C there is loss of mineral water and volatile components (Wang et al., 2018), at 400-600 °C organic matter decomposes (Wang et al., 2018; Rajeshwar et al., 1980) and cracks appear (Jha et al., 2016). The influence of kerogen decomposition on thermal conductivity is questionable as the degree of kerogen decomposition depends on the length of time during which the high temperature is maintained. For example, 90% kerogen decomposition required 100 hours at a temperature of 350 °C (Prats and O'Brien, 1975).

The results of experiments have shown that pressure has only a small effect on the thermal conductivity of shales in a temperature range of 25-400 °C. For Conasauga formation the effective thermal conductivity of shales at the initial temperature increased by 2% with a pressure increase from 2.5 MPa to 10 MPa (Smith, 1978). For shale samples from the Green River formation, effective thermal conductivity also increased by 2% with pressure increase from 0.7 MPa to 12 MPa (Prats and O'Brien, 1975). However, pressure increase from 0.8 MPa to 4.1 MPa at high temperatures of 400-600 °C was shown to increase the effective thermal conductivity of shales much more significantly, by 10-20 % (DuBow et al., 1980).

The degree of reduction in thermal conductivity is related to the percentage of organic content in shale samples. It was shown for the Green River formation that the dependence of effective thermal conductivity of shale samples with various oil yields (7-82 gal/t) on temperature is weak. However, an increase in oil yield in a shale sample is associated with a lower decrease in thermal conductivity as the temperature rises (Rajeshwar et al., 1980).

The thermal behavior of oil shales was observed to be sensitive to the atmosphere surrounding the sample during measurements. Differential thermal analysis (DTA) carried out on shale samples from the Green River formation showed the difference in the thermal behavior of shales in air and inert atmosphere (nitrogen) when rock sample temperature exceeds 300 °C. Thermal decomposition of kerogen was observed at two DTA peaks (440 and 500 °C) in the presence of air and one DTA peak (500 °C) in the presence of nitrogen (Rajeshwar et al., 1979). Similar thermal behavior was observed for samples from the Green River, Kentucky, and Michigan formations using differential scanning analysis. Exotherms observed in the range 300-500 °C are related to oxidation effects and decomposition of kerogen. Decomposition of organic matter in shale in an inert atmosphere occurred in a temperature range of 400-500 °C (Rajeshwar et al., 1980).

**Table 1.** Effective thermal conductivity of shales and experimental conditions of high-temperature measurements for different shale formations obtained from the literature.

Literature reference	Shale formation	Heat flow direction relative to the bedding plane	Thermal conductivity range, W/(m·K)	Temperature range, °C	Atmosphere	Number of studied samples	Oil yield, g/t*	Measurement technique	Metrological control of measurement quality
Prats and O'Brien, 1975	Green River, US	Parallel	0.44-1.82	25-400	Nitrogen	5	0-35	Transient line heat-source (probe) method	Tested on pyrex
Smith, 1978	Conasauga US	30°/40°/45°	1.00-2.80	55-400	Nitrogen	5	Not mentioned	Comparator / guarded hot plate method	Tested on pyroceram, average error-2.6%
Nottenburg et al., 1978	Green River, US	Parallel	0.90-1.50	25-350	Inert gas	3	6-79	Comparator	Tested on pyroceram (standard deviation (STD) = 5%) and pyrex (STD = 6%)
		Perpendicular	0.25-1.75			4			
DuBow et al., 1980	Green River, US	Parallel	0.40-1.70	35-430	Air	5	21.6-47.9	Comparator	Tested on pyrex (STD = 4%)
Rajeshwar et al., 1980	Kentucky, US	Parallel	0.80-1.00	25-350	Nitrogen	1	52	Comparator	Tested on pyroceram (STD = 5%) and pyrex (STD = 6%)
	Michigan, US					1	28		
	Utah, US					11	7-82		
	Wyoming, US					3	18-40		
Sokolova et al., 1986	Bazhenov, Russia	Not mentioned	0.90-1.60	25-200	Air	3	Not mentioned	Comparator	Not mentioned
Gilliam and Morgan, 1987	Devonian, US	Parallel	0.73-1.09	25-200	Not mentioned	19	Not mentioned	Comparator	Tested on pyrex
	Pierre, US		0.68-1.01			4			
	Green River, US		1.00-1.45			2			
Yu et al., 2015	Fushun, China	Parallel	1.35-1.84	25-300	Air	3	Not mentioned	Laser analyzer	Not mentioned
		Perpendicular	0.75-1.00			3			
Jha et al., 2016	Jhiri, India	Not mentioned	1.77-4.36	25-900	Air	1	Not mentioned	Guarded hot plate method	Tested on mild steel and asbestos (uncertainty** = 6%)
Wang et al., 2018	Fushun, China	Parallel	0.70-1.89	20-600	Argon	1	Not mentioned	Laser analyzer	Not mentioned
		Perpendicular	0.25-0.73	20-600		1	Not mentioned		

\*g/t – gallons per ton; \*\* – uncertainty is based on an estimated accounting for accuracy and precision.

## 2.2 Coefficient of linear thermal expansion at elevated temperatures – current state of the art

The experimental data on coefficient of linear thermal expansion (CLTE) of shales with different orientations of rock samples relatively to bedding plane and within a wide temperature range (up to 800 °C) were published earlier. The data demonstrate that CLTE of shales increases with temperature, but sometimes CLTE stops its increasing within a particular temperature range. For example, for Devonian formation (USA) some shale samples went deformation above 200 °C, and CLTE started to decrease (Gilliam and Morgan, 1987). Such deformation is explained by the collapse of contained clays that can have a reduction of the spacing between platelets (Gilliam and Morgan, 1987). Similar oil-rich shale behavior was observed for Fushun formation (China) and Devonian formation (US) where CLTE decrease began at temperature 60 °C and 430 °C correspondingly (Gilliam and Morgan, 1987; Yu et al., 2015). These experimental data show the complicated character of CLTE variations of shales with temperature. The previous experimental data show a wide range of CLTE variations when a CLTE component parallel to bedding varies within a range of  $(8-80) \cdot 10^{-6} \text{ K}^{-1}$ , a CLTE component perpendicular to bedding varies within a range of  $(6-350) \cdot 10^{-6} \text{ K}^{-1}$ , and CLTE component inclined by 45° to the bedding plane varies within a range of  $(40-200) \cdot 10^{-6} \text{ K}^{-1}$  at temperature range (25-800 °C) (Smith, 1978; Gilliam and Morgan, 1987; Yu et al., 2015; MacGillivray and Dusseault, 1998). For Queenston and Mancos formations, a study of CLTE anisotropy coefficient of shales was performed on samples with orientation parallel, perpendicular, and 45° to bedding within a temperature range 25-75 °C when the CLTE anisotropy coefficient values were found to be 1.04-1.29 for Queenston shales and 1.04-1.71 for Mancos shale (MacGillivray and Dusseault, 1998). Experiments on CLTE variations of shales with different heating rates, organic matter content, and orientations showed that:

- the heating rate has a little effect on thermal rock expansion;
- organic matter content has no effect on CLTE behavior with temperature before kerogen starts decomposing;
- perpendicularly oriented shale samples have the largest CLTE values (Duvall et al., 1983).

The previous results of CLTE measurements on shales and characteristics of the experimental procedure for different shale formations are shown in *Table 2*.

An effect of oil grade on thermal expansion was observed for the Anvil Points Mine shale samples cut at a different orientation to bedding (Duvall et al., 1983). An increase in the grade of oil shale leads to thermal expansion increase within a temperature range of 350-450 °C when

decomposition of kerogen occurs. Within a temperature range of 100-200 °C, the effect of oil grade was observed only for samples cut perpendicular to bedding.

Shale samples have a high degree of thermal anisotropy (Popov et al., 2016a); therefore studying CLTE anisotropy is important for such samples. However, investigation of CLTE anisotropy of rocks and rock-forming minerals was previously provided rarely: for clay minerals (McKinstry, 1965), dolomitic marbles (Luque et al., 2011), sandstones (Zhou et al., 2016), and Mancos and Queenstone shales (MacGillivray and Dusseault, 1998). Detection of main axes direction of CLTE anisotropy for shale samples was not performed previously according to our analysis of publications, except our previous study (Gabova et al., 2017).

**Table 2.** Summary of published CLTE studies of shales.

Shale formation	Temperature range, °C	Pressure, MPa	Number of samples	Bedding orientation	CLTE range, $10^{-6} \text{ K}^{-1}$	Atmosphere	CLTE Anisotropy	Measurement technique	Presence of CLTE standards for testing, description of metrology	Literature
Conasauga	25-400	No pressure	4	parallel	8-13	—	—	NETZSCH 402E dilatometer	Borosilicate glass, measurement error $\pm 1.2\%$	Smith, 1978
			4	perpendicular	6-16					
Anvil Points Mine	25-800	No pressure	3	parallel	20-80	Nitrogen	?	In-house*	$\pm 40\%^{**}$ , no information on standards and metrology	Duvall et al., 1983
			3	perpendicular	50-350				$\pm 12\%^{**}$ , no information on standards and metrology	
			3	45°	40-200				$\pm 30\%^{**}$ , no information on standards and metrology	
Devonian	25-300	No pressure	4	perpendicular	9-325	Nitrogen	—	NETZSCH 402E dilatometer	Vacromium reference material, no information on metrology	Gilliam and Morgan, 1987
Queenstone	25-75	0-13.8 MPa	4	axial	10.1-15.3	—	1.0-1.5	Waterloo TE Cell	Aluminum sample, no information on metrology	MacGillivray and Dusseault, 1998
Mancos	25-75	0-7 MPa	4	diametric	9.6-11.9					
			3	axial	16-22					
Green River	25-800	No pressure	3	axial	16-22	Nitrogen	?	Thermomechanical Analyzer 2490 model	—	Grebowicz, 2014
			3	diametric	13.7-15.4					
Fushun	25-300	No pressure	1	parallel	100	—	1.7	NETZSCH dilatometer	—	Yu et al., 2015
			1	perpendicular	3500					
Bazhenov	25-300	No pressure	3	parallel	14	Air	1.2-2.2	Quartz dilatometer	Precision not more than 4%, absolute error $1.8 \cdot 10^{-7} \text{ K}^{-1}$	Gabova et al., 2017
			3	perpendicular	23.6					
Bazhenov	25-300	No pressure	4	parallel	4.4-22.8	Air	1.2-2.2	Quartz dilatometer	Precision not more than 4%, absolute error $1.8 \cdot 10^{-7} \text{ K}^{-1}$	Gabova et al., 2017
			5	perpendicular	14.4-143.0					

Remarks:

Dash (—) means the absence of corresponding information in the literature source.

Question mark (?) means that anisotropic behavior was observed, but no values are presented.

\*Setup was designed and built in the laboratory of the Department of Metallurgy and Metallurgical Engineering, University of Utah.

\*\* Values calculated from the error bars shown in graphs representing the maximum and minimum values of the relative linear thermal expansion values observed in the temperature range 25-300 °C.

### 2.3 Volumetric heat capacity at elevated temperatures – current state of the art

The volumetric heat capacity of rocks (VHC) depends on the VHC of the components - the mineral matrix, pore fluid, organic matter, as well as the temperature of the rocks. The VHC of rock-forming minerals varies in the range of 1.8 - 2.6 MJ/(m<sup>3</sup>·K). For water, the VHC is 4.19 MJ/(m<sup>3</sup>·K), for oil - 1.3-1.7 MJ/(m<sup>3</sup>·K), for air - 0.001 MJ/(m<sup>3</sup>·K)) (Dobrynin et al., 2004).

The previous results of specific heat capacity measurements on shales and characteristics of the experimental procedure for different shale formations are shown in *Table 3*. Gilliam and Morgan (1987) studied the specific heat capacity of shale formations with a differential scanning calorimeter. For Devonian formation slight decrease of specific heat capacity at 200 °C is observed. The average percent of specific heat capacity increasing at temperature range 25-200 °C is 40% for Devonian shale formation, 55% - for Pierre shale formation, 50 % - for Green River shale formation. Investigations of Kendyrylyk and Shubarkol shale formations provided by Kasenov et al. (2016) showed that specific heat capacity increases more than by 100% at temperature range 25-200 °C. Investigations of specific heat capacity for Baltic oil shale showed that increasing kerogen content increases the value of heat capacity. The average percent of specific heat capacity increasing at temperature range 0-350 °C is 90%. Rajeshwar and DuBow (1980) also studied the specific heat capacity of shale formations with differential scanning calorimeter. The average percent of specific heat capacity increasing at temperature range 100-350 °C is 50% for Michigan shale, 20% - for Kentucky shale. Smith (1978) studied 5 samples from Conasauga shale formations that showed that the average percent of specific heat capacity increasing at temperature range 20-400 °C is 35%. Somerton (1992) studied the specific heat capacity of 1 shale sample with a Bunsen-type calorimeter. The average percent of specific heat capacity increasing at temperature range 25-350 °C is 48%. Determination of VHC for shales is not presented in publications, only analytical solutions can be found.

**Table 3.** Summary of published specific heat capacity studies of shales.

Literature reference	Shale formation	Specific heat capacity range, J/(kg·K)	Temperature range, °C	Number of studied samples	Measurement technique	Measurement uncertainties
Gilliam and Morgan, 1987	Devonian, US	840-1465	25-200	14	differential scanning calorimeter	Standard deviation – 126-293 J/(kg·K)
	Pierre, US	1047-1675		3		
	Green River, US	1047-1570		1		
Kasenov et al., 2016	Kendyrlyk, Kazakhstan	400-1600	25-200	1	IT-S-400 calorimeter	Maximum measurement error of the calorimeter is ±10.0%
	Shubarkol, Kazakhstan	600-1400		1		
Savest and Oja, 2013	Baltic shale	1000-1900	0-350	1	aqueous calorimeter	Calculation accuracy - 3%
Rajeshwar and DuBow, 1980	Michigan shale	840-1260	100-350	1	differential scanning calorimeter	-
	Kentucky shale	1050-1260		1		
Smith, 1978	Conasauga shale	800-1200	20-400	5	differential scanning calorimeter	Measurement error is estimated at ±1.5%
Somerton, 1992	Shale	800-1180	25-530	1	Bunsen-type calorimeter	Experimental results are reproducible within ±0.5 percent

#### 2.4 Thermal conductivity measurements on rock cuttings and unconsolidated rocks at elevated temperatures – current state of the art

Nowadays, there are a few methods of measuring the thermal properties of particles of solid materials at elevated temperatures. One of them is a divided-bar method, which allows us to measure the thermal conductivity of solid material at different temperatures in a specified temperature range on samples with fixed dimensions, cylindrical shape, and parallel-sided surfaces (Lemenager et al., 2018). Another method consists of mixing particles of solid material with water, determining the volume fractions of particles of solid material and water in the mixture, measuring the effective thermal conductivity of the mixture of particles of solid material with water at different temperatures using the linear source method, determining the thermal conductivity of particles of solid material at different temperatures using a ratio (Lichtenecker model) describing the effective thermal conductivity of a mixture of solid particles with water (Pribnow and Sass, 1995). The methods mentioned above have the following disadvantages:

- measurements are carried out on solid samples that can withstand hold-down pressure (without any failure) required to reduce the thermal resistance on the surfaces of the sample under study;
- the effect of free convection in a liquid mixed with particles of a solid material before measurements during heating by a heat source in the process of measurements on the results of measurements of the thermal conductivity of the mixture; uncontrolled convection of a liquid introduces significant distortions in the measurement results, which are obtained using a formula that does not take into account the effect of convection of a liquid;
- the temperature range in which measurements of the thermal conductivity of a mixture of particles of solid material with a liquid can be made is limited by the boiling point of the liquid.

Disadvantages mentioned above were excluded in the method of determination of thermal conductivity of rock cuttings and non-consolidated rocks (Popov et al., 2018) including grinding particles of non-consolidated material, preparation of the mixture of ground particles with material-filler, and following mixture pressing until the solid sample of the pressed mixture. Then volume fractions of particles of non-consolidated material, material-filler and volume fraction of air in the sample of the pressed mixture are determined. Next, the effective thermal conductivity of the sample of the pressed mixture is measured and the thermal conductivity of particles of non-consolidated material is determined by the ratio, describing the link between the effective thermal conductivity of the sample of a pressed mixture of particles of non-consolidated material with material-filler with thermal conductivity of particles of non-consolidated material. However, this method does not provide the determination of the thermal conductivity of particles of solid material at elevated temperatures and does not include operations that determine the thermal conductivity of particles of solid material at elevated temperatures. Another disadvantage of the method is that preparation of a solid sample of the pressed mixture does not ensure the choice of material filler that allows the sample made from the mixture to withstand the hold-down pressure required for measurements and maintain strength properties in the studied temperature range.

## **2.5 Summary**

As can be seen from the overview of previous publications, careful metrological analysis or measurement quality and levels of uncertainty in the results were provided only in a few publications. This is unfortunate since shale rocks are very sensitive to mechanical treatment. It is

not easy to obtain the flatness of the rock, which is required for the divided-bar method, so it is essential to check the degree of uncertainty in the results due to deviation from flatness. Most of the rock sample collections, which have been the objects of previous studies, were not representative; only two previous publications (Gilliam and Morgan, 1987; Rajeshwar et al., 1980) have a representative number of samples. Shale rocks are highly anisotropic, so the main axes of thermal conductivity and the anisotropy coefficient of studied rock samples should be defined before high-temperature measurements. It should be taken into account that the point position of the temperature sensors (thermocouples) when the divided-bar method is applied to highly heterogeneous shales (Popov et al., 2017) results in a significant measurement uncertainty so that careful control of heterogeneity of the selected rock samples is required.

Kerogen, even at a relatively low heating temperature, undergoes significant transformations, since, in comparison with all hydrocarbons of petroleum origin, kerogen has the most complex molecules that are unstable to thermal effects. In laboratory conditions at atmospheric pressure, free hydrocarbons are released from kerogen samples at a temperature of 200-300 °C. A significant number of experiments have been carried out to study the thermal transformation of kerogen contained in oil shale, which provides a qualitative idea of the possible behavior and kerogen of the rocks of the Bazhenov Formation. The beginning of thermal decomposition of shale is observed at 170–180 °C; at 70-290 °C active release of pyrogenic moisture begins, at 325-350 °C – gas, and tar. The semi-coking process ends mainly at 450-500 °C, but further decomposition of the solid residue continues at higher temperatures. All these processes influence thermal properties of rocks at high temperatures (Yudin et al, 2015).

The previous studies have found different degrees of effective thermal conductivity decrease in the 25-300 °C temperature range for each shale formation, with variations of 5-35% (Prats and O'Brien, 1975; Smith, 1978; Nottenburg et al., 1978; DuBow et al., 1980; Rajeshwar et al., 1980; Sokolova et al., 1986; Gilliam and Morgan, 1987; Yu et al., 2015; Jha et al., 2016; Wang et al., 2018). There is a necessity in new experimental investigations on representative shale sample collections, taking account of the experimental problems described above.

Analysis of published experimental data on rock CLTE showed insufficient information on thermal expansion of shales at different temperatures, namely:

- non-representative collections of investigated samples for organic-rich shale formations;
- lack of CLTE anisotropy analysis;

- the absence of standard procedure of sampling core plugs for CLTE investigation (the sampling point significantly influences results of shale formation characterization as most shale samples and formations are highly heterogeneous);
- lack of combined integrated investigations of CLTE together with other physical characteristics of shales (density, thermal conductivity, total organic carbon, etc.).

Reliable information on thermal expansion of particular shale formation could not be obtained from literature data and requires experimental investigation of CLTE on particular representative rock samples collection with advanced equipment and methodology, accounting for rock anisotropy.

The VHC of unconventional reservoir rocks at elevated temperatures is not presented in publications and requires a new approach for determining this parameter. Only specific heat capacity values are presented and the number of studied rock samples is not represented (see *Table 3*).

Methods of determination of thermal conductivity of rock cuttings and non-consolidated rocks do not provide the determination of the thermal conductivity of particles of solid material at elevated temperatures and require a new approach.

## Chapter 3. Experimental

### 3.1 Enhancement of experimental basis for thermal conductivity measurements at elevated temperatures

#### 3.1.1 Method of measuring thermal conductivity at elevated temperatures

##### 3.1.1.1 Thermal conductivity measurements procedure using a DTC-300 instrument

Effective thermal conductivity measurements in a temperature range of 30-300 °C were carried out with the well-known divided-bar method (Beck, 1957; Popov et al., 2016b) using a DTC-300 instrument (*Figure 1*) (TA Instruments, <http://www.tainstruments.com/dtc-300>). By the manufacturer's instructions, the rock samples were treated before the measurements and were prepared as cylindrical core plugs with a diameter of (50±1) mm and a height of (20±1) mm. The thermal conductivity measurements are based on the guarded heat flow meter method and satisfy the requirements of ASTM E1530-11 (2016). The instrument scheme can be found in (Popov et al., 2016b; TA Instruments, <http://www.tainstruments.com/dtc-300>).



**Figure 1.** DTC-300 instrument for measuring thermal conductivity of rock samples at elevated temperatures.

Technical characteristics of the DTC-300 are as follows (TA Instruments, <http://www.tainstruments.com/dtc-300>):

- thermal conductivity range: 0.1-30 W/(m·K)
- temperature range: -20 °C to 300 °C with an interval between measurements of at least 5 °C;

- range of compressive pressure: 0.03 – 0.41 MPa;
- measurement rate: 40-60 min at a particular temperature;
- uncertainty of the measurements is within from (3 to 8) % (depends on the thermal resistance of studied sample);

For measurements with the DTC-300, the samples should have a cylindrical form with a thickness of  $20\pm 1$  mm and a diameter of  $50\pm 1$  mm. The samples must have smooth and parallel-sided surfaces without any damage or cracks. Before the measurements, a thermal compound is applied on the flat surfaces of the sample to minimize thermal resistance between the sample and the closeout surfaces according to the recommendations of the DTC-300 manufacturer. The studied sample with some amount of thermal compound is set between two parallel flat surfaces (each of them has incorporated thermocouple inside) regulated by different temperatures. The temperature difference applied to the rock from the upper to lower surface is 30 °C. During measurements, a compressive load is applied to the stack (to minimize contact resistance) and axial temperature gradient is provided in the stack as heat is supplied from the upper surface through the sample to the lower surface. Compressive load for all experimental data was 7kPa and constant with temperature. Thermal expansion of studied rock samples does not exceed 0.1 mm (that is just 0.5% of the height of studied samples). It results in negligible changes in the compressive load and does not have an effect on thermal conductivity during heating that takes about 1 hour for each temperature to reach a steady state. The thermal conductivity of studied samples is calculated using measured temperature drop along with the sample and the sample thickness. An automatically controlled system provides continuing measurements during the studied temperature range. The heat isolation is performed by the guard that surrounds the stack during the experiment and is kept at the mean temperature of the two plates, to minimize lateral heat flow to and from the stack. A number of samples with known thermal resistance that covers the necessary range of studied samples are used for calibration of the instrument. Five certified reference standards (Vespel, titanium alloy VT-6, plexiglass, single-crystal quartz, and technical glass K-8) within the temperature range of 30-300 °C have been used for calibration and the accuracy and precision determination.

### **3.1.1.2 Metrological study of DTC-300 instrument**

For the metrological study of thermal conductivity measurements at elevated temperatures with DTC-300 instrument following standard samples were used: plexiglass, Vespel, technical glass K-8, single-crystal quartz, titanium alloy VT-6. These materials were chosen in such a way

because their thermal conductivity covers the range of thermal conductivity of rocks – 0.19-6.40 W/(m·K) (see *Table 4*). For all materials a precision of thermal conductivity measurements with temperature was estimated with experiments. Precision (random error) was determined using the formula:  $P = (\sigma \cdot t_{n,0.95}) / (\sqrt{n} \cdot \langle \lambda_{meas} \rangle \cdot 100\%)$ , where  $\sigma$  is root mean square deviation,  $t_{n,0.95}$  – Student’s coefficient at confidence level 95%;  $n$  – number of the measurements,  $\langle \lambda_{meas} \rangle$  – average measured thermal conductivity value. A number of measurements are presented in *Table 4*. The precision of thermal conductivity measurements on technical glass K-8, quartz, and titanium with temperature showed polynomial behavior (*Figure 2*). For technical glass K-8 it is in the range of 0-3%, for single-crystal quartz – 0-8%, for titanium alloy VT-6 – 2-7% (*Figure 2*). The precision of thermal conductivity measurements on vespel with temperature showed unstable behavior in the range of 0.5-2.5% (*Figure 2*). The precision of thermal conductivity measurements on plexiglass showed stable behavior with temperature and is in the range of 0.4-0.6% (*Figure 2*).

Accuracy (systematic error) was estimated with the formula:  $A = \frac{\langle \lambda_{meas} \rangle - \lambda_{certif}}{\langle \lambda_{meas} \rangle} \cdot 100\%$ , where  $\langle \lambda_{meas} \rangle$  – average measured thermal conductivity value;  $\lambda_{certif}$  – certified value of thermal conductivity. The values of thermal conductivity measurements with DTC-300 instrument at room temperature are shown in *Table 4*. The accuracy of thermal conductivity measurements for studied certified materials is in the range from -12 to -1%.

**Table 4.** Results of accuracy estimation using standard reference samples on DTC-300 instrument at room temperature.

Material	$\lambda_{certif}$ , W/(m·K)	$\lambda_{average}$ (DTC-300), W/(m·K)	Number of measurements (DTC-300)	Accuracy of DTC-300 measurements, %
Plexiglass	0.194 (Sergeev and Shashkov, 1983; Russian Standard Bureau VNIIM)	0.179	4	-8
Vespel	0.374 (NIST)	0.371	6	-1
Glass K-8	1.094 (Sergeev and Shashkov, 1983; Russian Standard Bureau VNIIM)	0.96	5	-12
Quartz, single crystal	6.05 (Beck, 1988; Popov et al., 2016b)	5.66	5	-6
Titanium alloy VT-6	6.52 (Popov et al., 2016b)	6.37	5	-2

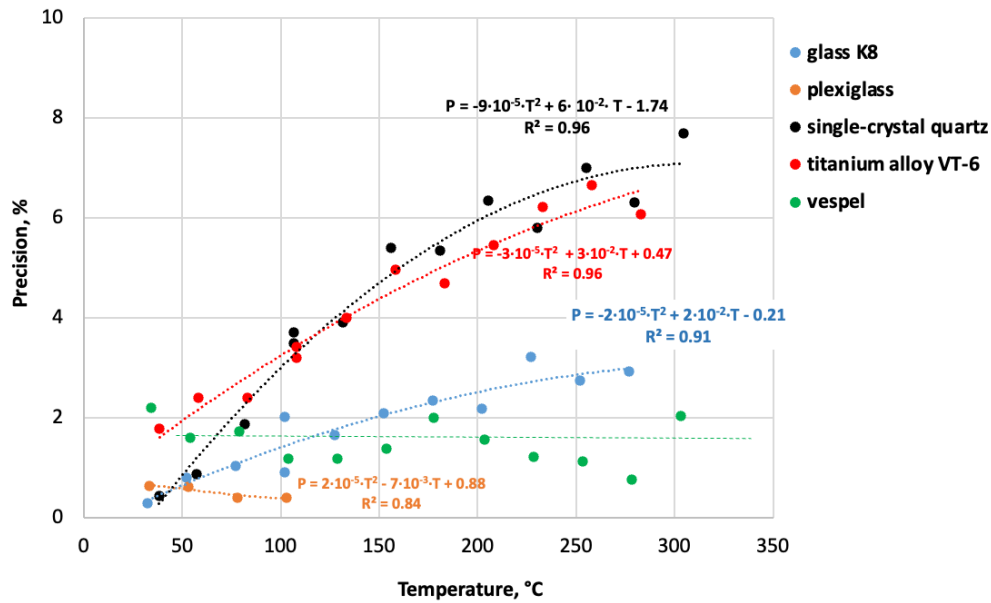


**Figure 2.** The precision of thermal conductivity measurements with DTC-300 instrument with temperature estimated from experiments on standard samples.

Metrological study of thermal conductivity measurements of standard samples on DTC-300 instrument showed that precision and accuracy of measurements are enough high and can reach 9% and -12% respectively. A new approach for thermal conductivity measurements at elevated temperatures is required to provide better measurement quality.

### 3.1.2 New measuring methodology for thermal conductivity by combining DTC-300 results with those of TCS

To account for rock anisotropy and heterogeneity and to provide better measurement quality, the DTC-300 was used in combination with Thermal Conductivity Scanner (TCS). The TCS offers contact-free non-destructive profiling of rock thermal conductivity and thermal diffusivity on the flat or cylindrical surface of full-diameter or split core samples. It measures thermal properties (thermal conductivity parallel ( $\lambda_{||}$ ) and perpendicular ( $\lambda_{\perp}$ ) to bedding, thermal diffusivity, the thermal heterogeneity factor obtained from scanning the sample along ( $\beta_1$ ) and perpendicular ( $\beta_2$ ) to the core axis, and the thermal anisotropy coefficient ( $K = \lambda_{||}/\lambda_{\perp}$ )) as well as the volumetric heat capacity of rock samples with flat or cylindrical surfaces in atmospheric conditions. The thermal conductivity component parallel to the bedding plane ( $\lambda_{||}$ ) is determined by optical scanning in a direction perpendicular to the rock bedding plane (normally equivalent to scanning along the axis of the core sample on the cylindrical surface of full-diameter core samples

for sub-vertical wells). The additional optical scan in a direction parallel to the rock bedding plane provides a determination of the effective thermal conductivity component perpendicular to the bedding plane ( $\lambda_{\perp}$ ) using the formula:

$$\lambda_{\perp} = \lambda_{\text{app}}^2 / \lambda_{\parallel}, \quad (1)$$

where  $\lambda_{\text{app}}$  is ‘apparent’ thermal conductivity measured by optical scanning in a direction perpendicular to the rock bedding plane (Popov et al., 2016b). The instrument scheme can be found in (Popov et al., 2016b).

The procedure of thermal conductivity measurements using the TCS instrument is following. The studied rock samples are placed between two reference standards on the platform. The reference standards are chosen in accordance with the range of thermal conductivity of the studied rock samples. Eight certified reference standards (VespeI, stainless steel, pyrex, plexiglass, fused quartz, technical glass K-8, titanium alloy VT-6 and anisotropic single crystal of quartz) have been used for calibration and the accuracy and precision determination (description of standards can be found in Popov et al., 2016b). The samples and two reference standards are scanned successively by three infrared temperature sensors that indicate temperature distribution along with the samples and reference standards before and after heating. Thermal conductivity values are calculated by comparing the temperature excess of the samples with that of reference standards (with known thermal conductivity), in accordance with the theoretical model of the optical scanning method (Popov et al., 2016b). The thermal heterogeneity factors ( $\beta_1, \beta_2$ ) of every studied rock sample are determined from the thermal conductivity profile in order to establish the degree of rock heterogeneity caused by variations of texture, structure, porosity, and mineral composition of the rocks (Popov et al., 2003). The thermal heterogeneity factor is defined as  $\beta = (\lambda_{\text{max}} - \lambda_{\text{min}}) / \lambda_{\text{aver}}$ , where  $\lambda_{\text{max}}$ ,  $\lambda_{\text{min}}$ , and  $\lambda_{\text{aver}}$  are the maximum, minimum, and average values of the thermal conductivity component with the recorded thermal conductivity profile of the rock sample. The number of experimental data points along the thermal conductivity profiles for  $\beta$  calculation is about 40.

The advantages of TCS instruments are as follows (Popov et al., 2016b):

- the high spatial resolution of continuous profiling of thermal properties (about 1 mm);
- non-destructive contact-free approach to measurement;
- measurement of principal components of the thermal conductivity tensor;
- high quality of the thermal conductivity measurements with accuracy (A) and precision (P) not exceeding, respectively (Popov et al., 2016b):

- $\pm 2\%$  (A) and  $\pm 1.5\%$  (P) for thermal conductivity  $\lambda_{\parallel}$  parallel to a rock bedding plane,
- $\pm 3\%$  (A) and  $\pm 2.5\%$  (P) for thermal conductivity  $\lambda_{\perp}$  perpendicular to a rock bedding plane (confidence level in both cases is 0.95).

That corresponds to measurement uncertainties of  $\pm 3\%$  for thermal conductivity  $\lambda_{\parallel}$  parallel to a rock bedding plane and  $\pm 4\%$  for thermal conductivity  $\lambda_{\perp}$  perpendicular to a rock bedding plane as the uncertainty U is determined as:

$$U = (A^2 + P^2)^{1/2} \quad (2)$$

Effective thermal conductivity measurements with the TCS were carried out on every rock sample before and after thermal conductivity measurements with the DTC-300 at high temperatures in order to:

- determine principal axes of the thermal conductivity tensor by making measurements with rotation of the flat surface of the samples at different angles to the scanning line (Popov et al., 2016b);
- determine principal components of the rock thermal conductivity tensor;
- analyze thermal heterogeneity and variations of the thermal anisotropy coefficient along with the core samples, from which the rock samples (core plugs) are taken for measurements with the DTC-300; this enables us to select a homogeneous zone with representative thermal anisotropy, from which to take a small cylindrical specimen (50 mm in diameter and 20 mm in height) for subsequent measurements with the DTC-300 (Popov et al., 2014) taking account of the local (point) location of temperature sensors in the metal layers of the DTC-300;
- enable metrological control of thermal conductivity measurements, since the optical scanning method provides contact-free thermal conductivity measurements with significantly better accuracy and precision for heterogeneous shale samples, which may be damaged by mechanical treatment, so that is it not possible to properly polish and obtain parallelism of flat surfaces of the rock sample, as would be required in order to achieve accurate measurements using the divided-bar technique;
- compare the above-mentioned thermal properties before and after measurements with the DTC-300 instrument at high temperatures.

Continuous profiling of full-diameter core samples from the studied depth intervals was carried out with the TCS before the measurements using the DTC-300 instrument. Full-diameter

core samples with a small thermal heterogeneity factor were then selected from the thermal conductivity profile along the well. The cylindrical samples sized 50×20 mm for measurements at high temperatures with the DTC-300 were drilled from the least heterogeneous zones of the full-diameter core samples. We thus select core samples with representative thermal properties for measurements of effective thermal conductivity at high temperatures, according to the research objectives, and avoid significant variations of thermal properties along the core sample (Popov et al., 2014) that could cause uncertainty in the DTC-300 measurement results. In order to control for any changes in the rock samples within the temperature range studied, all of the cylindrical rock samples were scanned by the TCS to obtain effective thermal conductivity in two mutually perpendicular directions – parallel and perpendicular to bedding – for the determination of the thermal anisotropy coefficient before and after high-temperature measurements by the DTC-300.

Correction for change in the structure of the rock samples during heating (due to the appearance of cracks) was carried out using thermal conductivity data obtained with the TCS after heating. Considering that thermal conductivity changes are related to the appearance of cracks after heating the difference between thermal conductivity before and after heating obtained with TCS was included as correction for results (obtained with DTC-300). Correction of experimental data at high temperatures using the TCS data consisted of the following steps:

1. Thermal conductivity measurements at room temperature with TCS before heating.
2. Thermal conductivity measurements at temperature range 30-300 °C with DTC-300.
3. Correction the dependence obtained at step 2 using the value of thermal conductivity obtained at step 1.
4. Thermal conductivity measurements at room temperature with TCS after heating up to 300 °C.
5. Calculation the proportional relative decrease in thermal conductivity values (obtained with TCS) within temperature interval between atmospheric temperature and 300 °C using results of steps 1 and 4.
6. Gradual correction (from 0% at room temperature up to the value obtained in step 5 at 300 °C) of the data obtained at step 3. The percent of thermal conductivity decreasing after heating was equally spread at all temperature intervals.

Changing in rock samples structure during heating is supposed to be a gradual process and the percentage of correction of thermal conductivity monotonically increases with temperature.

### 3.1.3 Modification of DTC-300 results

#### 3.1.3.1 Accounting for rocks flatness deviation

The difference in the rock sample thickness, caused by non-parallelism of the two flat surfaces of the core plug, leads to uncertainty in the thermal conductivity measurements obtained using the DTC-300 instrument. *Figure 3* shows experimental data, which demonstrate how a difference  $\Delta h$  in the rock sample thickness produces a difference  $\delta\lambda$  between effective thermal conductivity  $\lambda_{DTC-300}$  obtained with the DTC-300 at room temperature and effective thermal conductivity  $\lambda_{TCS}$  measured with the TCS. Determination coefficient  $R^2 = 0.70$ , root mean square error (*RMSE*) is 5.8%. The parameter  $\delta\lambda$  was defined by the formula:

$$\delta\lambda = (\lambda_{TCS} - \lambda_{DTC-300})/\lambda_{TCS} \quad (3)$$

The difference in rock sample thickness  $\Delta h$  was measured using a dimensional height gauge and relative difference  $\delta h$  in the core plug thickness was calculated as:

$$\delta h = \Delta h/h, \quad (4)$$

where  $\Delta h$  is a maximum difference in the rock sample thickness and  $h$  is the average height of the rock samples.

The deviation  $\delta\lambda$  is caused by the uncontrolled increase of thermal resistance between rock samples and metallic layers of the DTC-300 surrounding the rock sample when parallelism of the two flat surfaces of the core plug is disturbed. Peculiarities of organic-rich rocks do not permit adequate mechanical treatment of the rock samples to remove non-parallelism of the rock sample surfaces and exclude the thermal conductivity measurement error  $\delta\lambda$  when using the DTC-300. The combined use of the TCS and DTC-300 enables the correction of the effective thermal conductivity values obtained using the DTC-300. In the actual performed experiments collection of organic-rich rocks was used with the range of  $\delta h$ : 0.5-5%.

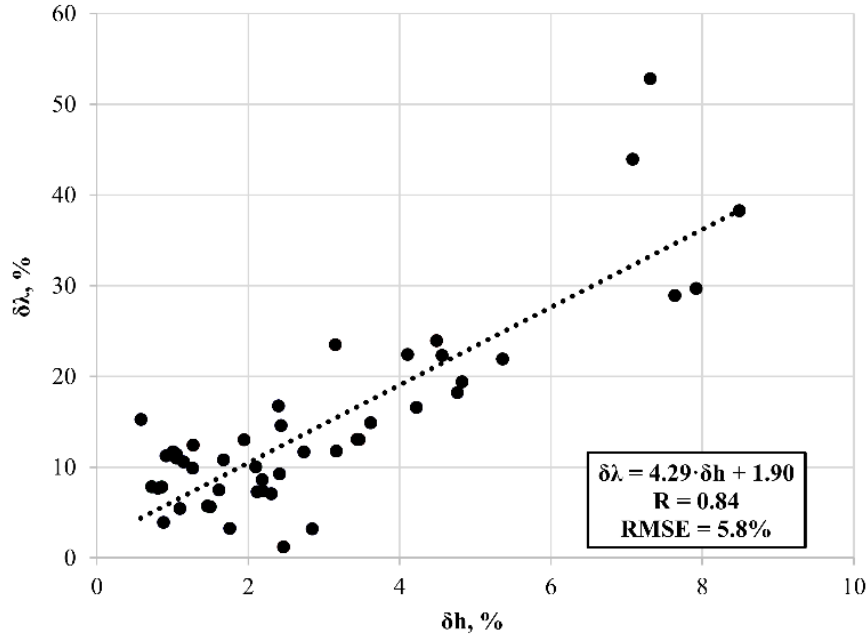


**Figure 3.** Influence of difference in rock sample flatness on the relative difference between effective thermal conductivity measured with DTC-300 and TCS instruments at room temperature.  $R$  is the correlation coefficient,  $RMSE$  is the root mean square error.

### 3.1.3.2 Variations in rock sample diameters

DTC-300 instrument allows us to measure the thermal conductivity of samples with a diameter of 50 mm at elevated temperatures. However, there is a necessity in measurements of rock samples with less diameter, as it is not always possible to drill rock samples or to make synthetic samples with a diameter of 50 mm. For checking the possibility of thermal conductivity measurements on samples with a diameter less than 50 mm a number of experiments on synthetic samples of marbles with different diameters were carried out. Marble samples with different diameters (25-50 mm) were made using a press machine (PP 25, Retsch). Results of thermal conductivity measurements on marble samples at elevated temperatures with the DTC-300 instrument are presented in *Figure 4*. The dependence of thermal conductivity of marble samples on samples diameter is shown in *Figure 5*. The results showed that the thermal conductivity of samples is decreasing with decreasing of samples diameter. To exclude dependence of thermal conductivity of samples on diameter following correction was applied:

$$\lambda_{corr} = \lambda \cdot \left(\frac{D_{50}}{D}\right)^2, \quad (5)$$

where  $\lambda_{corr}$  – correction of thermal conductivity value on diameter,  $\lambda$  – measured thermal conductivity,  $D_{50}$  – diameter of 50 mm,  $D$  – diameter of the studied sample.

Results of thermal conductivity correction using formula (5) are presented in *Figure 6*. It was observed that correction of thermal conductivity values on diameter can be used for samples with diameters 38-50 mm.

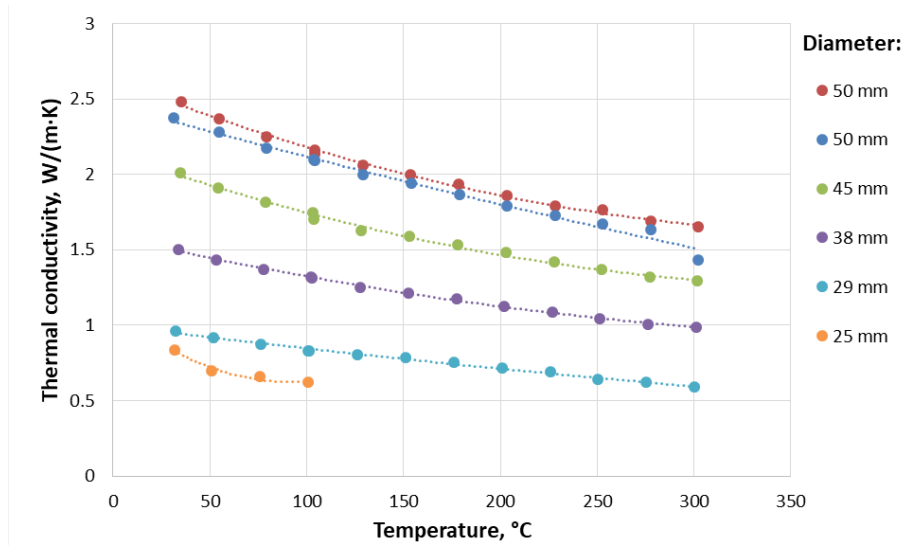


*Figure 4.* Thermal conductivity of marble samples with different diameters with the temperature.

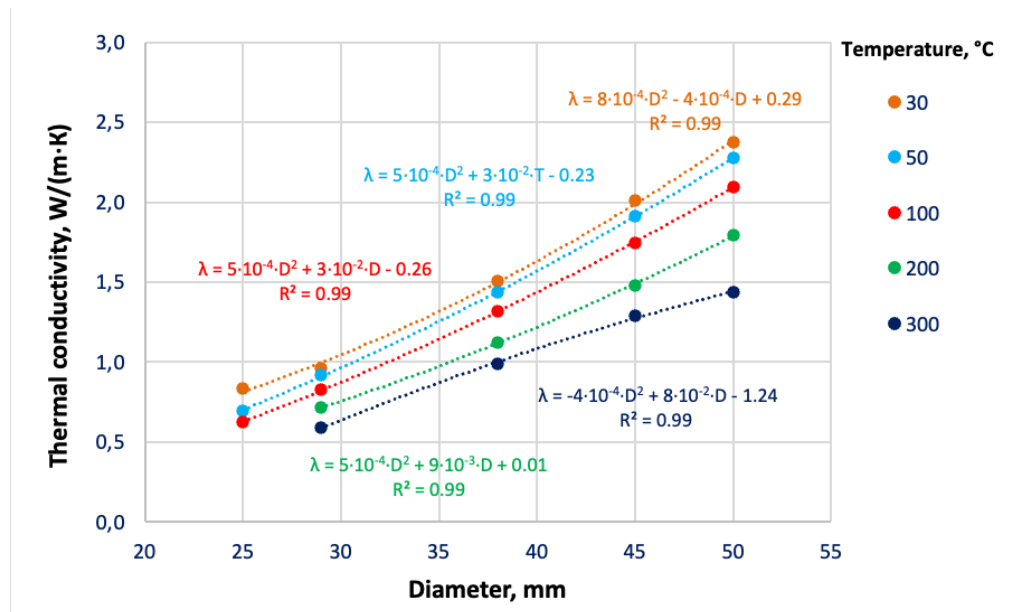


*Figure 5.* The dependence of thermal conductivity of marble samples on samples diameter.

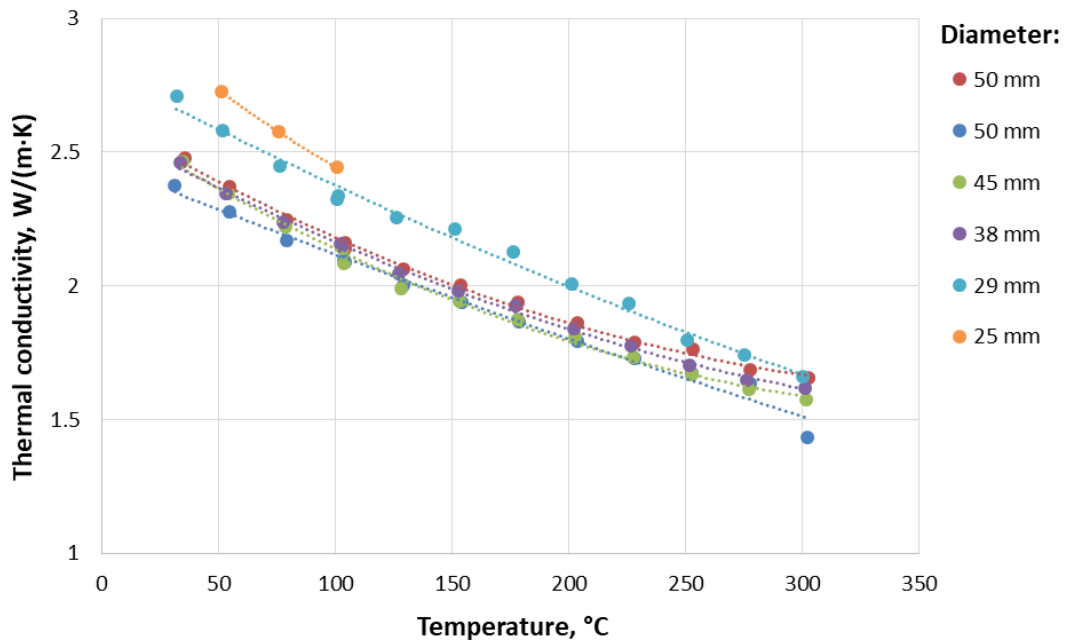


**Figure 6.** Corrected thermal conductivity values of marble samples with different diameters at elevated temperatures.

### 3.2 The technique of measurements of thermal conductivity of rock cuttings and non-consolidated rocks at elevated temperatures

#### 3.2.1 Materials and methods

Method of determining the thermal conductivity of particles of solid materials at elevated temperatures includes the following steps:

1. Thermal conductivity of the material-filler (solid-state) is measured at different temperatures in the specified temperature range. It is also possible to measure thermal diffusivity and volumetric heat capacity of the material-filler (solid-state) at different temperatures in a given temperature range and determine the dependence of thermal diffusivity and volumetric heat capacity of material-filler (solid-state) on temperature.
2. Rock cuttings are prepared with a ball mill with a certain particle size, which is controlled by the duration and frequency of the ball mill oscillation. The frequency and the duration of the ball mill oscillation are chosen based on the results of preliminary studies of the influence of these factors, as well as the properties of the rock cuttings (hardness, porosity, etc.) on the size of the particles.
3. The mixture of rock cuttings with material-filler is prepared at a specified proportion. It is also possible to use a mixture of several different materials (one of which is in a liquid

state) as a material filler. At first, rock cuttings are mixed with solid components of the material filler until a homogeneous mixture is obtained and then the liquid component of the material filler is added and the mixture is put into a homogeneous state. Removing as much air as possible from the mixture a solid sample mixture is formed.

4. The volume fractions of the following components of the solid sample mixture are determined: rock cuttings, material filler, and air.
5. The effective thermal conductivity of the solid sample mixture is measured at different temperatures in a specified temperature range. It is also possible to measure the thermal diffusivity or volumetric heat capacity of solid sample mixture at different temperatures.
6. The thermal conductivity of rock cuttings is determined at different temperatures in a specified temperature range by the ratio describing the effective thermal conductivity of a solid sample mixture of rock cuttings and material filler.

### 3.2.2 Theoretical approach

There are several theoretical procedures based on microstructure analysis and solution of the inverse homogenization problem for the determination of thermal conductivity of rock cuttings from effective thermal conductivity of the specimen. Among such methods are non-interaction approximation, Mori-Tanaka-Benveniste scheme, Maxwell scheme (Popov et al., 2018). In this work modified Lichtenecker formula was used which links the effective thermal conductivity of a solid sample mixture with the thermal conductivity of rock cuttings.

The problem of the determination of thermal conductivity of rock cuttings is an inverse problem. The objective of the inverse problem is to find the thermal conductivity of the matrix material based on given properties of the remaining constituents and measured effective properties of specimen.

The thermal diffusivity of a material can be calculated from the relation connecting thermal diffusivity, thermal conductivity, and volumetric heat capacity of materials:

$$\alpha(T) = \frac{\lambda(T)}{c(T)} \quad (6)$$

where  $C(T)$ ,  $\lambda(T)$ , and  $\alpha(T)$  are volumetric heat capacity, thermal conductivity, and the thermal diffusivity of the material at given temperature of  $T$ , respectively.

The effective volumetric heat capacity of solid sample mixture is determined from the measurement results of the effective thermal conductivity and thermal diffusivity of a solid sample mixture using the following relationship:

$$C_{mixture}(T) = \frac{\lambda_{mixture}(T)}{\alpha_{mixture}(T)} \quad (7)$$

where  $C_{mixture}(T)$ ,  $\lambda_{mixture}(T)$ , and  $\alpha_{mixture}(T)$  are effective volumetric heat capacity, effective thermal conductivity, and effective thermal diffusivity of solid sample mixture at temperature T correspondingly.

The volumetric heat capacity of rock cuttings is determined by the ratio connecting the volumetric heat capacity of rock cuttings with the effective volumetric heat capacity of the solid sample mixture, the volumetric heat capacities of material-filler and air, as well as the volume fractions of the components of the solid sample mixture:

$$C_{mixture}(T) = C_M(T) \cdot V_M + C_A(T) \cdot V_A + C_B(T) \cdot V_{AB} \quad (8)$$

where  $C_M(T)$  is the volumetric heat capacity of rock cuttings at temperature T,  $C_A(T)$  is the volumetric heat capacity of air at temperature T,  $C_B(T)$  is the volumetric heat capacity of material-filler at temperature T,  $V_M$  is the volume fraction of rock cuttings,  $V_A$  is the volume fraction of air,  $V_B$  is the volume fraction of material-filler in the solid sample mixture.

Thermal diffusivity of rock cuttings can be determined from relations (6)-(8):

$$\alpha_M(T) = \lambda_M(T) \cdot \frac{V_M}{\left( \frac{\lambda_{mixture}(T)}{\alpha_{mixture}(T)} - \lambda_A(T) \cdot \frac{V_A}{\alpha_A(T)} - \lambda_B(T) \cdot \frac{V_B}{\alpha_B(T)} \right)} \quad (9)$$

where  $\lambda_A(T)$  is the thermal conductivity of air at temperature T,  $\lambda_B(T)$  is the thermal conductivity of material-filler at temperature T,  $\alpha_A(T)$  is thermal diffusivity of air at temperature T,  $\alpha_B(T)$  is thermal diffusivity of material-filler at temperature T.

The thermal conductivity of rock cuttings can be determined in two ways. In accordance with the first method, the thermal conductivity of rock cuttings is determined by the Lichtenecker-Asaad ratio (Asaad, 1995), which links the effective thermal conductivity of a solid sample mixture with the thermal conductivity of rock cuttings, the thermal conductivity of air, the thermal conductivity of a material-filler, their volume fractions in a solid sample mixture and a parameter characterizing the structural features of the material under study:

$$\lambda_M(T) = \left( \lambda_{mixture}(T) \cdot \lambda_A(T)^{-\beta(T) \cdot V_A} \cdot \lambda_B(T)^{-\beta(T) \cdot V_B} \right)^{1/(1-\beta(T) \cdot (V_A+V_B))}, \quad (10)$$

where  $\beta(T)$  is a parameter characterizing structural features of the material under study at temperature T. The parameter  $\beta(T)$  is chosen on the basis of prior information about the material under study. If there is no prior information the parameter  $\beta(T)$  is assumed to be 1.

In accordance with the second way of the method for determining the thermal conductivity of rock cuttings, the value of thermal conductivity of rock cuttings is calculated by solving an equation based on the modified Lichtenecker formula (Edvabnik, 2015):

$$\lambda_{mixture}(T) - \left( V_M \cdot \lambda_M(T) + V_A \cdot \lambda_A(T) + V_B \cdot \lambda_B(T) \right)^{\beta(T)} \left( \frac{V_M}{\lambda_M(T)} + \frac{V_A}{\lambda_A(T)} + \frac{V_B}{\lambda_B(T)} \right)^{\beta(T)-1} = 0, \quad (11)$$

where parameter  $\beta(T)$  is chosen on the basis of prior information about the material under study. If there is no prior information, the parameter  $\beta(T)$  is calculated using the empirical formula depending on the measured parameters of the solid sample mixture.

A material filler consisting of a solid and a liquid phase is prepared by mixing solid and liquid phases in a mass ratio of 2:1. After that air bubbles are removed from the material filler by vacuuming and the material filler is placed for 12 hours in the oven at 70 °C until complete crystallization. Crystallization of material filler occurs due to the chemical reaction of material filler components during which crystalline hydrates are formed. After removal from the furnace, the material-filler is weighed and a sample of a cylindrical shape with required dimensions determined by the requirements of the measuring equipment is made of material-filler. Using the DTC-300 instrument (TA Instruments) the effective thermal conductivity of a sample of material-filler is measured at different temperatures in a specified temperature range, limited by the temperature at which the structure of the material filler is destroyed. According to the measurement results, the dependence of the thermal conductivity of the material-filler on the temperature in a temperature range is determined. Particles of solid material are ground with a ball mill (MM 400, Retsch) for 2 minutes at an oscillation frequency of 25 Hz. Then, 20 g of ground particles of unconsolidated material are mixed with 9 g of the solid phase of the initial material-filler using a ball mill for 2 minutes at a frequency of 15 Hz. The mixture is weighed and put into a shape with an internal diameter of 40 mm and mixed with 5 g of the liquid phase of the material-filler to homogeneous condition. Then, air bubbles are removed from the mixture using a vacuum, and the mixture is weighed again. Next, the mixture is put for 12 hours in an oven at 70 °C until complete crystallization. After removal from the furnace, the mixture is weighed and a cylindrical sample of the required size is made from it. The solid sample mixture, consisting of a mixture of ground particles of solid material, material-filler, and air, is weighed, its thickness and diameter are measured as well as the porosity to determine the volume fractions of the components of the solid sample mixture. Using the DTC-300 instrument, the effective thermal conductivity of a solid sample mixture is measured at different temperatures in a specified temperature range. After that according to the dependencies of thermal conductivity of material-filler and air on the temperature in a specified temperature range, the thermal conductivity of the solid material particles is determined for the specified temperature values by relations (10) or (11), describing the effective thermal conductivity of the mixture of ground solid particles, material-filler, and air.

Using a sample made of CEREOX wax (BM-0002-1 FLUXANA) molten under vacuum for maximizing air removal and cooled to a solid wax state at room temperature, the effective thermal conductivity of solid wax is measured using a DTC-300 instrument (TA Instruments) at

different temperatures in a specified temperature range, which is limited by the melting point of wax - 140 °C. Then, the dependence of the thermal conductivity of solid wax on the temperature is determined in a specified temperature range. Particles of solid material are ground using a ball mill (MM 400, Retsch) for 2 minutes at an oscillation frequency of 25 Hz. Then 20 g of ground particles of solid material is mixed with 4 g of the initial powdered wax using the same ball mill for 2 minutes at a frequency of 15 Hz. The prepared mixture is put into a press cell with an internal diameter of 40 mm of a press machine (PP 25, Retsch) and heated to 105 °C in an oven, after which it is pressed at a pressure of 1800 bar for 5 minutes. After removing from the press machine a solid sample mixture consisting of a mixture of ground particles of solid material, wax, and air, is weighed, its thickness and diameter are measured, and the porosity of the solid sample mixture is measured to determine the volume fraction of its components. Using the instrument DTC-300 (TA Instruments) the effective thermal conductivity of a solid sample mixture at different temperatures in a specified temperature range is measured. After that according to the dependences of thermal conductivity of air and wax on the temperature in a specified temperature range the thermal conductivity of the solid material particles is determined for the specified temperature values by the relations (10) or (11) describing the effective thermal conductivity of the mixture of ground solid particles with wax and air.

### **3.3 Enhancement of experimental basis for CLTE measurements at elevated temperatures on core samples**

#### **3.3.1 Experimental basis of CLTE measurements**

The CLTE measurements at elevated temperatures were performed with a quartz dilatometer (*Figure 7a*) specially adapted for the measurements on standard core plugs (cylinders 30×30 mm) within a temperature range of 25-300 °C (Popov et al., 2012). The basic requirements of the ASTM standard (ASTM D4535-85, 2000) were accounted for during CLTE measurements.

Quartz dilatometers are widely used for both laboratory and industrial studies of CLTE that is related to the following reasons (Yanchenko, 2009):

- dilatometers design is simple enough for construction;
- studied rock samples do not require complicated special treatment as the main requirement for the tested samples is the presence of two plane-parallel surfaces;
- the dilatometers provide sufficient elongation sensitivity for the satisfactory quality of the CLTE measurements.

The instrument used in our experiments has been developed specially for the CLTE measurements on rock samples (Popov et al., 2012) and allows us to measure CLTE on standard core plugs (30×30 mm) or cubes (30×30×30 mm). It allows us to measure differential CLTE within every temperature interval of 20 °C on core plugs with different bedding orientations and obtain CLTE anisotropy on the same core plug. The technical characteristics of the dilatometer are as follows:

- temperature range is 20...300 °C;
- accuracy of the elongation measurement is 0.05÷0.1 µm;
- accuracy of the temperature measurement is 0.1 °C;
- range of the heating rate is 0.1÷3.0 °C/min;
- the precision of the CLTE measurements is not more than 4%;
- uncertainty of the CLTE measurements is not more than  $1.8 \cdot 10^{-7} \text{ K}^{-1}$  (all at the confidence level 0.95).

Average CLTE is calculated from the following formula:

$$\alpha = \Delta l_0 / (l_0 \cdot (T_f - T_i)) + \alpha_{q.s.}, \quad (12)$$

$\alpha$  – CLTE of the sample in the temperature range  $T_i - T_f$ ,  $\Delta l_0$  – samples elongation, defined by the instrument with initial and final values difference,  $l_0$  – initial the length of the sample at the temperature  $T_i$ ,  $\alpha_{q.s.}$  – correction for expansion of dilatometer the quartz system at the temperature range  $T_i - T_f$ ,  $T_i$  – initial temperature,  $T_f$  – final heating temperature. The initial temperature is related to surrounding air temperature providing samples holding at room temperature for a time that is enough for samples thermodynamical equilibrium with the atmosphere inside the furnace.

Considering that transmitting elements of dilatometer (tube and push bar) can be made of different quartz glass with unknown CLTE values and temperatures of push bar and tube are different, it is necessary to correct expansion of dilatometer quartz system. Such correction is made with a standard sample of quartz glass with a calibration certificate. CLTE of quartz glass is calculated with the following formula:

$$\alpha_q = \Delta l_q / (l_0 \cdot (T_f - T_i)) + \alpha_{q.s.} \quad (13)$$

where the correction for expansion of dilatometer the quartz system is given by

$$\alpha_{q.s.} = \alpha_q - \Delta l_q / (l_0 \cdot (T_f - T_i)), \quad (14)$$

Here  $\alpha_q$  – average CLTE value of quartz glass standard sample in particular temperature range according to certificate,  $\Delta l_q$  – elongation of quartz glass standard sample with dilatometer quartz system, defined by the instrument for length calibration (Micron-02). Calculations are checked considering elongation measured by instrument Micron-02. Quartz glass standard sample is

measured a minimum of three times in a particular temperature range and average  $\Delta l_q$  is applied for calculation  $\alpha_{q.s.}$  by formula (14), which is used in basic formula (12).

Metrological studies of quartz dilatometer were provided with recommendations mentioned in (Miklashevsky, 2007).

For the CLTE measurements, cylindrical core plugs with a diameter and height of  $30 \pm 1$  mm were drilled from full-size core samples perpendicularly to the full-size core axis (i.e., parallel to bedding). Core plug dimensions were controlled by triple measurements of diameter and height with a slide-gauge. The preparation procedure included quality control when the core plugs having damages and cracks were excluded from the following measurements. Surfaces of studied core plugs were cleaned from dust particles, surfaces of dense samples, and standard samples were cleaned with ethanol. For the CLTE measurements on core plugs in radial direction polishing of side, the surface was performed in contact points with a sample holder of the dilatometer. A sampling of small pieces of core plugs was done and TOC measurements with the pyrolysis method (*Figure 7c*) for each small core piece were performed before the CLTE measurements.

Measurement workflow on the core plugs included the following step-by-step operations:

1. Density measurements with the gas volumetric method.
2. The measurements of thermal conductivity, thermal heterogeneity, and anisotropy on both flat surfaces of every core plug with the laser optical scanning instrument at seven different directions of the optical scanning (including directions parallel and perpendicular to bedding) (Popov et al., 2016b). Firstly, CLTE of 6 core plugs were measured in different directions (through every  $30^\circ$ ) in the temperature range 25-50 °C for detection of the direction of CLTE main axes. Each core plug was placed in two mutually perpendicular directions and was measured in axial direction and seven different points in the radial direction with sample rotation by every  $30^\circ$ . For these measurements, special preparation of a core plug was provided with a smoothing surface in measurement points. The temperature regime that was used during measurements is heating from room temperature (25 °C) to 50 °C. Room temperature was held for 60 minutes, 50 °C was kept for 90 minutes for the thermodynamical equilibrium of core plug and atmosphere inside the furnace.
3. The measurements of the mass of every core plug before the CLTE measurements.
4. Measurements of CLTE values on six core plugs at seven different directions (including directions parallel and perpendicular to bedding) at temperature range 25-50 °C.
5. Measurements of CLTE within a temperature range of 25-300 °C in the direction parallel and perpendicular to the bedding plane.

6. The measurements of the mass of every core plug after the CLTE measurements and cooling the core plugs up to room temperature.

### **3.3.2 Integration of dilatometer and Thermal Conductivity Scanner**

#### **3.3.2.1 Influence of rock anisotropy**

For studying CLTE anisotropy of shales a measurement methodology was developed that consists of two stages. At the first stage, the CLTE measurements were carried out for the heating temperature range of 25-50 °C on the core plugs with different bedding orientations relative to the dilatometer axis for anisotropy estimation (detection of main axis direction and values of principal components). Such a heating temperature range of 25-50 °C for the CLTE anisotropy study is chosen to avoid irreversible changes of structure and properties of studied shale samples. At the second step, the CLTE measurements were carried out within a wide temperature range of 25-300 °C when the bedding orientation of the core plug corresponded to the principal axes of the CLTE established in the first stage.

The high-precision measurements of the thermal conductivity of shale samples under study were performed within the CLTE investigation. The principal thermal conductivity tensor components were determined for every core plug and additional measurements were performed with several optical scanning lines inclined to the rock bedding plane with different angles to determine principal axes of the rock thermal conductivity. The complemented thermal conductivity measurements were performed for every core plug twice - before and after the CLTE measurements. The goals of the thermal conductivity measurements were as follows:

- to fix changes in the shale sample properties happened during the CLTE measurements when the shale samples were heated up to 300 °C;
- to determine principal axes of the rock thermal conductivity to compare the principal thermal conductivity axes directions with the principal CLTE axes directions.



**Figure 7.** Main (a) and auxiliary equipment (b, c) used in the study; a - Quartz dilatometer with an installed core sample, b - Thermal Conductivity Scanner, c - HAWK pyrolysis instrument.

The laser thermal conductivity scanner was used for the thermal conductivity measurements and thermal anisotropy investigation including detection of principal axes of the studied core plug thermal conductivity (*Figure 7b*) (Popov et al., 2016b). The instrument provides determination of the following rock characteristics:

- thermal conductivity components parallel ( $\lambda_{||}$ ) and perpendicular to bedding plane ( $\lambda_{\perp}$ );
- coefficient of thermal conductivity anisotropy  $K = \lambda_{||} / \lambda_{\perp}$ ;
- thermal heterogeneity factor calculated separately for scanning parallel ( $\beta_1$ ) and perpendicular to bedding plane ( $\beta_2$ );  $\beta = (\lambda_{\max} - \lambda_{\min}) / \lambda_{\text{average}}$ , where  $\lambda_{\max}$ ,  $\lambda_{\min}$ ,  $\lambda_{\text{average}}$  – maximum, minimum and average values of thermal conductivity along every scanning line.

The laser thermal conductivity scanner (TCS) allows us to measure thermal conductivity on standard core plugs prepared for the CLTE measurements and on full-size core samples as well. It gives the possibility for comprehensive studying correlations CLTE vs thermal conductivity excluding the influence of essential heterogeneity of shales if the correlation studying is performed with CLTE and thermal conductivity measurements on different core plugs. The laser thermal

conductivity scanner was used for the same shale collection in combination with the quartz dilatometer for the following objectives:

- control of thermal anisotropy and heterogeneity of shales from the measurements on full-size core samples and core plugs as well;
- selection of a representative collection of full-size core samples along a well under study for the following CLTE investigations;
- selection of representative areas with the full-size core samples selected for the following core plug drilling accounting for heterogeneity and variations in thermal conductivity anisotropy coefficient within the full-size core samples selected;
- detection of the direction of thermal conductivity main axes;
- investigation of the correlation thermal conductivity vs CLTE.

### **3.4 The technique of measurements of volumetric heat capacity of rocks at elevated temperatures**

#### **3.4.1 Measurements of specific heat capacity at elevated temperatures**

A differential scanning calorimeter DSC 214 Polyma (NETZSCH) was used to measure the specific heat of the rocks. Technical characteristics and image of the calorimeter are given in *Table 5* and *Figure 8*.

The measurement results were processed using the Proteus 7.0 software. NETZSCH - Concavus aluminum crucibles were used for measurements. To calibrate the heat flux, a synthetic sapphire weighing 25.02 mg was used. Calibration was carried out every day before the start of measurements.

The measurement program in various temperature ranges consists of three stages:

1. Isothermal segment at 35 °C - 10 min;
2. Dynamic segment 35 - 310 °C, heating rate - 10 °C / min;
3. Isothermal segment at 310 °C - 10 min.

High purity nitrogen (99.999%) was used as a purge and shielding gas. The volumetric flow rates of the purge and shielding gases were 40 and 60 ml/min, respectively. The mass of the samples was determined with an accuracy of  $\pm 0.01$  mg. Measurements and calculations of specific heat were carried out in accordance with the requirements of ASTM E1269-11 (ASTM E1269-11, 2018).



**Figure 8.** Differential scanning calorimeter NETZSCH - DSC 214 Polyma.

**Table 5.** Main technical characteristics of the calorimeter DSC NETZSCH 214 Polyma.

<b>Description of characteristics</b>	<b>Value</b>
Temperature reading range T, °C	-170-600
Temperature measurement range, °C	30-600
Specific heat measurement range, kJ/kg	10-1000
Specific heat capacity measurement range, J/(kg·K)	200-2000
Limits of permissible uncertainty of temperature measurements, °C	±0.8
Limits of permissible relative error of specific heat measurements, %	±3.0
Limits of permissible relative error of specific heat capacity measurements, %	±2.5
Temperature change rate, °C/min	0.001-500
Supply voltage, V	230
Supply voltage frequency, Hz	50
Power consumption, κV·A,	1.0
<b>Operating conditions</b>	
Ambient temperature range, °C	15-35
Atmospheric pressure range, κPa	84-106.7
Relative humidity range, %	5-80

### **3.4.2 Integration of differential scanning calorimeter and dilatometer for measuring volumetric heat capacity at elevated temperatures**

For volumetric heat capacity, determination new methodology was applied as only analytical solutions are applied for the calculation of this parameter (*Chapter 1.1*). Experimental data for shale formations are presented only for specific heat capacity (*Chapter 1.1*). The methodology is based on a combination of measurements on differential scanning calorimeter, dilatometer, and hydrostatic weighing method. It includes the following steps:

1. Specific heat capacity of rock sample  $C_p(T)$  within temperature is measured with differential scanning calorimeter.

2. The coefficient of linear thermal expansion on rock sample sized 30×30 mm  $\alpha(T)$  within temperature is measured with dilatometer DKT-40 (*Chapter 3.3.1*).
3. The density of rock sample at room temperature  $\rho_0$  is measured by hydrostatic weighing method (GOST 25281-82, 1982).
4. The dependence of density of rock sample on temperature is determined using the following formula (Zhdanov, 1984):

$$\rho(T) = \frac{\rho_0}{(1+\beta \cdot (T-25))} \quad (15)$$

$\rho_0$  – density of rock sample at room temperature  $T = 25^\circ\text{C}$ ,  $\beta = 3\alpha$ ,  $\alpha$  – coefficient of linear thermal expansion of rock sample.

5. Volumetric heat capacity of rock sample within temperature is determined by the following formula:

$$C(T) = C_p(T) \cdot \rho(T), \quad (16)$$

where  $C_p(T)$  – specific heat capacity of a rock sample,  $\rho(T)$  – density of rock sample within the temperature.

For volumetric heat capacity of rock sample determination the following formula can be applied:

$$C(T) = C^M(T) \cdot (1-x) + c_a(T) \cdot \rho_a(T) \cdot x, \quad (17)$$

$C^M(T)$  – volumetric heat capacity of the matrix,  $x$  – air fraction in the sample,  $c_a$ ,  $\rho_a$  – specific heat capacity and density of air.

From formula (17) volumetric heat capacity of the matrix can be determined:

$$C^M(T) = \frac{(C_p^m(T) \cdot \rho_0 - c_a(T) \cdot \rho_a(T) \cdot x)}{(1-x)} \quad (18)$$

where  $c^m$ ,  $\rho_0$  – measured heat capacity and density of a sample at room temperature.

## Chapter 4. Experimental results

### 4.1 Unconventional reservoir rocks under study

The collections of organic-rich sedimentary rock samples, which were studied, are from unconventional reservoirs in Russia's West-Siberian and Volga-Ural oil and gas basins. The number of unconventional reservoir rocks for studying effective thermal conductivity, coefficient of linear thermal expansion (CLTE), and volumetric heat capacity (VHC) at elevated temperatures are shown in *Table 6*. The organic-rich samples were selected after continuous non-destructive contact-free profiling of all core samples recovered during the drilling of the respective wells. The profiling was carried out using TCS (Popov et al., 2016b) in bench conditions on all full-diameter cores from wells for the formations to be studied (Popov et al., 2017; Chekhonin et al., 2018). Thermal core logging provided a thermal conductivity profile along every core sample. A thermal conductivity tensor component was defined along the bedding plane with a spatial resolution of 1 mm (Popov et al., 2017; Chekhonin et al., 2018). Additional profiling for a perpendicular direction on every core sample (along one or several lines on the core sample surface) enabled the definition of thermal conductivity tensor components for a direction perpendicular to the bedding plane (Popov et al., 2016b; Popov et al., 2017). The thermal anisotropy coefficient was then determined as a ratio of the parallel and perpendicular components of thermal conductivity. The most representative core samples for every formation were selected based on statistical processing of the thermal core logging data and geological description of all the core samples (accounting for data on multiscale rock thermal heterogeneity and anisotropy obtained from the thermal core logging).

**Table 6.** Number of unconventional reservoir rocks for studying thermal conductivity, CLTE, and VHC at elevated temperatures.

Formation	Thermal conductivity	CLTE	VHC
Bazhenov	19	31	27
Abalak	9	6	4
Golchih	4	7	-
Domanic	7	-	-
Total	39	44	31

## 4.2 Thermal conductivity at elevated temperatures

### 4.2.1 Rock collection for studying thermal conductivity at elevated temperatures

Rock collection for studying thermal conductivity at elevated temperatures includes 5 oil fields of West-Siberian and Volga-Ural oil and gas basins.

#### Oil field 1

The collection of 6 West-Siberian rock samples (50×20 mm) of Oil field 1 are from Bazhenov and Abalak formations and were all drilled along a single well (see *Table 7*). The Bazhenov formation (3 samples) is composed of organic-rich clayey-siliceous and carbonaceous siliceous-clayey rocks with total organic carbon (TOC) of 3-15%. The Abalak formation (3 samples) is composed of silty argillites with TOC of about 1-3%.

**Table 7.** The collection of studied rocks from Oil field 1.

№ of sample	Formation	Lithology
3BF	Bazhenov	Clayey-siliceous with lentils siltstone
4 BF	Bazhenov	Clayey-siliceous
5 BF	Bazhenov	Clayey-siliceous
1AB	Abalak	Silty argillite
2 AB	Abalak	Silty argillite
5 AB	Abalak	Silty argillite

#### Oil field 2

The collection of 8 West-Siberian rock samples (50×20 mm) of Oil field 2 are from Golchih and Abalak formations and were all drilled along a single well. The Golchih and Abalak formations are composed of bituminous argillites with TOC of 2-6%.

#### Oil field 3

The collection of 5 West-Siberian rock samples (50×20 mm) of Oil field 3 are from Bazhenov formation and were drilled along and perpendicular to a single well (*Table 8*). The Bazhenov formation is composed of clayey-siliceous and carbonaceous siliceous-clayey rocks with TOC of 3-14%.

**Table 8.** The collection of studied rocks from Oil field 3.

№ of sample	Formation	Axis direction of the cylinder to be drilled	Lithology
1B	Bazhenov	perpendicular	Clayey-siliceous
2B	Bazhenov	perpendicular	Clayey-siliceous
3B	Bazhenov	perpendicular	carbonaceous siliceous-clayey
4B	Bazhenov	parallel	Clayey-siliceous
5B	Bazhenov	perpendicular	Clayey-siliceous

#### **Oil field 4**

The collection of 12 West-Siberian rock samples (50×20 mm) of Oil field 4 are from Bazhenov formation presented by bituminous argillites and were drilled along a single well. The TOC of studied rocks is 5-8%.

#### **Oil field 5**

The collection of 22 Volga-Ural rock samples (50×20 mm) are from Mendym, Domanic, Sargaev, and Timan formations, also along one well (*Table 9*). The Mendym formation (10 samples) is composed of dolomites, limestones, and clayey limestones, with TOC of 0.3-0.6%. The Domanic formation (7 samples) is composed of carbonaceous clayey limestones and siliceous limestones, with TOC of 0.5-17.8%. The Sargaev formation (4 samples) consists of interbedded limestones and clayey limestones with TOC of 0.6-0.8%. And the Timan formation (1 sample) is represented by silty sandstone.

**Table 9.** The collection of studied rocks from Oil field 5.

№ of sample	Formation	Lithology
1Md	Mendym	Dolomite
2Md	Mendym	Dolomite
3Md	Mendym	Limestone
4Md	Mendym	Clayey limestone
5Md	Mendym	Limestone with fractures
6Md	Mendym	Limestone
7Md	Mendym	Limestone
8Md	Mendym	Clayey limestone
9Md	Mendym	Limestone with fractures
10Md	Mendym	Limestone
1Dm	Domanic	Clayey limestone
2Dm	Domanic	Clayey limestone
3Dm	Domanic	Limestone
4Dm	Domanic	Calcareous argillite
5Dm	Domanic	Calcareous argillite
6Dm	Domanic	Limestone

7Dm	Domanic	Limestone
1S	Sargaev	Limestone with fractures
2S	Sargaev	Limestone with fractures
3S	Sargaev	Limestone
4S	Sargaev	Clayey limestone
1Tm	Timan	Sandstone

#### 4.2.2 Results of measurements

##### Oil field 1

The effective thermal conductivity values of 6 rock samples from the Bazhenov (BF) and Abalak (AB) formations were measured with a TCS at room temperature and then with a DTC-300 instrument in a temperature range of 30-300 °C. The results of the measurements with the TCS are shown in *Table 10*. The BF and AB rocks have high variations in both thermal conductivity components: parallel to the bedding plane ( $\lambda_{||} = 2.08-2.73 \text{ W/(m}\cdot\text{K)}$ ) and perpendicular to the bedding plane ( $\lambda_{\perp} = 1.27-2.20 \text{ W/(m}\cdot\text{K)}$ ). Wide range of values of the thermal anisotropy coefficient (up to 1.79) and thermal heterogeneity factors ( $\beta_1 = 0.08-0.56$ ,  $\beta_2 = 0.04-0.15$ ) were established. High values of the heterogeneity factor  $\beta_1$  relative to  $\beta_2$  for the Bazhenov formation are explained by the local development of organic matter along the sample with the sub-parallel layering of organic matter that has lower thermal conductivity (0.2-0.5 W/(m·K)) than that of the surrounding rock matrix (2.5-3.2 W/(m·K)). The marked contrast between the thermal conductivity of organic matter and the mineral matrix as well as the significant content of organic matter and its sub-layering distribution in samples have a major effect on thermal conductivity, heterogeneity, and thermal anisotropy of organic-rich rock samples (Popov et al., 2016a). High values of the thermal heterogeneity factor in the Bazhenov rock samples are related to high values and variations in TOC (3-15%) within the formation as well as within the rock samples.

Rock samples from Abalak formations are less heterogeneous than rocks from Bazhenov formation due to low variations of TOC (0-3%). TOC values for the rock samples were measured using a HAWK pyrolysis instrument (<http://www.wildcattertechnologies.com>). Additional reasons for the high thermal anisotropy coefficient of Bazhenov and Abalak rocks are (1) sub-oriented layers of organic matter; and (2) oriented natural microcracks in the rocks and artificial microcracks caused by changes during core recovery from the well and further mechanical treatment of the core samples.

**Table 10.** Results of thermal property measurements of rock samples from Bazhenov and Abalak formations at room temperature with a TCS before measurements at elevated temperatures.

№ sample	Rock type	$\lambda_{  }$ , W/(m·K)	$\lambda_{\perp}$ , W/(m·K)	K	$\beta_1$	$\beta_2$
Bazhenov formation						
3BF	Clayey-siliceous with lentils siltstone	2.22	2.20	1.00*	0.56	0.15
4BF	Clayey-siliceous	2.08	1.33	1.56	0.25	0.04
5BF	Clayey-siliceous	2.42	1.48	1.63	0.18	0.13
Abalak formation						
1AB	Silty argillite	2.28	1.27	1.79	0.09	0.10
2AB	Silty argillite	2.22	1.30	1.70	0.20	0.07
5AB	Silty argillite	2.73	1.55	1.77	0.08	0.09

\*All measurements of the thermal anisotropy coefficient in a range of 1.00-1.02 were approximated as 1.00 due to real uncertainty concerning measurements of the thermal conductivity components  $\lambda_{||}$  and  $\lambda_{\perp}$ .

Thermal conductivity measurements in the 30-300 °C range show curvilinear dependences of thermal conductivity on temperature along bedding ( $\lambda_{||}$ ) of rock samples from the Bazhenov and Abalak formations. *Figure 9* shows the percentage decrease of thermal conductivity of corresponding rocks at a particular temperature relative to the initial temperature  $T_0 = 30$  °C. As the temperature increases, thermal conductivity decreases and the average value of thermal conductivity (for 6 studied samples) becomes lower than its value at 30 °C by 3-5% at 100 °C and 5-14% at 300 °C. However, the thermal conductivity change with temperature for sample 3BF is unique: average thermal conductivity at 100 °C and 300 °C is respectively 6% and 25% lower than its value at 30 °C. Such a sharp decrease of thermal conductivity with temperature can be explained by the presence of quartz grains with a size of ~0.1 mm in this sample as the thermal conductivity of quartz decreases by 30% at 100 °C and 50% at 300 °C (Clauser, 2006). Scattering the data of the sample 1AB compare to the other samples does not exceed the measurement error (*Chapter 3.1.1.1*) and, probably, explained by the increased volume of clay minerals: endothermic reactions in clay minerals around 130-190 °C (Milner, 1962) may decrease measured thermal conductivity due to features of the measurement technique. The increment values within the temperature range of 240-300 °C can be seen for two samples: 1AB and 2AB. Although the effect of increment values does not exceed the measurement error essentially (*Chapter 3.1.1.1*), this fact could correspond to specific peculiarities of the AB rock samples studied.

*Figure 10* shows curves that relate the average percentage of thermal conductivity decrease (relatively to initial thermal conductivity at room temperature) to temperature for the Bazhenov

and Abalak samples in the 30-300 °C temperature range. Equations that relate thermal conductivity to temperature for each formation are shown in *Table 17*. The equation for sample 3BF is shown separately due to its unique behavior. Correction for change in the structure of the rock samples during heating (due to the appearance of cracks) was carried out using thermal conductivity data obtained with the TCS after heating. Considering that thermal conductivity changes are related to the appearance of cracks after heating the difference between thermal conductivity before and after heating obtained with TCS was included as correction for results (obtained with DTC-300) shown in *Figure 10*. Correction of experimental data at high temperatures using the TCS data was made by steps described in *Chapter 3.1.2*. The correction was applied to the curves for each formation (*Figure 10*, dashed line) by taking account of the average change in thermal conductivity ( $\lambda_{||}$ ) after heating (*Table 11*), as measured by the TCS.

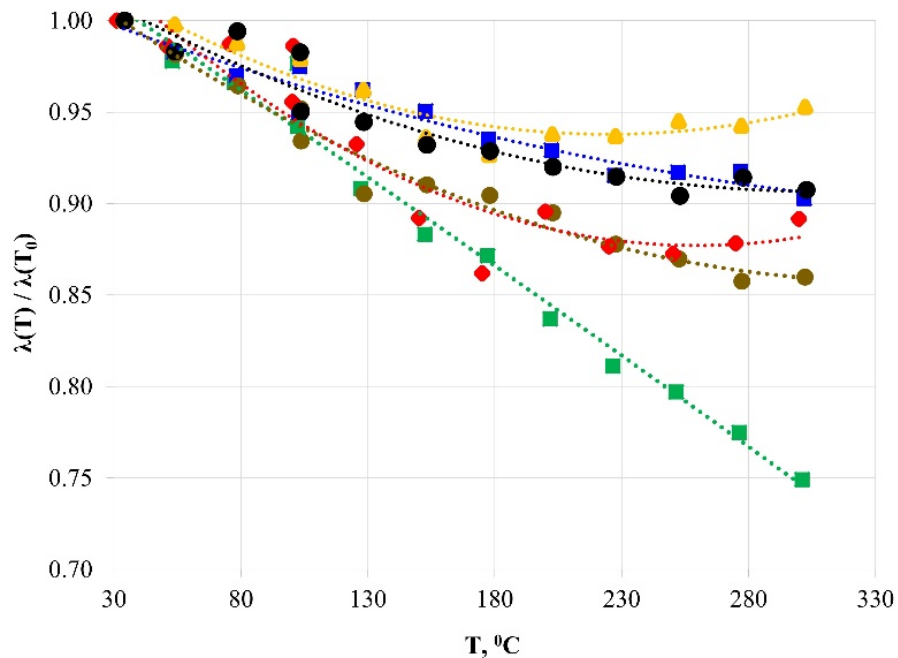


**Figure 9.** Thermal conductivity decrease for rock samples from the Bazhenov and Abalak formations in the 30-300 °C temperature range. Different colors refer to different rock samples: ♦ – 1AB, ▲ – 2AB, ● – 5AB, ■ – 3BF, ■ – 4BF, ● – 5BF. Thermal conductivity values at initial temperature  $T_0 = 30$  °C are shown in Table 11.

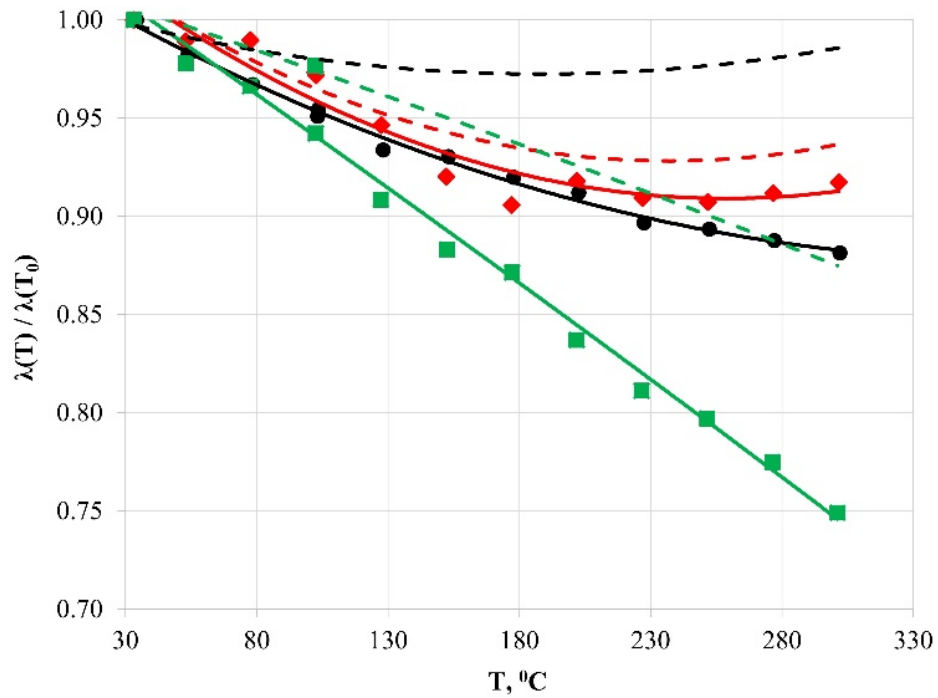


**Figure 10.** Curves drawn on a scatter diagram of average percentage of thermal conductivity decrease with temperature for rock samples from different formations:  $\blacklozenge$  – Abalak formation,  $\bullet$  – Bazhenov formation,  $\blacksquare$  – sample 3BF from the Bazhenov formation, - - correction for the Bazhenov formation, - - correction for the Abalak formation, - - correction for sample 3BF from the Bazhenov formation. Thermal conductivity values at initial temperature  $T_0 = 30\text{ }^\circ\text{C}$  are shown in Table 11.

**Table 11.** TCS measurements of thermal properties of Bazhenov and Abalak samples at room temperature after heating to  $300\text{ }^\circ\text{C}$  and subsequent cooling.

No sample	$\lambda_{  }$ after heating, W/(m·K)	$\lambda_{\perp}$ after heating, W/(m·K)	Variations in $\lambda_{  }$ after heating to $300\text{ }^\circ\text{C}$ , %	Variations in $\lambda_{\perp}$ after heating to $300\text{ }^\circ\text{C}$ , %	K after heating to $300\text{ }^\circ\text{C}$	Variations in K after heating to $300\text{ }^\circ\text{C}$ , %	$\beta_1$ after heating to $300\text{ }^\circ\text{C}$	$\beta_2$ after heating to $300\text{ }^\circ\text{C}$	Absolute difference in $\beta_1$ after heating to $300\text{ }^\circ\text{C}$	Absolute difference in $\beta_2$ after heating to $300\text{ }^\circ\text{C}$
Bazhenov formation										
3BF	1.93	1.87	-13.0	-15	1.03	2.2	0.55	0.12	0.01	0.03
4BF	1.87	1.14	-10.1	-14.3	1.64	5.2	0.19	0.11	0.06	-0.07
5BF	2.16	1.00	-10.7	-32.4	2.16	32.5	0.19	0.13	-0.01	0
Abalak formation										
1AB	2.29	1.18	0.4	-7.1	1.94	8.4	0.09	0.10	-	-
2AB	1.96	0.97	-11.7	-25.4	2.02	18.9	0.14	0.07	0.06	0
5AB	2.84	1.45	4.0	-6.5	1.96	10.7	0.08	0.06	0	0.03
Average	2.18	1.27	-6.9	-16.8	1.78	13.0	0.21	0.10	0.02	0.00

Analysis of the change in thermal conductivity of BF and AB rock samples after heating to  $300\text{ }^\circ\text{C}$  and subsequent cooling to room temperature was based on measurements using a TCS instrument (Table 11). After completion of measurements using the DTC-300, all samples were studied again with the TCS to determine thermal conductivity components for the same directions

as were gauged before the high-temperature measurements. The comparison results presented in *Tables 10-11* show that thermal conductivity parallel to bedding decreases by 7% on average and changes in thermal conductivity perpendicular to bedding ( $\lambda_{\perp}$ ) are more pronounced, averaging 17%. The thermal anisotropy coefficient increases by 13% on average after heating to 300 °C for the Bazhenov and Abalak samples. This behavior is explained by the presence of additional microcracks after heating to 300 °C. All changes are related to loss of intergranular contact and thermal resistance during heating. The absolute difference in thermal heterogeneity of the rock samples after heating showed small changes of 0.07 on average. A slight increase of thermal conductivity after measurements at elevated temperatures is observed due to the displacement of the scanning line for heterogeneous rock samples relative to scanning before the high-temperature measurements.

## Oil field 2

The thermal conductivity of 8 rock samples from the Golchih (GF) and Abalak (AB) formations from Oil field 2 was measured with a TCS at room temperature and then with a DTC-300 instrument in a temperature range of 30-300 °C. The results of the measurements with the TCS are shown in *Table 12*. The GF and AB rocks have low variations in both thermal conductivity components: parallel to the bedding plane ( $\lambda_{\parallel} = 1.39\text{-}1.49$  W/(m·K)) and perpendicular to the bedding plane ( $\lambda_{\perp} = 1.21\text{-}1.51$  W/(m·K)). A low range of values of the thermal anisotropy coefficient (up to 1.05) and thermal heterogeneity factors ( $\beta_1 = 0.08\text{-}0.17$ ,  $\beta_2 = 0.09\text{-}0.17$ ) were established.

**Table 12.** Results of thermal property measurements of rock samples from Golchih and Abalak formations at room temperature with a TCS before measurements at elevated temperatures.

No sample	$\lambda_{\parallel}$ , W/(m·K)	$\lambda_{\perp}$ , W/(m·K)	K	$\beta_1$	$\beta_2$
1G	1.39	1.36	1.02	0.16	0.17
2G	1.27	1.21	1.05	0.17	0.13
3G	1.23	1.21	1.01	0.09	0.12
4G	1.40	1.40	1.00	0.08	0.09
5A	1.41	1.39	1.02	0.15	0.10
6A	1.39	1.35	1.03	0.12	0.09
7A	1.49	1.51	1.00	0.09	0.12
8A	1.45	1.42	1.02	0.11	0.13

Thermal conductivity measurements in the 30-300 °C range show curvilinear dependences of thermal conductivity on temperature along bedding ( $\lambda_{\parallel}$ ) of rock samples from the Golchih and Abalak formations (*Figure 11*). *Figure 12* shows the relative decrease of thermal conductivity of

corresponding rocks at a particular temperature relative to the initial temperature  $T_0 = 30\text{ }^\circ\text{C}$ . As the temperature increases, thermal conductivity decreases and the average value of thermal conductivity (for 8 studied samples) becomes lower than its value at  $30\text{ }^\circ\text{C}$  by 1-5% at  $100\text{ }^\circ\text{C}$  and 5-25% at  $300\text{ }^\circ\text{C}$ .

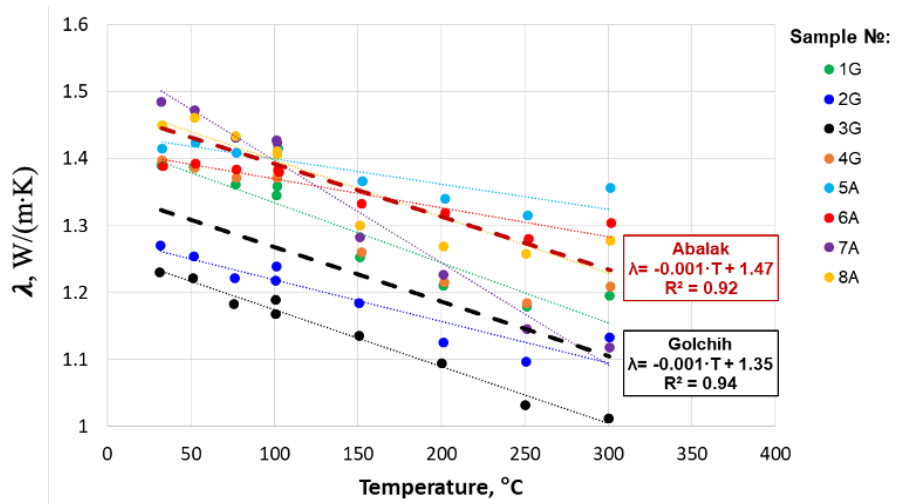


**Figure 11.** Changes in thermal conductivity for rock samples of the Golchih and Abalak formations of oil field 2 with increasing temperature. Black dotted line - curve obtained by averaging thermal conductivity overall rock samples of the Golchih formation; brown dotted line - curve obtained by averaging thermal conductivity overall rock samples of the Abalak formation.

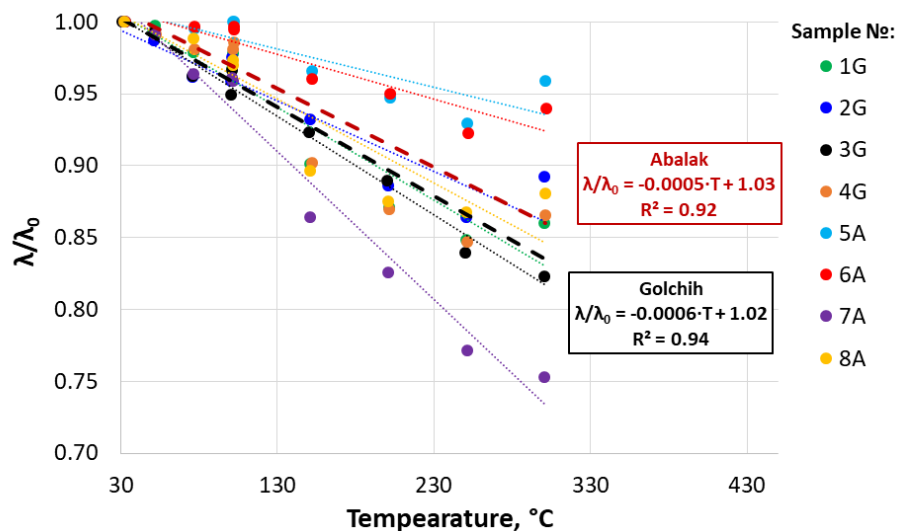


**Figure 12.** Relative change in thermal conductivity for rock samples from the Golchih and Abalak formations of oil field 2 with increasing temperature. Black dotted line - curve obtained by averaging the relative change in thermal conductivity for all rock samples of the Golchih formation; brown dotted line - curve obtained by averaging the relative change in thermal conductivity for all rock samples of the Abalak formation. Thermal conductivity values at initial temperature  $T_0 = 30\text{ }^\circ\text{C}$  are shown in Table 12.

The comparison results presented in *Tables 11-12* show that thermal conductivity parallel and perpendicular to bedding decreases by 15% on average. The thermal anisotropy coefficient increases by 2% on average after heating to 300 °C for the Gochih and Abalak samples.

**Table 13.** TCS measurements of thermal properties of Golchih and Abalak formations samples at room temperature (after heating to 300 °C and subsequent cooling).

№	$\lambda_{  }$ after heating, W/(m·K)	$\lambda_{\perp}$ after heating, W/(m·K)	Variations in $\lambda_{  }$ after heating to 300 °C, %	Variations in $\lambda_{\perp}$ after heating to 300 °C, %	K after heating to 300 °C	Variations in K after heating to 300 °C, %	$\beta_1$ after heating to 300 °C	$\beta_2$ after heating to 300 °C	Absolute difference in $\beta_1$ after heating to 300 °C	Absolute difference in $\beta_2$ after heating to 300 °C
1G	1.18	1.14	-15	-17	1.03	2	0.21	0.15	33	-11
2G	1.06	1.04	-17	-14	1.01	-3	0.23	0.16	33	20
3G	1.01	1.00	-17	-18	1.01	0	0.08	0.11	-18	-11
4G	1.24	1.19	-12	-15	1.04	4	0.14	0.09	63	6
5A	1.18	1.15	-17	-17	1.02	0	0.15	0.13	-1	29
6A	1.22	1.15	-12	-15	1.07	3	0.13	0.14	4	57
7A	1.32	1.24	-11	-18	1.07	8	0.08	0.13	-13	5
8A	1.28	1.27	-12	-11	1.00	-2	0.17	0.14	50	7

Thermal conductivity of the rock samples of the Golchih formation decreases by an average of 9% relative to the thermal conductivity at an initial temperature of 30 °C when the temperature rises to 150 °C; for the rocks of the Abalak formation, the decrease in thermal conductivity is 8%.

### Oil field 3

The thermal conductivity of 5 rock samples from the Bazhenov formation (BF) from Oil field 3 was measured with a TCS at room temperature and then with a DTC-300 instrument in a temperature range of 30-300 °C. The results of the measurements with the TCS before and after heating are shown in *Table 14*. The BF rocks have high variations in thermal conductivity perpendicular to the bedding plane ( $\lambda_{\perp}$  = 0.84-1.91 W/(m·K)).

**Table 14.** TCS measurements of thermal conductivity of Bazhenov formation samples at room temperature (after heating to 300 °C and subsequent cooling).

№ sample	$\lambda_{\perp}$ , W/(m·K)	$\lambda_{\perp}$ after heating, W/(m·K)	Variations in $\lambda_{\perp}$ after heating to 300 °C, %
1B	0.84	0.81	-4
2B	1.00	0.88	-11
3B	1.76	1.74	-1
4B	1.60	1.43	-11
5B	1.91	1.65	-13

Thermal conductivity measurements in the 30-300 °C range show curvilinear dependences of thermal conductivity on temperature perpendicular to bedding ( $\lambda_{\perp}$ ) of rock samples from the Bazhenov formations (Figure 13). Figure 14 shows the relative decrease of thermal conductivity of corresponding rocks at a particular temperature relative to the initial temperature  $T_0 = 30$  °C. As the temperature increases, thermal conductivity decreases and the average value of thermal conductivity (for 5 studied samples) becomes lower than its value at 30 °C by 0-2% at 100 °C and 5-20% at 300 °C.

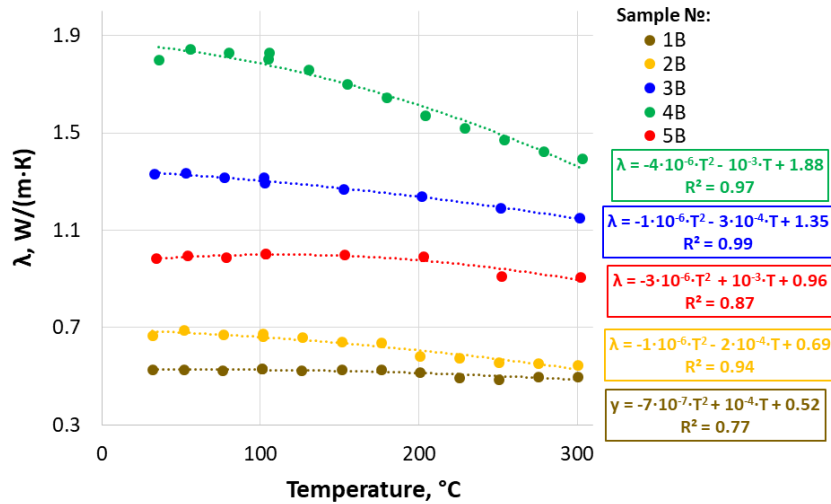


**Figure 13.** Changes in thermal conductivity for rock samples of Bazhenov formations of oil field 3 with increasing temperature.

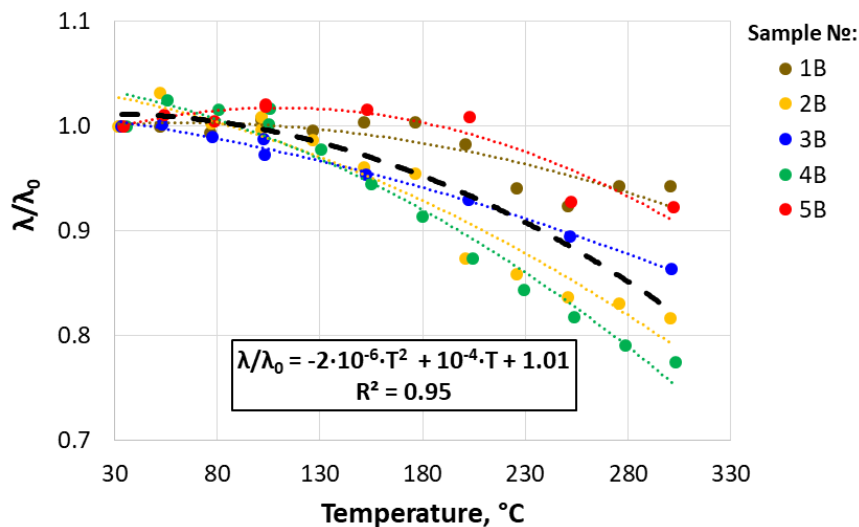


**Figure 14.** Relative change in thermal conductivity for rock samples from the Bazhenov formation of oil field 3 with increasing temperature. Black dotted line - curve obtained by averaging the relative change in thermal conductivity for all rock samples of the Bazhenov formation. Thermal conductivity values at initial temperature  $T_0 = 30$  °C are shown in Table 14.

The comparison results presented in *Table 14* show that thermal conductivity perpendicular to bedding decreases by 6% on average after heating. The thermal conductivity of the rock samples of the Bazhenov formation decreases by an average of 13% relative to the thermal conductivity at an initial temperature of 30 °C when the temperature rises to 300 °C.

#### Oil field 4

The thermal conductivity of 12 rock samples from the Bazhenov formation from Oil field 4 was measured with a DTC-300 instrument in a temperature range of 30-300 °C. Thermal conductivity measurements in the 30-300 °C range show curvilinear dependences of thermal conductivity on temperature perpendicular to bedding ( $\lambda_{\perp}$ ) of rock samples from the Bazhenov formations (*Figure 15*). *Figure 16* shows the percentage decrease of thermal conductivity of corresponding rocks at a particular temperature relative to the initial temperature  $T_0 = 30$  °C. As the temperature increases, thermal conductivity decreases and the average value of thermal conductivity (for 12 studied samples) becomes lower than its value at 30 °C by 0-5% at 100 °C and 1-6% at 300 °C.

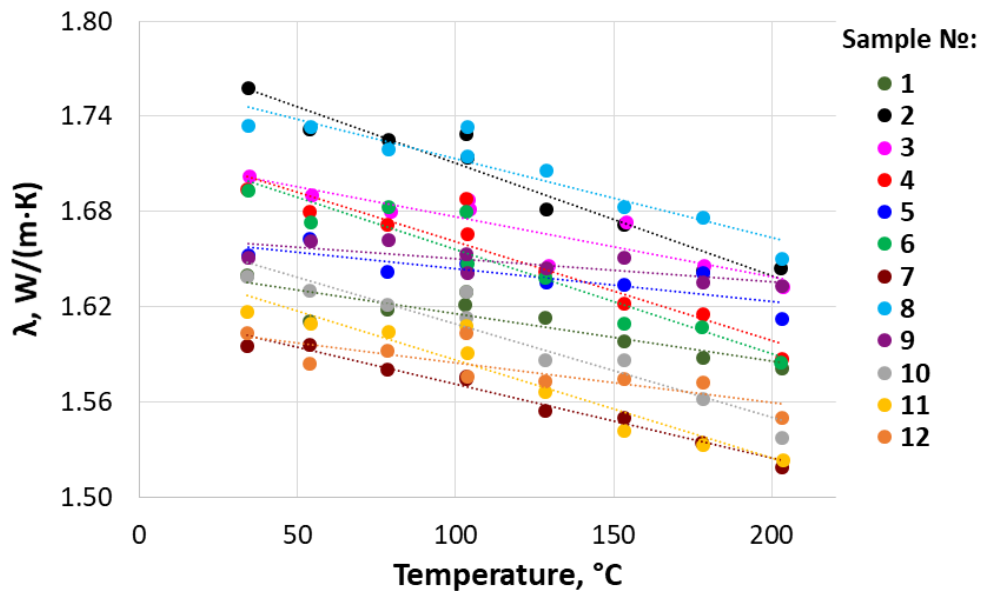


**Figure 15.** Changes in thermal conductivity for rock samples of Bazhenov formations of oil field 4 with increasing temperature.

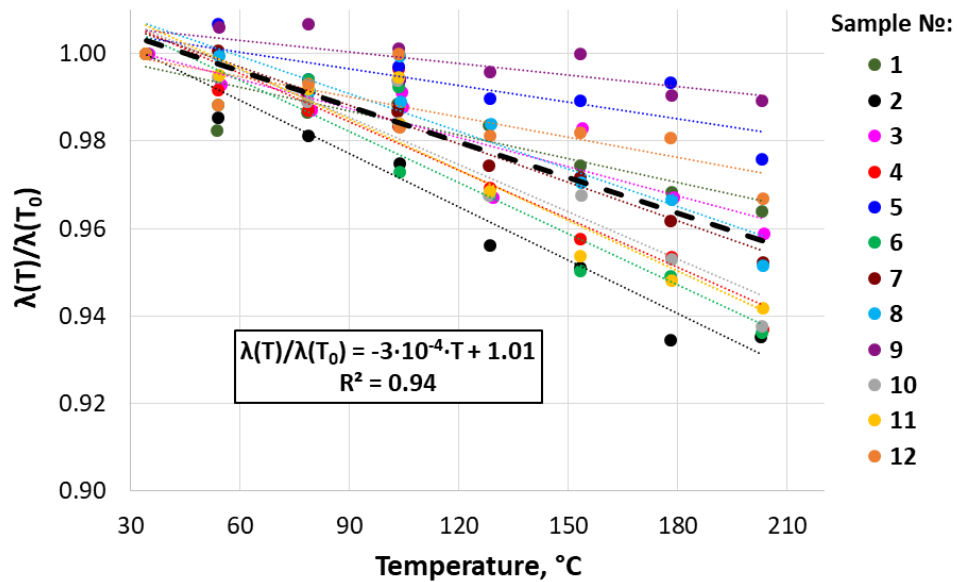


**Figure 16.** Relative change in thermal conductivity for rock samples from the Bazhenov formation of oil field 4 with increasing temperature. Black dotted line - curve obtained by averaging the relative change in thermal conductivity for all rock samples of the Bazhenov formation.

### Oil field 5

Thermal conductivity measurements on 22 rock samples from formations in Russia's Volga-Ural region were carried out using the DTC-300 instrument in a temperature range of 30-300 °C. Results of thermal property measurements with the TCS before heating of the samples (Table 15) showed significant variations of thermal conductivity of samples from the Mendym formation (2.30-3.74 W/(m·K)), which is related to the presence of dolomites (samples 1Md, 2Md). Thermal conductivity of dolomites is 1.2-1.4 times higher than that of limestones, due to the presence of rock-forming dolomite and calcite minerals with higher thermal conductivity (thermal conductivity of dolomite single crystal is 5.7-6.3 W/(m·K), the thermal conductivity of calcite single crystal is 3.35-3.50 W/(m·K)) (Popov et al., 1987). Variations of the thermal anisotropy coefficient were up to 1.20 for samples from the Mendym, Domanic, and Sargaev formations, and 1.53 for the sample from the Timan formation. Variations of the thermal heterogeneity coefficient were 0.07-0.22 for samples from the Mendym, Sargaev, and Timan formations and 0.08-0.48 for the Domanic samples. The high thermal heterogeneity coefficient of the Domanic rocks is related to essential lithological heterogeneity and significant variations of organic matter in the rock samples (from a few millimeters to tens of centimeters).

**Table 15.** TCS measurements of thermal properties of Mendym, Domanic, Sargaev, and Timan samples at room temperature before measurements at high temperatures.

№ sample	Rock type	$\lambda_{  }$ , W/(m·K)	$\lambda_{\perp}$ , W/(m·K)	K	$\beta_1$	$\beta_2$
Mendym formation						
1Md	Dolomite	3.74	3.13	1.20	0.12	0.16
2Md	Dolomite	3.40	3.16	1.07	0.11	0.09
3Md	Limestone	2.55	2.55	1.00	0.10	0.09
4Md	Clayey limestone	2.39	2.39	1.00	0.13	0.10
5Md	Limestone with fractures	2.40	2.40	1.00	0.21	0.13
6Md	Limestone	2.39	2.38	1.00	0.07	0.07
7Md	Limestone	2.45	2.43	1.00	0.11	0.14
8Md	Clayey limestone	2.37	2.20	1.08	0.09	0.09
9Md	Limestone with fractures	2.30	1.98	1.16	0.18	0.21
10Md	Limestone	2.44	2.42	1.00	0.08	0.06
Domanic formation						
1Dm	Clayey limestone	2.29	2.29	1.00	0.08	0.11
2Dm	Clayey limestone	2.39	2.39	1.00	0.15	0.10
3Dm	Limestone	2.58	2.58	1.00	0.30	0.14
4Dm	Calcareous argillite	2.69	2.28	1.18	0.16	0.48
5Dm	Calcareous argillite	2.31	2.21	1.05	0.30	0.30
6Dm	Limestone	2.42	2.36	1.03	0.13	0.12
7Dm	Limestone	2.48	2.32	1.07	0.12	0.12
Sargaev formation						
1S	Limestone with fractures	2.76	2.59	1.07	0.09	0.11
2S	Limestone with fractures	2.49	2.44	1.00	0.22	0.10
3S	Limestone	2.33	2.01	1.16	0.18	0.13
4S	Clayey limestone	2.34	2.00	1.17	0.15	0.11
Timan formation						
1Tm	Sandstone	3.40	2.23	1.53	0.15	0.15

Figures 17-20 show the relative decrease of thermal conductivity of rocks from the Mendym, Domanic, Sargaev, and Timan formations at a particular temperature relative to the initial temperature ( $T_0 = 30$  °C). The average decrease of thermal conductivity for rock samples from the Mendym formation at 100 °C and 300 °C relative to room temperature is 9% and 23% respectively; for the Domanic rock samples it is 10% and 24%; for the Sargaev samples, 8% and 20%; and 10% and 27% for the Timan sample. The lowest decrease of thermal conductivity in the 30-300 °C temperature range is observed for the Sargaev sample 4S and Mendym sample 4Md and

is related to the high clay content in these samples. *Figure 21* show curves of thermal conductivity change averaged for different lithotypes and formations in the 30-300 °C temperature range. *Figure 22* show three curves with similar average thermal conductivity behavior at 30-300 °C for the following types: clayey limestones (determination coefficient  $R^2 = 0.92$ ); limestones and argillites ( $R^2 = 0.89$ ); and dolomites and sandstone ( $R^2 = 0.97$ ). Correction for changing structure of samples during heating was applied to the curves as described above for the Abalak and Bazhenov formations (*Figure 22*, dashed lines).

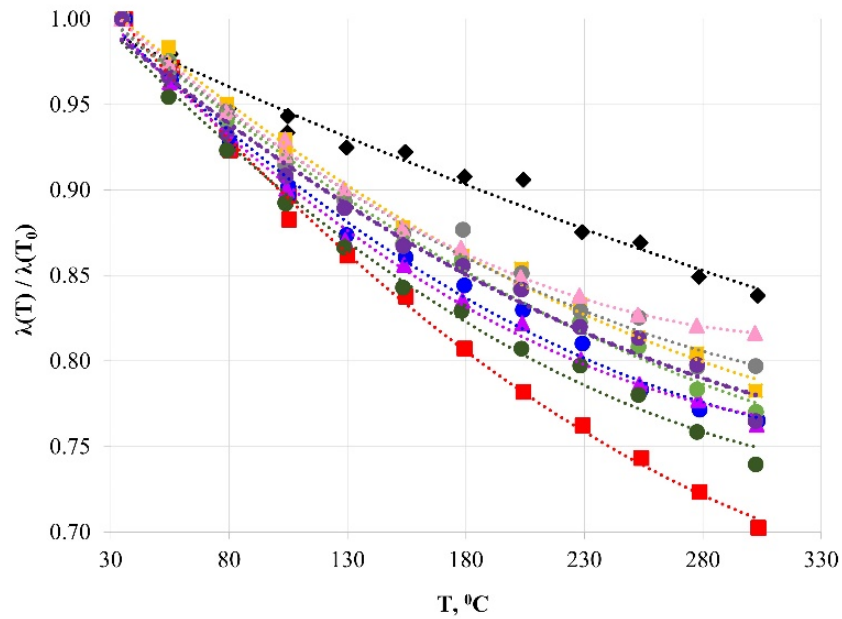


**Figure 17.** Curves drawn on the thermal conductivity-temperature scatter diagram for Mendym samples (■ – 1Md, ● – 2Md, ▲ – 3Md, ◆ – 4Md, ■ – 5Md, ● – 6Md, ● – 7Md, ● – 8Md, ▲ – 9Md, ● – 10Md) in the 30-300 °C temperature range. Thermal conductivity values at initial temperature  $T_0 = 30$  °C are shown in Table 15.

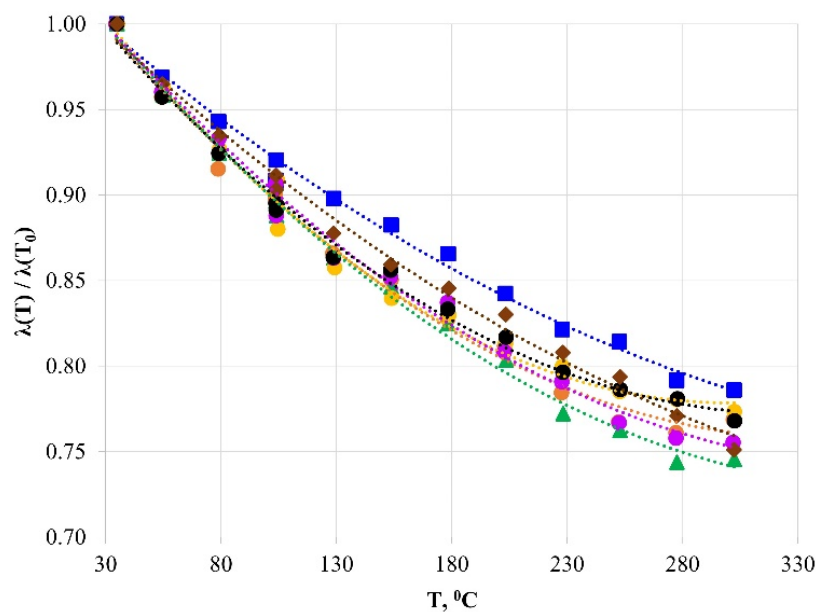


**Figure 18.** Curves lines drawn on the thermal conductivity-temperature scatter diagram for Domonic samples (■ – 1Dm, ○ – 2Dm, ▲ – 3Dm, ● – 4Dm, ◆ – 5Dm, ● – 6Dm, ◆ – 7Dm) in the 30-300 °C temperature range. Thermal conductivity values at initial temperature  $T_0 = 30$  °C are shown in Table 15.

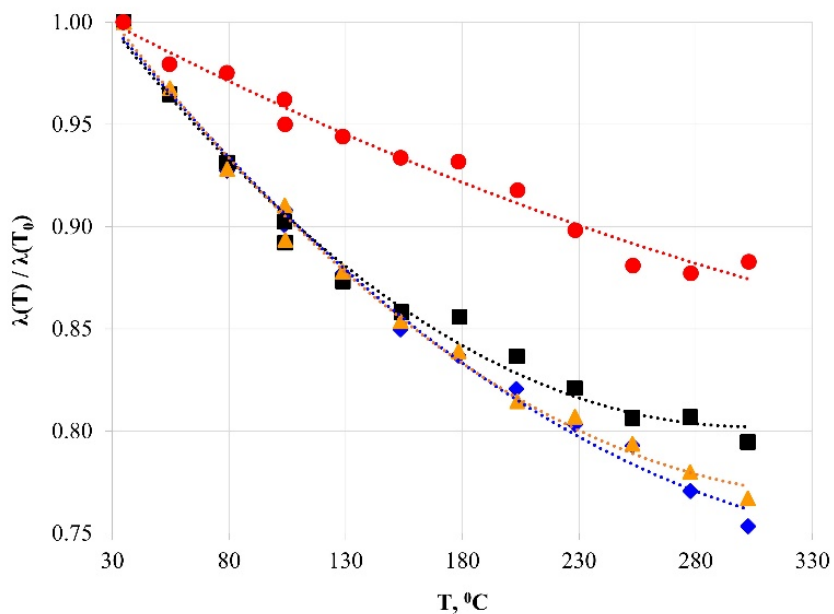


**Figure 19.** Curves lines drawn on the thermal conductivity-temperature scatter diagram for Sargaev samples (◆ – 1S, ■ – 2S, ▲ – 3S, ● – 4S) in the 30-300 °C temperature range. Thermal conductivity values at initial temperature  $T_0 = 30$  °C are shown in Table 15.

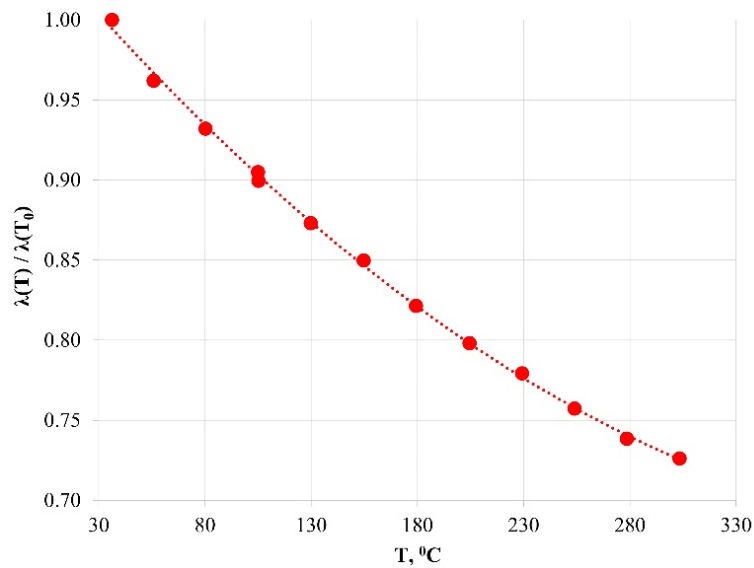


**Figure 20.** The curve drawn on the thermal conductivity-temperature scatter diagram for the Timan sample (Tm) in the 30-300 °C temperature range. Thermal conductivity values at initial temperature  $T_0 = 30$  °C are shown in Table 15.

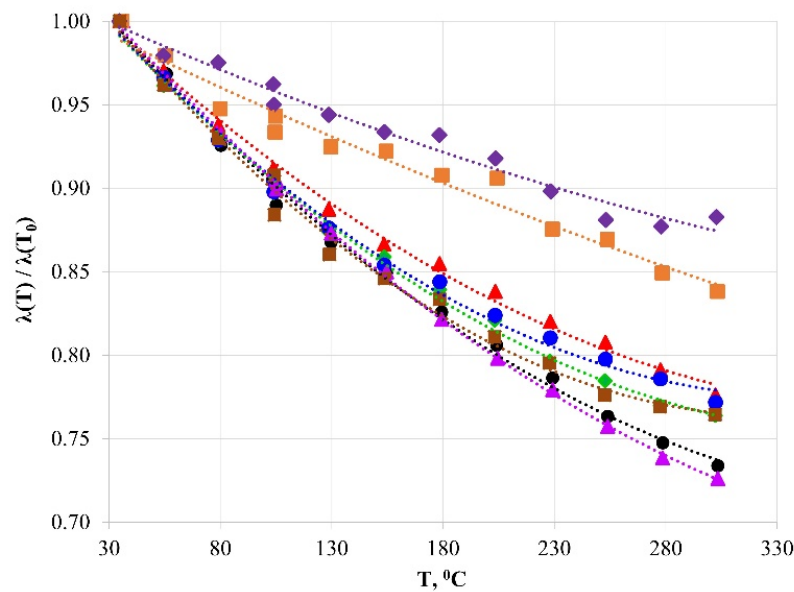


**Figure 21.** Curves drawn on the average thermal conductivity- temperature scatter diagram for lithotypes from different formations in the 30-300 °C temperature range. Different colors are related to different lithotypes: ● – dolomites (Mendym), ▲ – limestones (Mendym), ◆ – limestones (Domanic), ● – limestones (Sargaev), ▲ – sandstone (Timan), ■ – argillites (Domanic), ■ – clayey limestones (Mendym), ◆ – clayey limestones (Sargaev). Thermal conductivity values at initial temperature  $T_0 = 30$  °C are shown in Table 15.

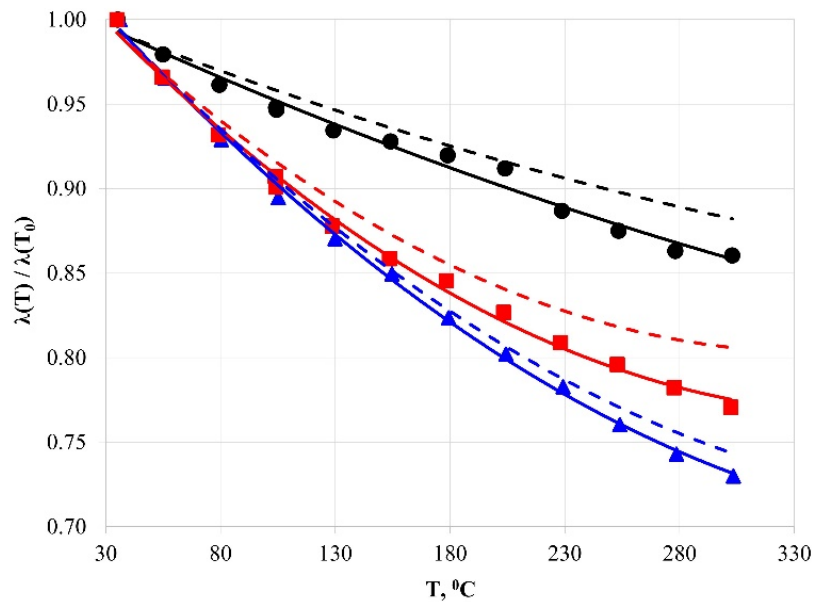


**Figure 22.** Curves drawn on the average thermal conductivity- temperature scatter diagram for different lithotypes from different formations (● – clayey limestones, ▲ – dolomites and sandstones, ■ – limestones and argillites, - - clayey limestones with correction, - - dolomites and sandstones with correction, - - limestones and argillites with correction) in the 30-300 °C temperature range. Thermal conductivity values at initial temperature  $T_0 = 30$  °C are shown in Table 15.

After thermal conductivity measurements with the DTC-300 instrument at high temperatures, all samples from the Mendym, Domanic, Sargaev, and Timan formations were studied again with the TCDS to gauge thermal conductivity components for the same directions as had been studied before the high-temperature measurements (*Table 16*). The comparison results in *Tables 15 and 16* show that the thermal conductivity components ( $\lambda_{||}$ ,  $\lambda_{\perp}$ ) decrease by 2-3% on average and that the thermal anisotropy coefficient was almost unchanged (~1%) after heating to 300 °C. Significant change of thermal properties after heating for samples 9Md and 10Md from the Mendym formation, 3Dm and 6Dm from the Domanic formation, and 4S from the Sargaev formation is related to the presence of numerous fractures in these samples. *Figures 23a, b* show photographs of one of the Bazhenov samples before and after heating to 300 °C. The cracks oriented along the bedding are a change induced by the high temperatures.

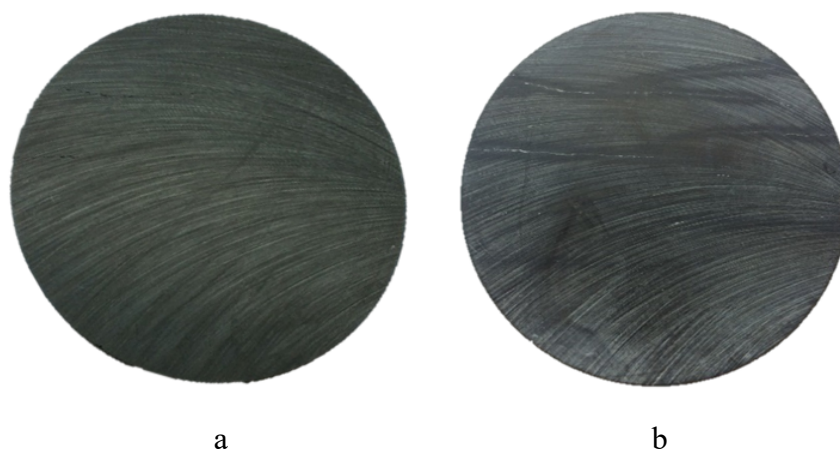


**Figure 23.** A Bazhenov sample before heating (a) and after heating to 300 °C (b).

**Table 16.** TCS measurements of thermal properties of Mendym, Domanic, Sargaev, and Timan samples at room temperature (after heating to 300 °C and subsequent cooling)

№	$\lambda_{  }$ after heating, W/(m·K)	$\lambda_{\perp}$ after heating, W/(m·K)	Variations in $\lambda_{  }$ after heating to 300 °C, %	Variations in $\lambda_{\perp}$ after heating to 300 °C, %	K after heating to 300 °C, room temperature	Variations in K after heating to 300 °C, %	$\beta_1$ after heating to 300 °C	$\beta_2$ after heating to 300 °C	Absolute difference in $\beta_1$ after heating to 300 °C	Absolute difference in $\beta_2$ after heating to 300 °C
<b>Mendym formation</b>										
1Md	3.60	3.14	-3.7	0.3	1.15	-4.2	0.15	0.12	0.03	-0.04
2Md	3.24	3.02	-4.7	-4.4	1.07	0.0	0.15	0.12	0.04	0.03
3Md	2.62	2.57	2.7	0.8	1.00	0.0	0.10	0.11	0	0.02
4Md	2.46	2.43	2.9	1.7	1.00	0.0	0.09	0.10	-0.04	0
5Md	2.39	2.29	-0.4	-4.6	1.04	4.0	0.21	0.12	0	-0.01
6Md	2.35	2.28	-1.7	-4.2	1.03	3.0	0.08	0.10	0.01	0.03
7Md	2.26	2.20	-7.8	-9.5	1.03	2.0	0.12	0.15	0.01	0.01
8Md	2.25	2.13	-5.1	-3.2	1.06	-1.9	0.10	0.11	0.01	0.02
9Md	2.34	1.90	1.7	-4.0	1.23	6.2	0.19	0.12	0.01	-0.09
10Md	2.39	2.08	-2.0	-14.0	1.15	13.9	0.12	0.10	0.04	0.04
<b>Domanic formation</b>										
1Dm	2.19	2.19	-4.4	-4.4	1.00	0.0	0.11	0.09	0.03	-0.02
2Dm	2.21	2.21	-7.5	-7.5	1.00	0.0	0.12	0.11	-0.03	0.01
3Dm	2.56	2.56	-0.8	-0.8	1.00	0.0	0.23	0.15	-0.07	0.01
4Dm	2.58	2.20	-4.1	-3.5	1.17	-0.6	0.41	0.11	0.25	-0.37
5Dm	2.14	2.03	-7.4	-8.1	1.05	0.0	0.38	0.23	0.08	-0.07
6Dm	2.40	2.40	-0.8	1.7	1.00	-2.9	0.10	0.12	-0.03	0
7Dm	2.19	2.19	-11.7	-5.6	1.00	-6.5	0.19	0.11	0.07	-0.01
<b>Sargaev formation</b>										
1S	2.68	2.46	-2.9	-5.0	1.09	1.9	0.09	0.09	0	-0.02
2S	2.37	2.31	-4.8	-5.3	1.03	1.0	0.16	0.12	-0.06	0.02
3S	2.43	2.11	4.3	5.0	1.15	-0.9	0.17	0.13	-0.01	0
4S	2.16	2.02	-7.7	1.0	1.07	-8.5	0.15	0.12	0	0.01
<b>Timan formation</b>										
1Tm	3.56	2.31	4.7	3.6	1.54	0.7	0.16	0.22	0.01	0.07
Average	2.52	2.35	-2.8	-1.5	1.07	-1.3	0.16	0.13	0.02	-0.02

Comparison of thermal conductivity behavior with temperature for organic-rich samples from different formations shows that equations vary with formations and lithotypes. All of the equations with determination coefficients, root mean square error (RMSE), and the number of studied samples are shown in *Table 17*. It should be noted that these equations are correct only for the studied temperature range (30-300 °C) and their extrapolation to predict the thermal conductivity of oil shales, in general, could lead to serious error (Rajeshwar et al., 1979).

**Table 17.** Equations which relate average thermal conductivity to temperature in the 30-300 °C temperature range for studied lithotypes from different formations.

Formation	Lithotype	Equations	R <sup>2</sup>	RMSE	Number of studied samples
Bazhenov	Clayey-siliceous with lentils siltstone	$\lambda(T)/\lambda(T_0) = -10^{-7} \cdot T^2 - 4 \cdot 10^{-4} \cdot T + 1.02$	0.98	0.01	1
	Clayey-siliceous	$\lambda(T)/\lambda(T_0) = 10^{-6} \cdot T^2 - 4 \cdot 10^{-4} \cdot T + 1.01$	0.75	0.02	2
		$\lambda(T)/\lambda(T_0) = -2 \cdot 10^{-6} \cdot T^2 + 10^{-4} \cdot T + 1.01$	0.95	0.01	5
Golchih	Bituminous argillite	$\lambda(T)/\lambda(T_0) = -5 \cdot 10^{-4} \cdot T + 1.02$	0.94	0.01	20
Abalak	Silty argillite	$\lambda(T)/\lambda(T_0) = 2 \cdot 10^{-6} \cdot T^2 - 10^{-3} \cdot T + 1.05$	0.69	0.02	3
Mendym, Domanic, Sargaev, Timan	Clayey limestone	$\lambda(T)/\lambda(T_0) = 4 \cdot 10^{-7} \cdot T^2 - 6 \cdot 10^{-4} \cdot T + 1.01$	0.92	0.01	2
	Argillite, limestone	$\lambda(T)/\lambda(T_0) = 2 \cdot 10^{-6} \cdot T^2 - 15 \cdot 10^{-4} \cdot T + 1.04$	0.89	0.02	16
	Dolomite, sandstone	$\lambda(T)/\lambda(T_0) = 2 \cdot 10^{-6} \cdot T^2 - 16 \cdot 10^{-4} \cdot T + 1.05$	0.97	0.02	3

In reservoir conditions, temperature, pressure, and fluid influence the thermal conductivity of rocks. According to previous studies (Abdulagatov et al., 2006) pressure increases thermal conductivity values up to 5% for the rocks with low porosity at the pressure of 150 MPa. The rate of pressure increase is less than that of temperature. Therefore, the effect of pressure can be neglected in correction. In-situ temperature on particular depth can be calculated using temperature gradient. Temperature at a certain depth can be formulated as:  $T = T_0 + h \cdot \text{grad}T$ , where T is a temperature at a certain depth,  $T_0$  is land surface temperature, h is depth, and gradT is geothermal gradient. Using experimental data on thermal conductivity of studied rocks at elevated temperatures it is possible to make corrections for thermal conductivity values for certain depths and in-situ temperatures.

### Measurements on kerogen sample

For determining the thermal conductivity of kerogen at elevated temperatures a synthetic sample was made (*Figure 24*). The kerogen was received by the dissolution of all rock minerals,

as kerogen has maximum chemical resistance (Bugaev et al., 2014). Then kerogen particles were pressed by a press machine (PP 25, Retsch) to the tablet with a diameter of 40 mm (*Figure 24*). TOC is 31% that was measured by the HAWK pyrolysis instrument. Thermal conductivity values of the kerogen sample at elevated temperature measured with the DTC-300 instrument are shown in *Figure 25*. The results are shown after correction with TCS instrument measurements. It is observed that the thermal conductivity of kerogen is increasing with the temperature that is in agreement with the theoretical background: organic matter is an amorphous substance, the thermal conductivity of which increases with temperature (Chudnovsky, 1962; Yudin et al., 2015).

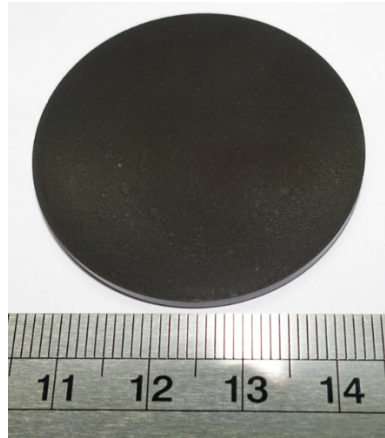


**Figure 24.** A synthetic sample of kerogen.

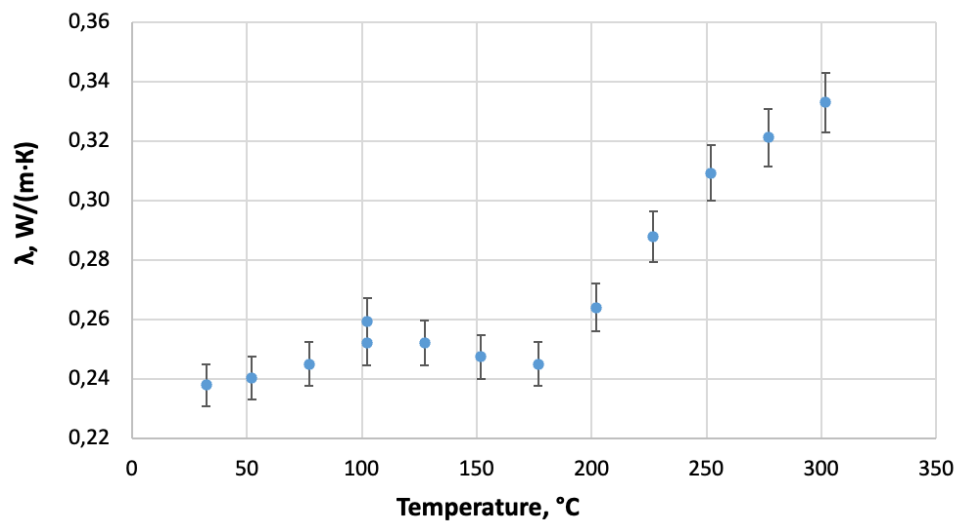


**Figure 25.** Thermal conductivity of kerogen sample at elevated temperatures measured with DTC-300 instrument. Bars values correspond to precision determined in *Chapter 3.1.1.2*.

### 4.2.3 Changes in thermal conductivity of unconventional reservoir rocks during heating and cooling

For determining the temperature range on which changes in samples structure appeared a number of experiments were provided on 5 rock samples from oil field 2. The thermal conductivity of 5 rock samples was measured in the temperature range 30-300 °C during heating and cooling. The results are shown in *Figure 26*. The thermal conductivity of rock samples during a heating cycle is decreasing and after the cooling cycle, the thermal conductivity value is lower that is related to structural changes in the sample.

Changes in thermal properties of unconventional reservoir rocks from 5 oil fields before and after heating are shown in *Table 18*. The decrease of thermal conductivity parallel to bedding after heating is 2-15%, the decrease of thermal conductivity perpendicular to bedding after heating is 1-20%. Variations in thermal conductivity anisotropy can reach 13%.

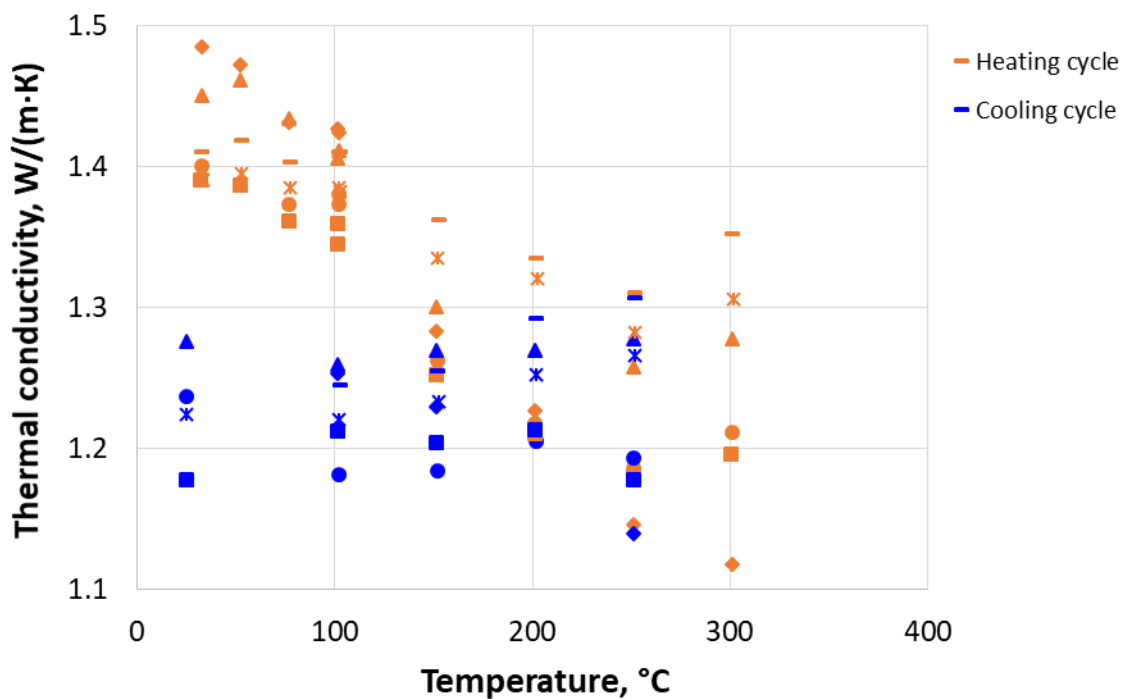


*Figure 26.* Thermal conductivity values of Golchih and Abalak formations rocks measured with the DTC-300 instrument during heating and cooling. Different symbols relate to different rock samples.

**Table 18.** Changes in thermal properties of unconventional reservoir rocks from 5 oil fields after heating.

Oil field	Formation	$\delta\lambda_{  }$ , %	$\delta\lambda_{\perp}$ , %	$\delta K$ , %
1	Bazhenov	-11	-20	13
	Abalak	-5	-14	13
2	Golchih	-15	-16	1
	Abalak	-15	-15	2
3	Bazhenov	-	-6	-
5	Mendym	-2	-4	2
	Domanic	-5	-4	-1
	Sargaev	-3	-1	-2
	Timan	5	4	1

#### 4.2.4 Analysis of thermal conductivity with temperature characteristic of unconventional reservoir rocks in comparison with other sedimentary rocks

The results of thermal conductivity measurements of unconventional reservoir rocks at elevated temperatures showed that the percentage of thermal conductivity decreasing is much lower than for other sedimentary rocks (*Figure 27*). These results agree with the experimental data for bituminous argillites from Bazhenov formations obtained earlier by Sokolova et al. (1986) where average thermal conductivity at 100-130 °C was found to be 10% lower than its value at room temperature. The decrease in thermal conductivity of Bazhenov rocks is much lower than in other sedimentary rock samples (sandstones, sands, siltstones), which show 10-15% reduction of thermal conductivity at 100 °C (Popov et al., 2013). This anomalously low decrease of thermal conductivity of organic-rich samples was also observed for other formations (Green River, Devonian) shown in *Table 1* (Prats and O'Brien, 1975; Rajeshwar et al., 1980). The effect is related to the presence of organic matter in the studied rock samples. Organic matter is an amorphous substance, the thermal conductivity of which increases with temperature (Chudnovsky, 1962; Yudin et al., 2015). So, the presence of organic matter in a sample limits the decrease of thermal conductivity as temperature increases. This was also demonstrated by measurements of thermal conductivity when temperature increases in shale samples with various oil yields from the Green River formation. The greater the oil yield in a shale sample, the less the decrease of thermal conductivity with temperature, and thermal conductivity even become constant for samples with high oil yield (27-82 gal/t) (Rajeshwar et al., 1980).

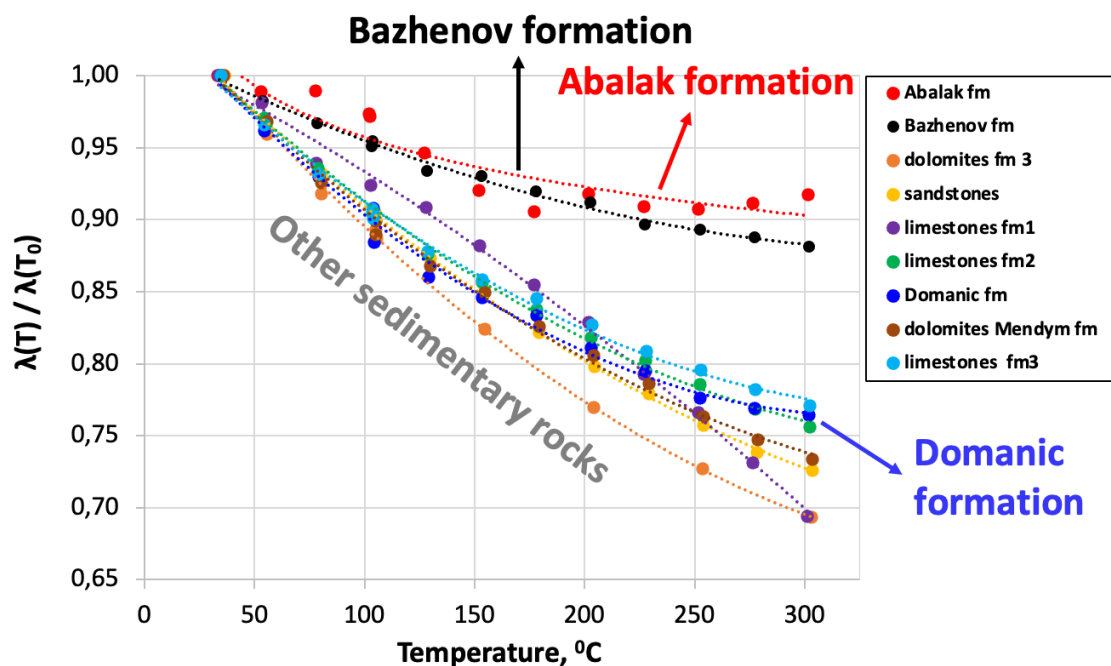


**Figure 27.** Relative change in thermal conductivity for unconventional and other sedimentary rock samples with increasing temperature.

### 4.3 CLTE investigations for unconventional reservoir rocks

#### 4.3.1 Rock collections for studying CLTE

Rock collection for CLTE at elevated temperatures includes 6 oil fields of the West-Siberian oil and gas basin.

##### Oil field 1

The collection of 15 rock samples (30×30 mm) of Oil field 1 are from Bazhenov (BF) and Abalak (AB) formations and were all drilled along a single well (see *Table 19*). BF samples are presented by high-carbonaceous shales that are composed of clayey, carbonate, and siliceous minerals in different proportions. Pyrite is presented as globules, finely disseminated inclusions, and nodules. Pyrite replaces organogenic remains tend to organic matter. The texture of shales is pelitic; the structure is silty-pelitic and straticulate thin-bedded, lightly massive. AF samples are presented by shales that are composed of argillites, silty argillites with glauconite inclusions, and siltstones. TOC range of studied rock samples is 1.3-8.3%, the density range is 2.21-2.70 g/cm<sup>3</sup>.

**Table 19.** Characteristics of studied rock samples from oil field 1.

Sample №	Formation	Brief geological description
10	Bazhenov	Shale (Carbonate - Clayey-Siliceous rock, pelitic, thin-bedded, carbonaceous)
11-14		Shale (Clayey-Siliceous rock, silty-pelitic, thin-bedded, carbonaceous)
15-17		Shale (Clayey-Siliceous rock, thin-bedded, pelitic, carbonaceous)
18		Shale (Clayey-Siliceous rock, silty-pelitic, thin-bedded, carbonaceous with glauconite inclusions)
19-21	Abalak	Silty argillites with glauconite inclusions, thin-bedded
22		Clayey siltstone, thin-bedded
23		Silty argillites with pyrite nodules

### **Oil field 2**

The collection of 8 rock samples (30×30 mm) of Oil field 2 are from Golchih formation (GF) and AB presented by bituminous argillites and were all drilled along a single well. GF and AB rock samples are presented by bituminous argillites. TOC range of studied rock samples is 1.6-10.9%, the density range is 2.31-2.70 g/cm<sup>3</sup>.

### **Oil field 3**

The collection of 12 rock samples (30×30 mm) of Oil field 3 are from BF presented by bituminous argillites and were all drilled along a single well. BF rock samples are presented by bituminous argillites. The density range of studied rock samples is 2.34-2.54 g/cm<sup>3</sup>.

### **Oil field 4**

The collection of 4 rock samples (30×30 mm) of Oil field 4 are from BF and were all drilled along a single well. BF rock samples are presented by high-carbonaceous shales that are composed of clayey, carbonate, and siliceous minerals in different proportions. TOC range of studied rock samples is 7.5-17.2%, the density range is 2.08-2.28 g/cm<sup>3</sup>.

### **Oil field 5**

The collection of 5 rock samples (30×30 mm) of Oil field 5 are from BF and were all drilled along a single well. BF rock samples are presented by high-carbonaceous shales that are composed of clayey, carbonate, and siliceous minerals in different proportions. TOC range of studied rock samples is 6.8-11.9%, the density range is 2.18-2.34 g/cm<sup>3</sup>.

### 4.3.2 CLTE and thermal conductivity measurements at room temperature

CLTE values for temperature range 25-50 °C for core plugs drilled from the full-size core samples of the BF and AF in the direction perpendicular to bedding are shown in *Table 20*. The data demonstrate that CLTE values perpendicular to the bedding plane are twice higher than CLTE values along the bedding plane. The BF rocks have high CLTE anisotropy coefficients (up to 2.2). *Table 20* also shows that CLTE measurement data for the shales are much higher (by 5-10 times) than for other sedimentary rocks as, for example, CLTE range is  $(3.5\div 10.2)\cdot 10^{-6} \text{ K}^{-1}$  for limestones, and  $(7.8\div 10.1)\cdot 10^{-6} \text{ K}^{-1}$  for sandstones (Popov et al., 2008). Such high CLTE values for the BF rocks are related to the presence of organic matter in studied rock samples as the CLTE of organic matter is much higher ( $\sim 3.4\cdot 10^{-4} \text{ K}^{-1}$  (Smith and Johnson, 1976)) than for mineral components of rocks. For example, CLTE of bitumen is  $200\cdot 10^{-6} \text{ K}^{-1}$  (Yarzev and Erofeev, 2004) and CLTE of kerogen was estimated as  $115\cdot 10^{-6} \text{ K}^{-1}$  (Kaevand and Lille, 2005) that is by 5-10 times higher than for CLTE of rock-forming minerals  $(16\div 50)\cdot 10^{-6} \text{ K}^{-1}$  (Anderson, 1989)). Average CLTE variations along bedding for the BF rocks from oil fields 5 ( $\text{CLTE}_{\text{average}} = 16.8\cdot 10^{-6} \text{ K}^{-1}$ ) and 4 ( $\text{CLTE}_{\text{average}} = 21.1\cdot 10^{-6} \text{ K}^{-1}$ ) are higher than for the BF and GF rocks from oil fields 1 ( $\text{CLTE}_{\text{average}} = 10.2\cdot 10^{-6} \text{ K}^{-1}$ ) and 2 ( $\text{CLTE}_{\text{average}} = 9.0\cdot 10^{-6} \text{ K}^{-1}$ ) that is related to different range of TOC along wells. Low density values for rock samples from *Table 20* are related to high TOC in such samples, as density of samples depends on TOC (see *Figure 30b*).

Results of the thermal conductivity measurements on core plugs of shale formations are presented in *Table 20*. The thermal conductivity component parallel to the bedding plane ( $\lambda_{\parallel}$ ) ranges within 1.63-3.58 W/(m·K) for BF, 1.67-2.09 W/(m·K) for GF and 2.05-3.74 W/(m·K) for AB. The thermal conductivity component perpendicular to the bedding plane ( $\lambda_{\perp}$ ) ranges within 0.95-2.15 W/(m·K) for BF, 1.14-1.52 W/(m·K) for GF and 1.35-2.55 W/(m·K) for AB. All formations are characterized by high variations of thermal anisotropy coefficient (K), which ranges within 1.06-3.74 for BF, 1.38-1.52 for GF, and 1.31-1.90 for AB (*Table 20*). Thermal heterogeneity factors inferred from the thermal conductivity profiles are also given in *Table 20*. The data in *Table 20* show that high values of thermal conductivity and thermal heterogeneity factors are related to samples that have pyrite inclusions (samples №11, 14). For most shale samples (№15-22) heterogeneity factor,  $\beta_1$  is larger than  $\beta_2$  and average values of  $\beta_1$  exceed average values of  $\beta_2$  essentially (correspondingly 0.19 and 0.11).

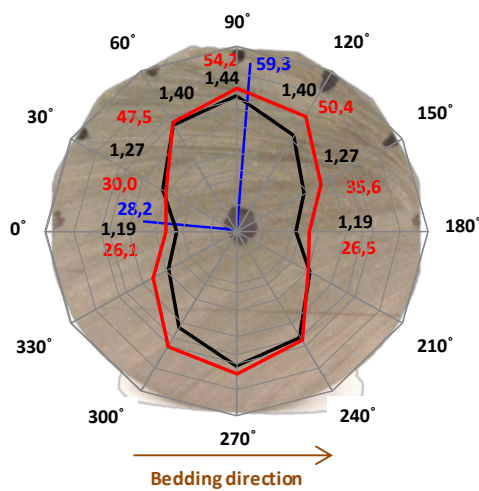
**Table 20.** Results of CLTE, CLTE anisotropy coefficient, density, TOC and thermal properties measurements

Sample №	Oil field	Formation	CLTE at 25-50 °C, 10 <sup>-6</sup> K <sup>-1</sup>		CLTE anisotropy coefficient	CLTE range at 25-300 °C, 10 <sup>-6</sup> K <sup>-1</sup>	Density, g/cm <sup>3</sup>	TOC, %	Thermal conductivity, W/(m·K)		Thermal conductivity anisotropy coefficient	Thermal heterogeneity factor	
			Along bedding	Perpendicular to bedding					λ <sub>  </sub>	λ <sub>⊥</sub>		β <sub>1</sub>	β <sub>2</sub>
1	5	Bazhenov	11.6	-	-	11.6-16.8 <sup>a</sup>	2.34	6.57	-	-	-	-	-
2			20.3	42.2	2.1	18.0-20.3 <sup>a</sup>	2.18	9.19	1.73	1.42	1.22	0.16	0.07
3			19.4	41.7	2.2	16.6-18.8 <sup>a</sup>	2.18	11.50	1.73	1.44	1.20	0.11	0.07
4			-	51.3	-	40.0-140 <sup>b</sup>	2.25	11.85	-	-	-	-	-
5			15.9	29.9	1.9	21.1-54.8 <sup>b</sup>	2.27	6.80	1.97	1.65	1.19	0.10	0.06
6	4	Bazhenov	14.9	18.5	1.2	14.4-18.4 <sup>b</sup>	2.28	16.39	2.28	2.15	1.06	0.08	0.06
7			-	27.7	-	19.6-27.7 <sup>b</sup>	2.26	7.50	-	-	-	-	-
8			26.0	54.2	2.1	16.5-143 <sup>b</sup>	2.08	15.43	1.44	1.19	1.21	0.08	0.08
9			22.3	41.0	1.8	4.4-22.8 <sup>a</sup>	2.20	17.19	1.63	1.48	1.10	0.09	0.07
10	1	Bazhenov	10.5	-	-	6.9-11.3 <sup>a</sup>	2.42	6.19	2.17	1.81	1.20	0.13	0.09
11			6.7	-	-	5.4-12.9 <sup>a</sup>	2.34	7.47	2.83	1.91	1.48	0.57	0.41
12			11.7	-	-	4.5-11.7 <sup>a</sup>	2.35	7.73	2.05	1.58	1.30	0.10	0.11
13			11.9	-	-	8.7-12.7 <sup>a</sup>	2.34	7.47	2.20	1.76	1.25	0.11	0.11
14			12.5	-	-	7.5-13.2 <sup>a</sup>	2.35	8.34	3.58	0.95	3.74	0.97	0.11
15			8.3	-	-	3.3-10.8 <sup>a</sup>	2.38	7.69	2.21	1.60	1.38	0.12	0.09
16			10.6	-	-	8.8-14.9 <sup>a</sup>	2.40	6.19	2.37	1.78	1.33	0.12	0.10
17			9.2	-	-	7.4-15.9 <sup>a</sup>	2.52	3.19	2.36	1.95	1.21	0.13	0.14
18			10.1	-	-	6.7-12.7 <sup>a</sup>	2.52	2.98	2.57	2.15	1.20	0.16	0.09
19			7.4	-	-	2.9-10.1 <sup>a</sup>	-	2.06	2.43	1.84	1.31	0.14	0.13
20		8.6	-	-	2.9-9.9 <sup>a</sup>	-	1.90	2.63	1.70	1.55	0.14	0.13	
21		5.3	-	-	2.07-9.3 <sup>a</sup>	-	2.38	-	-	-	-	-	
22		8.2	-	-	1.4-9.3 <sup>a</sup>	-	1.64	2.92	1.53	1.90	0.13	0.11	
23		6.8	-	-	4.7-9.2 <sup>a</sup>	-	2.35	2.82	1.93	1.46	0.18	0.12	
1GF	2	Golchih	7.0	-	-	3.1-7.5 <sup>a</sup>	2.69	2.03	2.09	1.38	1.52	0.23	0.13
2GF			7.5	-	-	3.6-8.4 <sup>a</sup>	2.65	1.60	1.97	1.52	1.30	0.36	0.25
3GF			8.1	-	-	7.9-8.5 <sup>a</sup>	2.63	3.45	2.07	1.39	1.50	0.19	0.16
4GF			9.6	-	-	5.1-9.6 <sup>a</sup>	2.70	2.99	2.08	1.41	1.47	0.19	0.17
5GF			10.3	-	-	1.8-10.3 <sup>a</sup>	2.37	7.40	1.67	1.14	1.47	0.12	0.14
6GF			10.0	-	-	3.0-10.0 <sup>a</sup>	2.46	4.28	1.77	1.24	1.43	0.32	0.20
7GF			10.3	-	-	9.8-11.6 <sup>a</sup>	2.31	10.90	1.71	1.24	1.38	0.19	0.13
1AF		Abalak	6.3	-	-	3.4-7.3 <sup>a</sup>	2.65	1.80	2.05	1.35	1.52	0.18	0.27

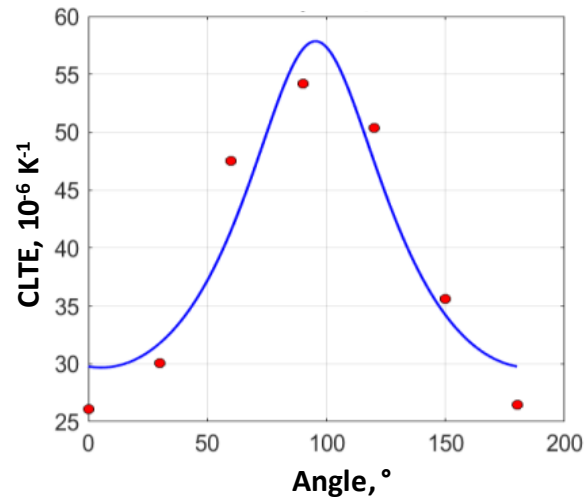
<sup>a</sup> Minimum-maximum CLTE values parallel to bedding at 25-300 °C range; <sup>b</sup> Minimum-maximum CLTE values perpendicular to bedding at 25-300 °C range.

### 4.3.3 CLTE anisotropy at room temperature

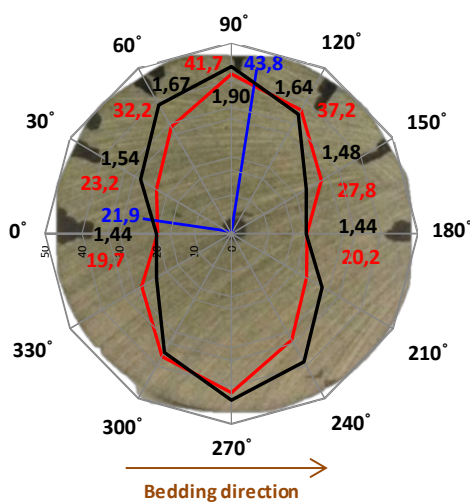
Measurements of CLTE anisotropy were carried out for six core plugs from BF in a reduced temperature range (25-50 °C) to prevent any changes of physical parameters of studied core plugs. Results of CLTE measurements on rock samples at different directions relative to the bedding plane are shown in *Figures 28a, c, e, g, i, k* by red lines and values, the measurement unit is  $10^{-6} \text{ K}^{-1}$ . Thermal conductivity measurements were provided with TCS on the core plugs in the same directions. Results are shown by black lines and values in *Figures 28 a, c, e, g, i, k*; measurement unit is  $\text{W}/(\text{m}\cdot\text{K})$ . Detection of main axes directions and CLTE values was provided by the application of ellipse with unknown semiaxes and rotation angle on experimental results and determination of unknown values by the least square method. The result of solving the optimization problem by the ellipse parameters method (blue line) is shown in *Figures 28 b, d, f, h, j, l*. The direction of main axes and CLTE values are also shown in *Figures 28 a, c, e, g, i, k* (blue lines and values). Results of experimental measurements are presented by red markers.



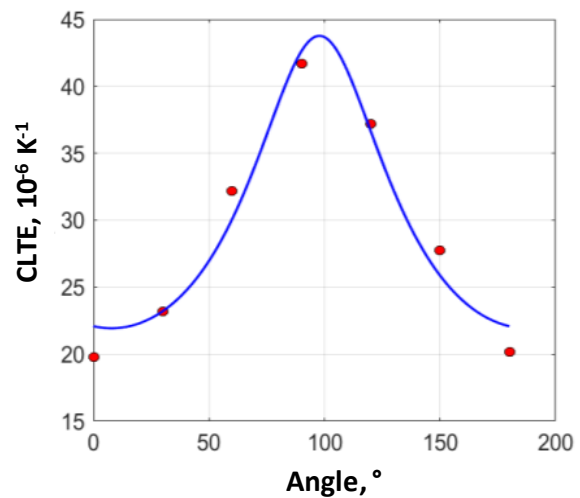
a



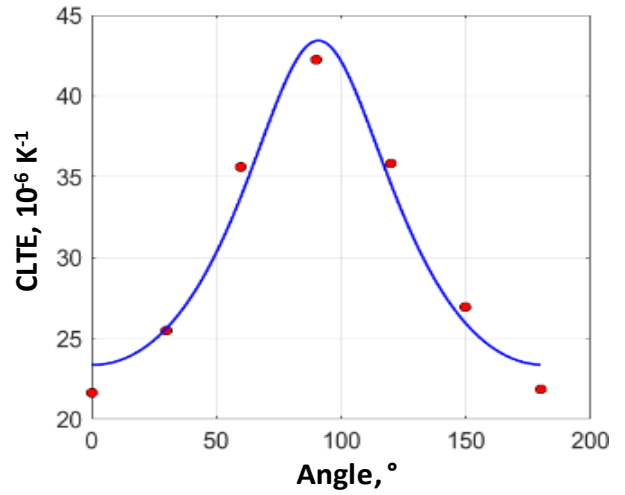
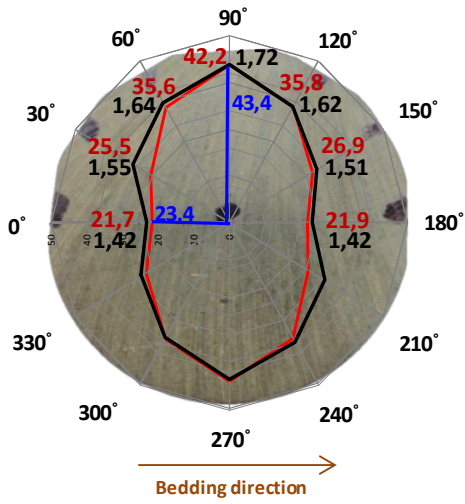
b



c

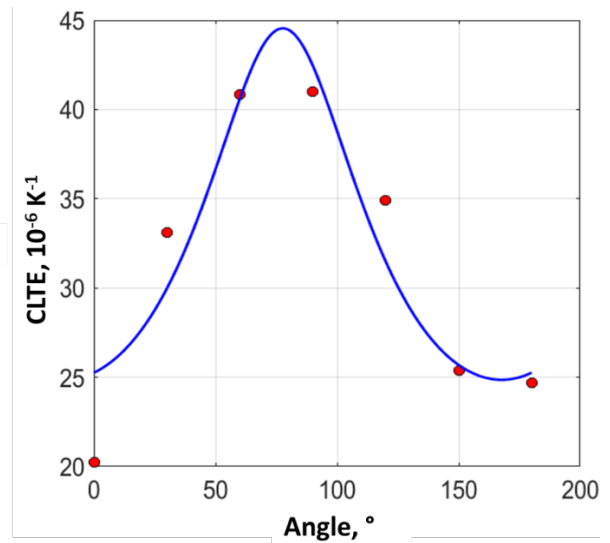
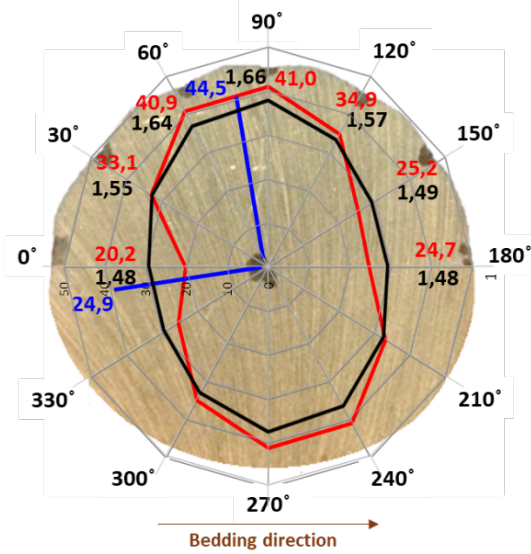


d



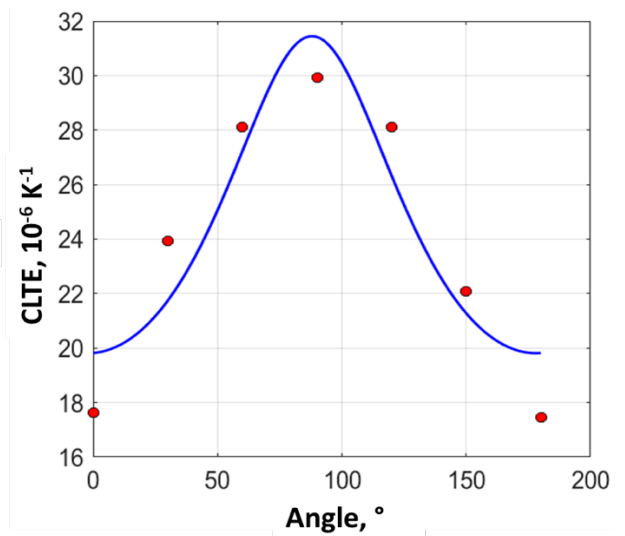
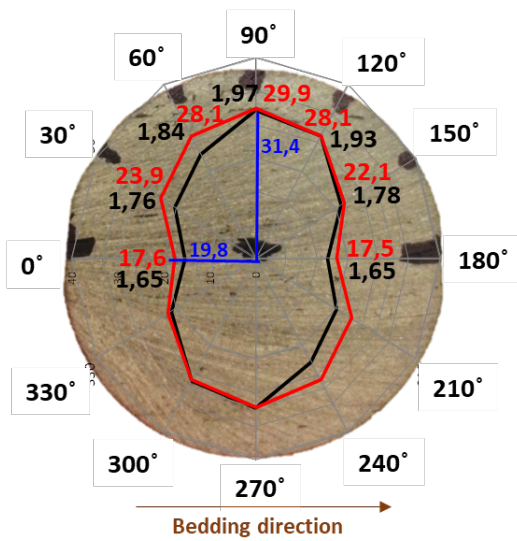
e

f



g

h



i

j

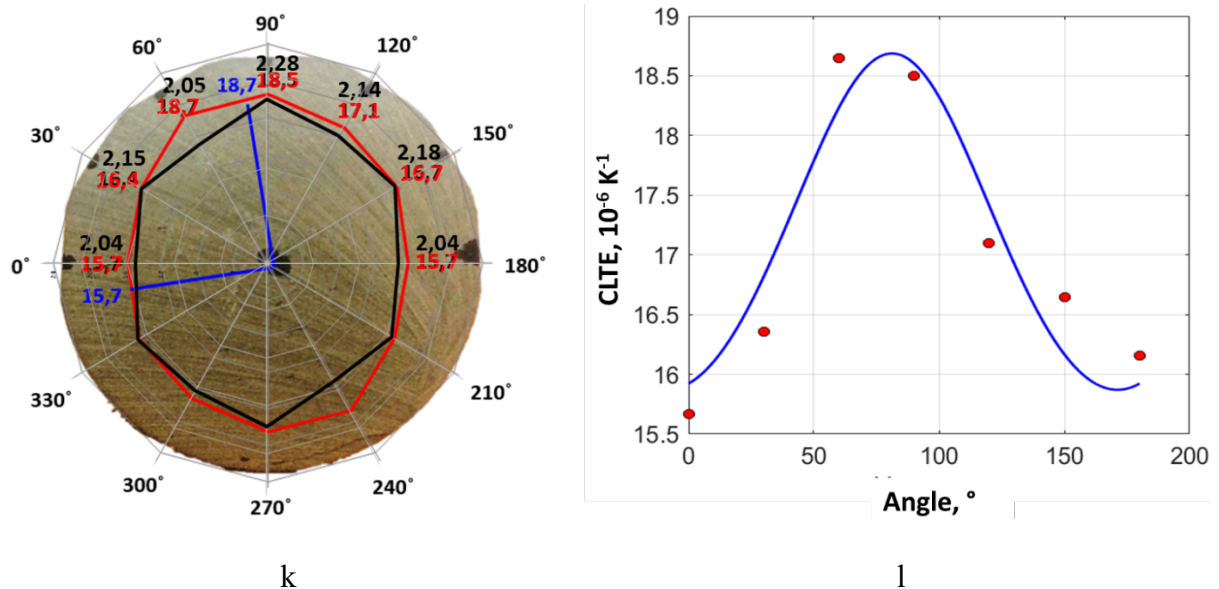


**Figure 28.** Results of CLTE (measurement unit is  $10^{-6} \text{ K}^{-1}$ , the data are shown by red lines and numbers) and thermal conductivity (measurement unit is  $\text{W}/(\text{m}\cdot\text{K})$ , black line and numbers) measurements of BF core plugs at different directions to the bedding plane (a, c, e, g, i, k). The results of solving the optimization problem by the ellipse parameters method (blue lines) and the CLTE measurement results (red markers) are shown in corresponding figures b, d, f, h, j, l.

The results given in *Figure 28* show that for the core plugs from BF main axes of CLTE anisotropy coincide with the main axes of thermal conductivity anisotropy. Though there is not enough data for fixing a reliable correlation dependence for CLTE anisotropy coefficient vs thermal conductivity anisotropy coefficient, the results showed the following tendency – the higher the thermal conductivity anisotropy coefficient is, the higher CLTE anisotropy coefficient is. It opens the possibility to predict CLTE anisotropy through the thermal conductivity anisotropy and vice versa.

#### 4.3.4 Integrated analysis and core state control

Comparison results of thermal profiling before and after CLTE measurements showed no significant changes in thermal conductivity parallel perpendicular to bedding (less than the uncertainty of thermal conductivity measurements) for most core plugs. As thermal conductivity is sensitive to any changes in rocks (Popov et al., 2017), it shows that there are no essential changes in rocks structure after high-temperature measurements for core plugs.

Integration of CLTE (parallel to bedding at temperature range 25-50 °C) and thermal conductivity measurements on core plugs allows us obtaining new correlation thermal conductivity vs CLTE (*Figures 29*):  $\lambda = 6.64 \cdot \alpha^{-0.45}$ , determination coefficient  $R^2 = 0.88$ , root

mean square error (RMSE) = 0.18 W/(m·K). The reason for such correlation is the sensitivity of thermal conductivity and CLTE of rock samples to the presence of organic matter (Popov et al., 2017). CLTE of organic matter is much higher (5-10 times) than for other sedimentary rock minerals. Similar correlation was obtained between CLTE (parallel to bedding at temperature range 25-50 °C) and mineral density of studied core plugs at room temperature:  $\rho = 3.38 \cdot \alpha^{-0.15}$ ,  $R^2 = 0.85$ , RMSE = 0.05 g/cm<sup>3</sup> (Figures 30a). Also, close correlations between density, TOC, and thermal conductivity measured at room temperature were observed (Figures 30 b, c).

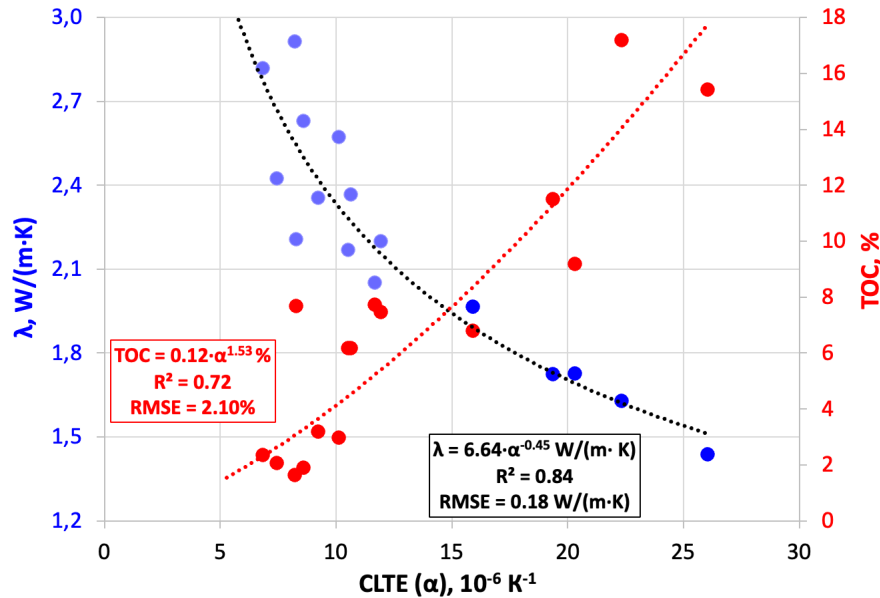


Figure 29. Correlation TC vs CLTE for core plugs from BF from 3 oil fields.

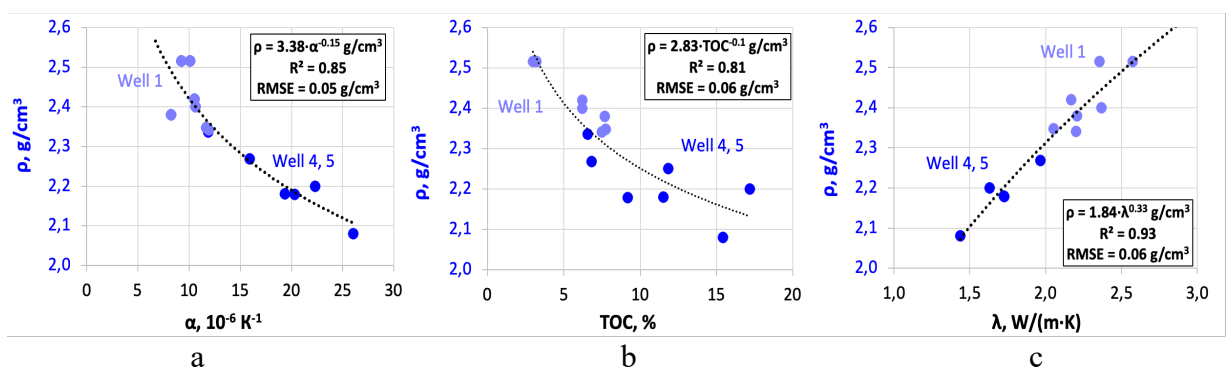
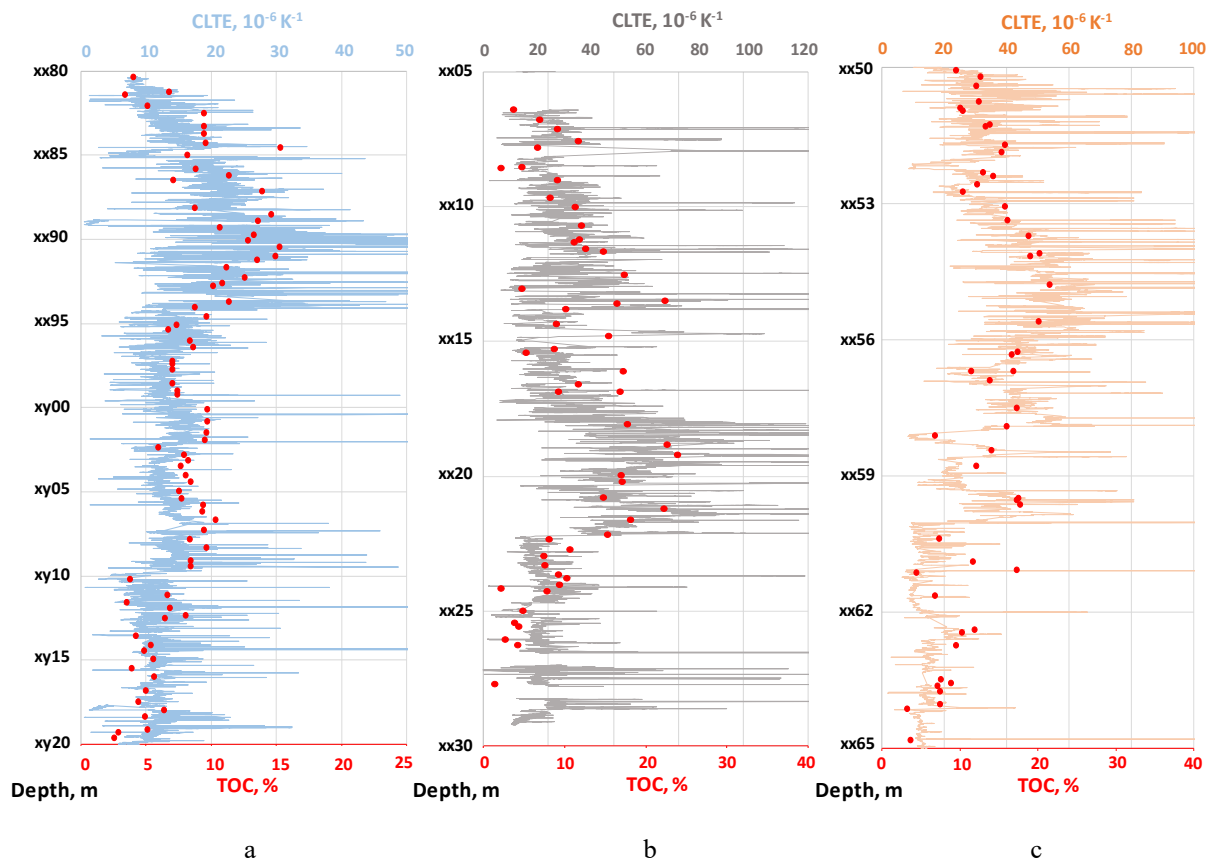
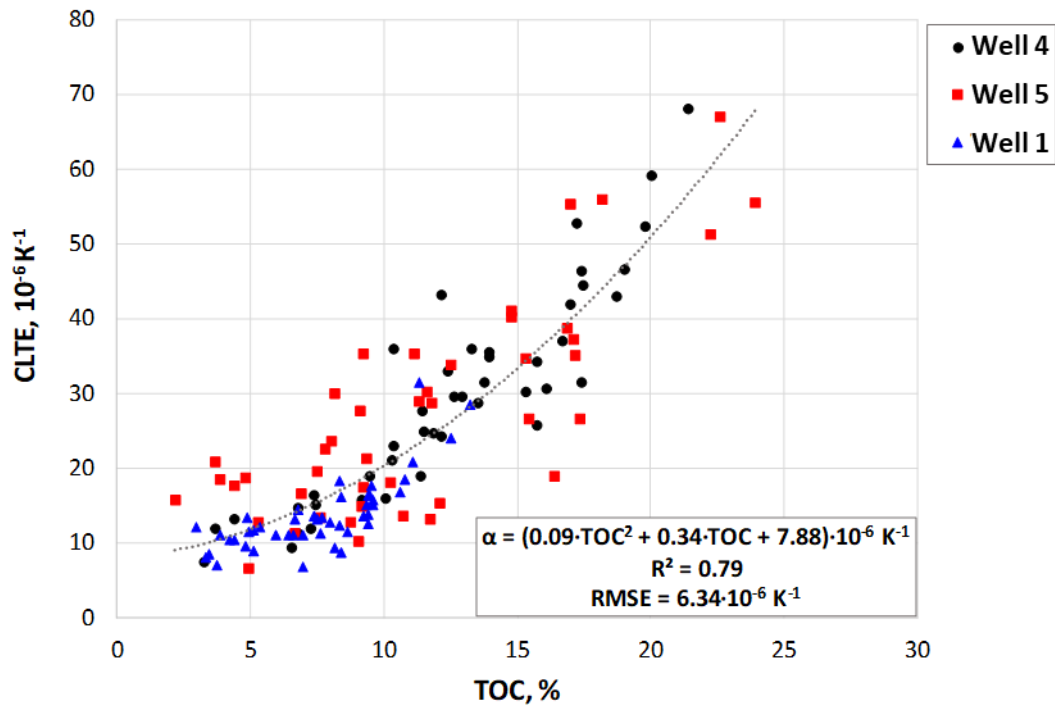


Figure 30. Correlations density vs CLTE (parallel to bedding at temperature range 25-50 °C) (a), density vs TOC (b), and density vs TC (c) for core plugs from BF from 3 oil fields. Dark blue points relate to samples from well 1; light blue points relate to samples from wells 4, 5.

Obtained correlations allow us to predict CLTE of BF rocks using density and thermal conductivity data. The observed correlation thermal conductivity vs CLTE for studied core plugs ( $\alpha = 52.82 \cdot \lambda^{-1.94}$ ,  $R^2 = 0.88$ ) gives the possibility to obtain a detailed CLTE profile (parallel to bedding at temperature range 25-50 °C) for wells 1, 4 and 5 (*Figure 31*) using the high resolution (1 mm) profiles of the thermal conductivity obtained from the continuous thermal core profiling performed on all full-size cores with the optical scanner. TOC for each well was obtained with the HAWK pyrolysis instrument and matched with CLTE profile along wells (*Figure 31*). Generalized correlation CLTE vs TOC for three studied wells was specified by CLTE profiles averaged in every 10 cm interval and pyrolysis data (*Figure 32*):  $\alpha = 0.09 \cdot \text{TOC}^2 + 0.34 \cdot \text{TOC} + 7.88$  ( $R^2 = 0.79$ ,  $\text{RMSE} = 6.34 \cdot 10^{-6} \text{ K}^{-1}$ ).



**Figure 31.** Detailed profile of CLTE and pyrolysis data (red markers) for BF rocks from well 4 (c), well 5 (b) and well 1 (a).



**Figure 32.** Correlation CLTE vs TOC for BF rocks from 3 wells.

#### 4.3.5 CLTE measurements at elevated temperatures

CLTE measurements at high temperatures (25-300 °C) were performed for each studied core plug. The measurement results are shown in *Figures 33-36*. The CLTE measurements at high temperatures were conducted for different directions – parallel and perpendicular to the bedding plane. The decrease of CLTE values within the temperature range of 25-140 °C for studied core plugs is probably related to the dehydration of water during heating. Clay minerals are very sensitive to temperature increase as they contain interlayer and physically adsorbed water. Dehydration of water during heating causes the decrease of interlayer spacing and thermal expansion of clay minerals. So, smectites lose interlayer water in the temperature range 100-200 °C and interlayer spacing decreases from 15-12 Å to 10-9.4 Å (Weaver, 1976). DTA curves of samples composed of illite-rich clay minerals were observed to have endothermic peaks within the temperature range of 98-114 °C that was related to dehydration of adsorbed water (Alver et al., 2016). It is demonstrated by the strong correlation of CLTE variations with a mass change of studied core plugs during the heating (*Figure 36*). Rock mass for each studied core plug was measured before, and after heating to 300 °C, CLTE variations were calculated as  $(\text{CLTE}_{\text{max}} - \text{CLTE}_{\text{min}}) / \text{CLTE}_{\text{average}}$ ,  $\text{CLTE}_{\text{max}}$ ,  $\text{CLTE}_{\text{min}}$ ,  $\text{CLTE}_{\text{average}}$  – maximum, minimum and average CLTE values correspondingly for each core plug within a temperature range of 25-300 °C. *Figure 37* demonstrates that more core plugs mass loss results in higher CLTE variations with

temperature. Moreover, for sample №1 evaporation of bitumen was observed after heating to 300 °C (Figure 38). The CLTE measurements on core plugs from the Bazhenov and Abalak formations at high temperatures showed that CLTE at high temperatures is 2.0-2.7 times higher than CLTE at initial temperature  $T_0$ . CLTE values measured for the directions perpendicular to the bedding plane reach  $(133\div 143)\cdot 10^{-6} \text{ K}^{-1}$  at temperature 160-200 °C (samples № 4 and 8, Figure 34).

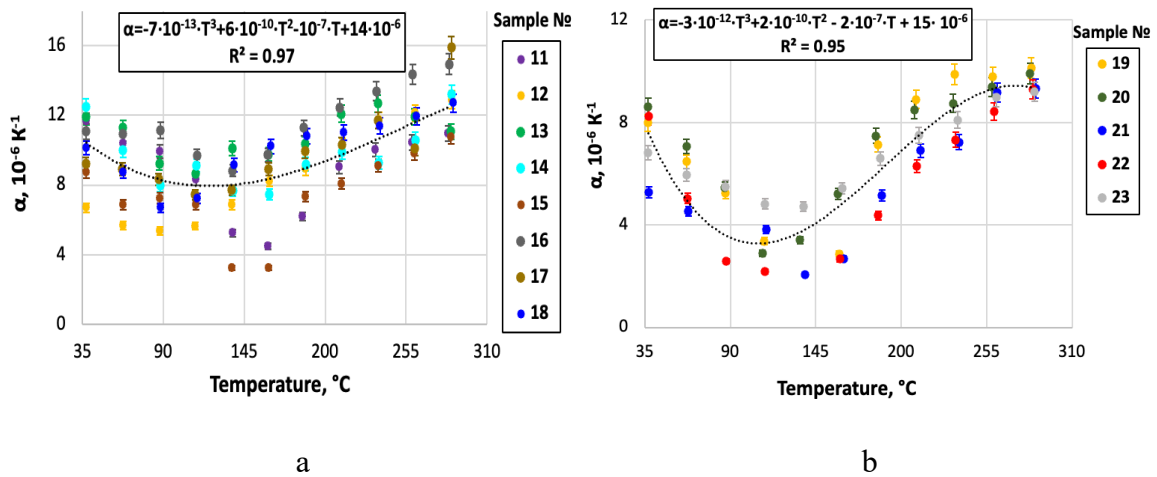


**Figure 33.** CLTE variations (parallel to the bedding plane) with a temperature increase for core plugs from the BF (a) and the AF (b) (well 1). Bars values correspond to the precision of CLTE measurements (Chapter 3.3.1).

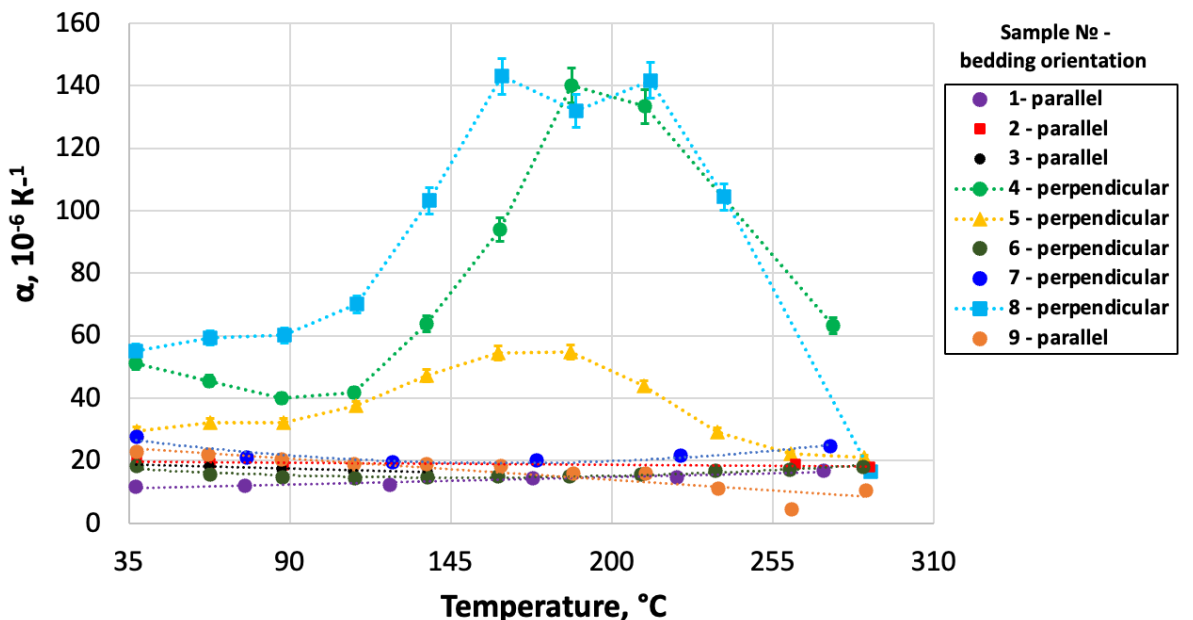


**Figure 34.** CLTE values change with temperature for core plugs from the BF (wells 4, 5). Bars values correspond to the precision of CLTE measurements (Chapter 3.3.1).

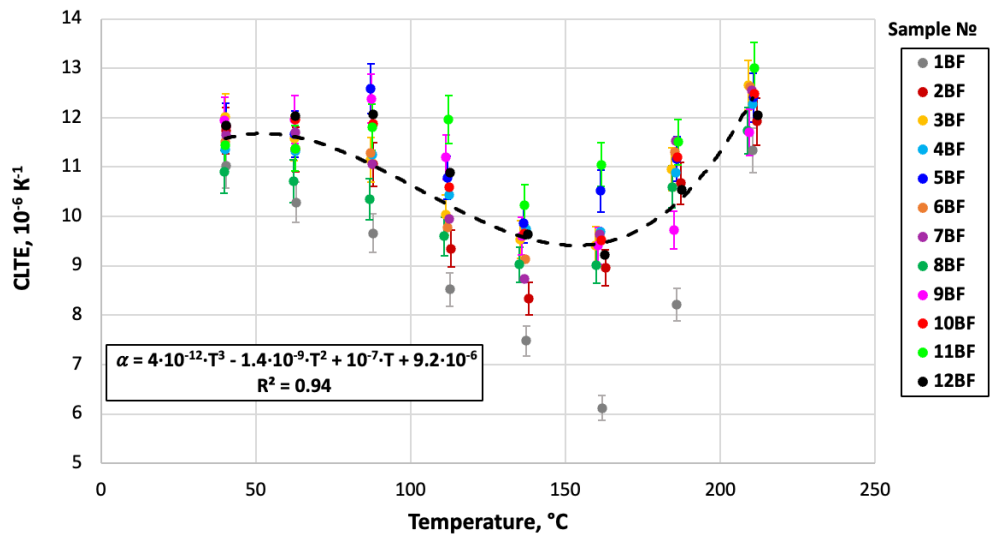


**Figure 35.** CLTE variations (parallel to the bedding plane) with a temperature increase for core plugs from the BF (well 3). Bars values correspond to the precision of CLTE measurements (Chapter 3.3.1).

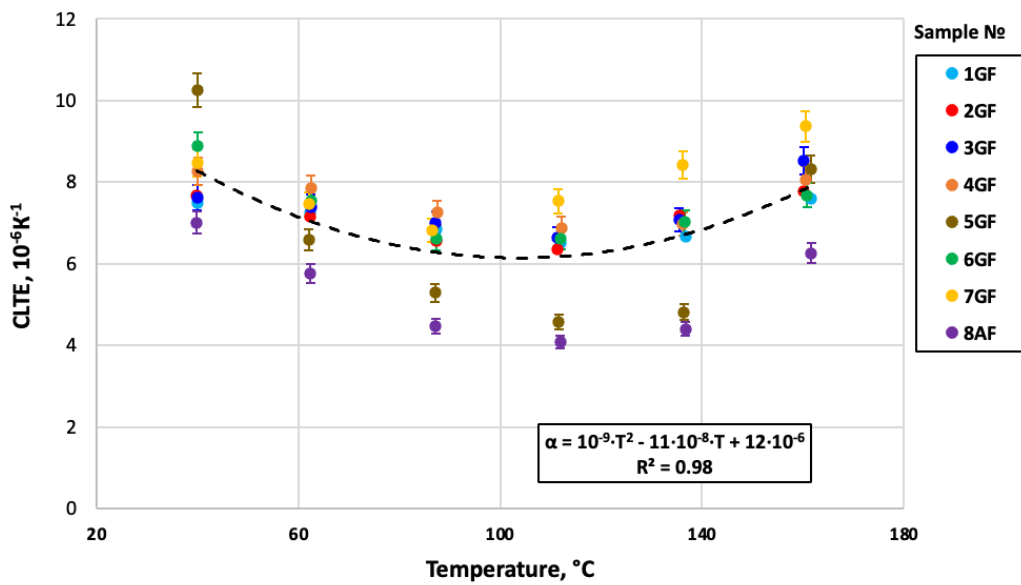


**Figure 36.** CLTE variations (parallel to the bedding plane) with a temperature increase for core plugs from the GF and AB (well 2). Bars values correspond to the precision of CLTE measurements (Chapter 3.3.1).

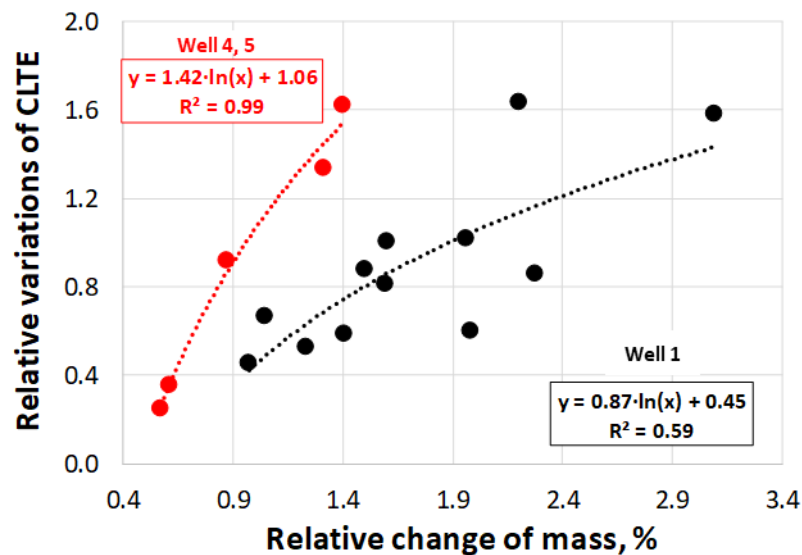


**Figure 37.** Variations of CLTE with a relative change of core plug mass after measurements at 300 °C for BF rocks (Samples №4, 5, 6, 7, 8, 10, 12-13, 15-23).

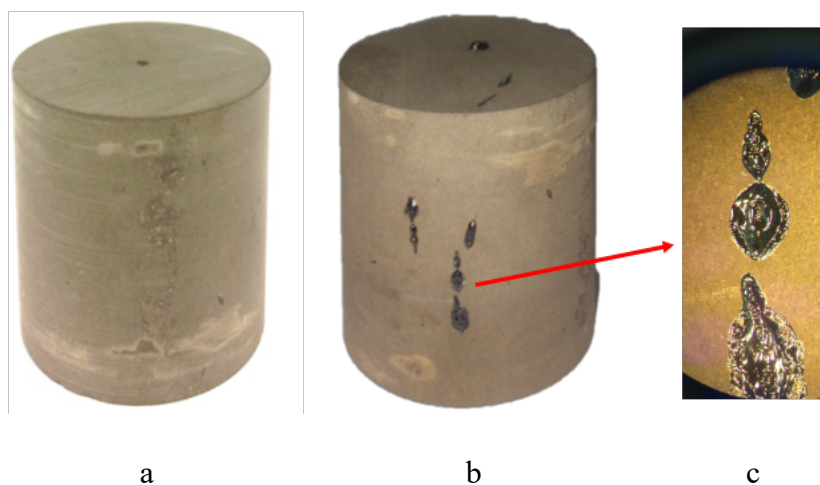


**Figure 38.** Photo of sample №1 before (a) and after (b) high-temperature measurements with a zoomed area of bitumen exudation (c).

#### 4.4 Volumetric heat capacity of unconventional reservoir rocks at elevated temperatures

##### 4.4.1 Rock collection for studying volumetric heat capacity at elevated temperatures

Rock collection for studying volumetric heat capacity (VHC) at elevated temperatures includes 4 oil fields of the West-Siberian oil and gas basin.

## Oil field 1

The collection of 11 rock samples (~15 g) of Oil field 1 are from Bazhenov and Abalak formations (see *Table 21*). Bazhenov formation (BF) samples are presented by argillites and siltstones, Abalak formation (AB) samples are presented by argillites.

**Table 21.** Characteristics of studied rock samples from oil field 1.

№ of sample	Formation	Lithology
1	Bazhenov	Argillite with quartz lenses
2	Bazhenov	Argillite with sand admixture
3	Bazhenov	Siltstone
4	Bazhenov	Silt-rich argillite
5	Bazhenov	Argillite with silty admixture
6	Bazhenov	Siltstone with fine-grained sand admixture
7	Bazhenov	Argillite with silty admixture and detritus
8	Bazhenov	Argillite
9	Abalak	Argillite with silty admixture
10	Abalak	argillite
11	Abalak	argillite

## Oil field 2

The collection of 8 rock samples (~15 g) of Oil field 2 are from Bazhenov and Abalak formations. Bazhenov and Abalak formation samples are presented by bituminous argillites.

## Oil field 3

The collection of 12 rock samples (~15 g) of Oil field 3 are from Bazhenov formation that is presented by bituminous argillites.

### 4.4.2 Results of measurements for unconventional reservoir rocks

#### Oil field 1

Volumetric heat capacity measurements in the temperature range of 25-200 °C were carried out on 11 non-extracted samples with a mass of 15 g from the most representative samples of full-sized core samples, selected based on the results of thermophysical profiling and geological description of the core. The determination of the volumetric heat was based on measurements of the specific heat capacity in the temperature range 25-200 °C on 11 non-extracted samples weighing 15 g, measurements of the density of rocks, estimates of changes in the density of rocks with a temperature in the temperature range of 25-200 °C according to the

results of measurements of the coefficient of linear thermal expansion in a given temperature range with the subsequent determination of the volumetric heat capacity by the ratio (16). To measure the specific heat capacity, tablets (4 mm in diameter) were prepared, which were obtained using a manual hydraulic press at a pressure of 8 MPa. *Tables 22-31* provide summary information on the results of measurements of the specific heat capacity of samples 1 - 11 at temperatures of 25, 50, 100, 150, and 200 °C. For rock samples, No.1-5 and No.9-11, the values of specific heat capacity obtained in the first and second experiments are in satisfactory agreement with each other within the error of the DSC method (according to ASTM E 1269-05, on average, the relative error of the method is 5-7%). For samples No.6-8, the specific heat capacity is in poor agreement according to the results of the first and second experiments. In the case of sample No.7, this may be due to the fact that measurements were carried out on a rock powder, and not on a tablet; therefore, an increased error in measurements on the powder could arise due to the fact that the condition of good and reproducible thermal contact between the crucible bottom was not met and a sample. The second reason for the discrepancy between the results can be associated with the high hygroscopicity of the samples - as a result of this, the error in determining the mass of the dried preparations could be increased.

**Table 22.** The results of measurements of the specific heat capacity of sample №1.

Sample №1					
$T, ^\circ\text{C}$	$c_p, \text{kJ}/(\text{kg}\cdot\text{K})$			Standard deviation, $\text{kJ}/(\text{kg}\cdot\text{K})$	Student's confidence interval ( $\alpha= 0.05$ ), $\text{kJ}/(\text{kg}\cdot\text{K})$
	Tablet 2	Tablet 3	Average		
25	0.830	0.796	0.813	0.02	0.2
50	0.879	0.840	0.859	0.03	0.2
100	0.976	0.918	0.947	0.04	0.4
150	1.055	0.988	1.021	0.05	0.4
200	1.098	1.048	1.073	0.03	0.3

**Table 23.** The results of measurements of the specific heat capacity of sample №3.

Sample №3					
$T, ^\circ\text{C}$	$c_p, \text{kJ}/(\text{kg}\cdot\text{K})$			Standard deviation, $\text{kJ}/(\text{kg}\cdot\text{K})$	Student's confidence interval ( $\alpha= 0.05$ ), $\text{kJ}/(\text{kg}\cdot\text{K})$
	Tablet 2	Tablet 3	Average		
25	0.860	0.781	0.820	0.06	0.5
50	0.905	0.824	0.865	0.06	0.5
100	1.033	0.917	0.975	0.08	0.7
150	1.159	1.031	1.095	0.09	0.8
200	1.259	1.189	1.224	0.05	0.4

**Table 24.** The results of measurements of the specific heat capacity of sample №4.

Sample №4					
$T, ^\circ\text{C}$	$c_p, \text{kJ}/(\text{kg}\cdot\text{K})$			Standard deviation, $\text{kJ}/(\text{kg}\cdot\text{K})$	Student's confidence interval ( $\alpha= 0.05$ ), $\text{kJ}/(\text{kg}\cdot\text{K})$
	Tablet 2	Tablet 3	Average		
25	0.867	0.836	0.852	0.02	0.2
50	0.936	0.877	0.907	0.04	0.4
100	1.035	0.968	1.002	0.05	0.4
150	1.111	1.069	1.090	0.03	0.3
200	1.192	1.177	1.185	0.01	0.1

**Table 25.** The results of measurements of the specific heat capacity of sample №5.

Sample №5					
$T, ^\circ\text{C}$	$c_p, \text{kJ}/(\text{kg}\cdot\text{K})$			Standard deviation, $\text{kJ}/(\text{kg}\cdot\text{K})$	Student's confidence interval ( $\alpha= 0.05$ ), $\text{kJ}/(\text{kg}\cdot\text{K})$
	Tablet 2	Tablet 3	Average		
25	0.816	0.803	0.810	0.01	0.1
50	0.875	0.847	0.861	0.02	0.2
100	0.951	0.922	0.937	0.02	0.2
150	0.995	0.971	0.983	0.02	0.2
200	1.029	1.053	1.041	0.02	0.2

**Table 26.** The results of measurements of the specific heat capacity of sample №6.

Sample №6					
$T, ^\circ\text{C}$	$c_p, \text{kJ}/(\text{kg}\cdot\text{K})$			Standard deviation, $\text{kJ}/(\text{kg}\cdot\text{K})$	Student's confidence interval ( $\alpha= 0.05$ ), $\text{kJ}/(\text{kg}\cdot\text{K})$
	Tablet 2	Tablet 3	Average		
25	0.723	0.871	0.797	0.1	0.9
50	0.773	0.916	0.845	0.1	0.9
100	0.859	1.003	0.931	0.1	0.9
150	0.927	1.074	1.001	0.1	0.9
200	0.979	1.124	1.051	0.1	0.9

**Table 27.** The results of measurements of the specific heat capacity of sample №7.

Sample №7					
$T, ^\circ\text{C}$	$c_p, \text{kJ}/(\text{kg}\cdot\text{K})$			Standard deviation, $\text{kJ}/(\text{kg}\cdot\text{K})$	Student's confidence interval ( $\alpha= 0.05$ ), $\text{kJ}/(\text{kg}\cdot\text{K})$
	Tablet 2	Tablet 3	Average		
25	0.954	0.774	0.864	0.1	1
50	1.000	0.822	0.911	0.1	1
100	1.067	0.898	0.982	0.1	1
150	1.113	0.960	1.036	0.1	1
200	1.178	1.023	1.101	0.1	1

**Table 28.** The results of measurements of the specific heat capacity of sample №8.

Sample №8					
$T, ^\circ\text{C}$	$c_p, \text{kJ}/(\text{kg}\cdot\text{K})$			Standard deviation, $\text{kJ}/(\text{kg}\cdot\text{K})$	Student's confidence interval ( $\alpha= 0.05$ ), $\text{kJ}/(\text{kg}\cdot\text{K})$
	Tablet 2	Tablet 3	Average		
25	0.821	0.738	0.779	0.06	0.5
50	0.892	0.784	0.838	0.08	0.7
100	0.983	0.867	0.925	0.08	0.7
150	1.030	0.942	0.986	0.06	0.6
200	1.069	0.994	1.031	0.05	0.5

**Table 29.** The results of measurements of the specific heat capacity of sample №9.

Sample №9					
$T, ^\circ\text{C}$	$c_p, \text{kJ}/(\text{kg}\cdot\text{K})$			Standard deviation, $\text{kJ}/(\text{kg}\cdot\text{K})$	Student's confidence interval ( $\alpha= 0.05$ ), $\text{kJ}/(\text{kg}\cdot\text{K})$
	Tablet 2	Tablet 3	Average		
25	0.820	0.784	0.802	0.03	0.2
50	0.859	0.830	0.844	0.02	0.2
100	0.932	0.912	0.922	0.01	0.1
150	0.998	0.984	0.991	0.01	0.1
200	1.043	1.023	1.033	0.01	0.1

**Table 30.** The results of measurements of the specific heat capacity of sample №10.

Sample №10					
$T, ^\circ\text{C}$	$c_p, \text{kJ}/(\text{kg}\cdot\text{K})$			Standard deviation, $\text{kJ}/(\text{kg}\cdot\text{K})$	Student's confidence interval ( $\alpha= 0.05$ ), $\text{kJ}/(\text{kg}\cdot\text{K})$
	Tablet 2	Tablet 3	Average		
25	0.836	0.797	0.817	0.03	0.2
50	0.879	0.837	0.858	0.03	0.3
100	0.958	0.912	0.935	0.03	0.3
150	1.018	0.975	0.996	0.03	0.3
200	1.074	1.026	1.050	0.03	0.3

**Table 31.** The results of measurements of the specific heat capacity of sample №11.

Sample №11					
$T, ^\circ\text{C}$	$c_p, \text{kJ}/(\text{kg}\cdot\text{K})$			Standard deviation, $\text{kJ}/(\text{kg}\cdot\text{K})$	Student's confidence interval ( $\alpha= 0.05$ ), $\text{kJ}/(\text{kg}\cdot\text{K})$
	Tablet 2	Tablet 3	Average		
25	0.728	0.751	0.739	0.02	0.1
50	0.764	0.791	0.777	0.02	0.2
100	0.835	0.862	0.849	0.02	0.2
150	0.884	0.918	0.901	0.02	0.2
200	0.918	0.960	0.939	0.03	0.3

The dependence of density on temperature can be taken into account using the equation (15). According to the results of the measurements of the CLTE (*Chapter 4.3*) and the results of density measurements ( $2.01\text{-}2.89 \text{ g}/\text{cm}^3$ ) (measurements were carried out laboratory by the

method of hydrostatic weighing), it was found that for this collection of samples the density of the samples is practically independent of temperature: the difference in density at 25 °C and 200 °C when calculating by formula (15) is less than 0.5% (*Figure 39*). In this regard, for this collection of samples, it is quite correct to assume that  $\rho(T) \approx \rho_0$ . Taking into account this assumption, formula (16) for calculating the volumetric heat capacity takes the form:

$$C(T) = C_p(T) \cdot \rho_0 \quad (19)$$

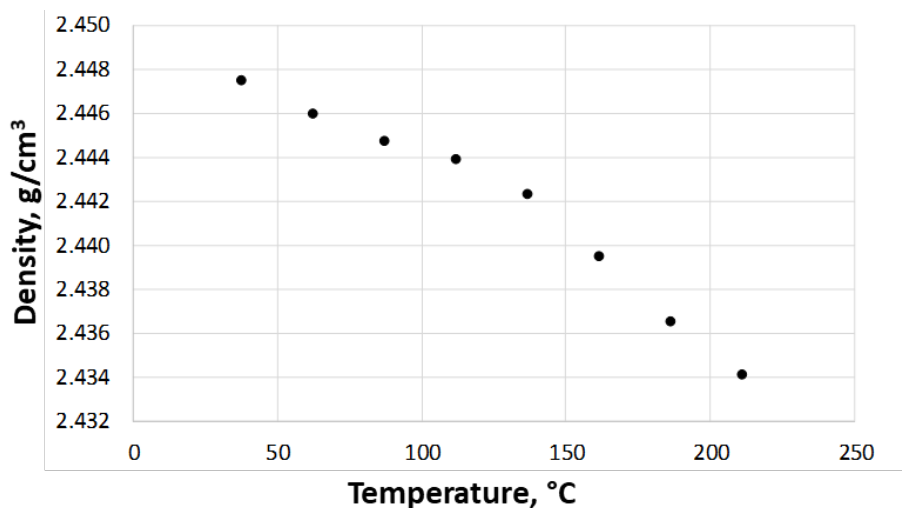


**Figure 39.** The dependence of the density on temperature, calculated by the formula (15), for a sample from the studied collection of rocks, which has the maximum CLTE ( $\alpha = 15.9 \cdot 10^{-6} \text{ K}^{-1}$ ).

*Figures 40-41* show the dependence of the volumetric heat capacity on temperature for the collection of the studied samples, calculated by the formula (19). The range of volumetric heat capacity variations for Bazhenov formation rocks in the temperature range 25-200 °C is 1.86-2.78 MJ/(m<sup>3</sup>·K), for Abalak formation rocks - 1.64-2.74 MJ/(m<sup>3</sup>·K). The average percentage of volumetric heat capacity increasing with temperature relative to initial volumetric heat capacity ( $T = 25 \text{ °C}$ ) for Bazhenov formation rocks is 34%, for Abalak formation rocks – 27% (*Figures 42-43*).

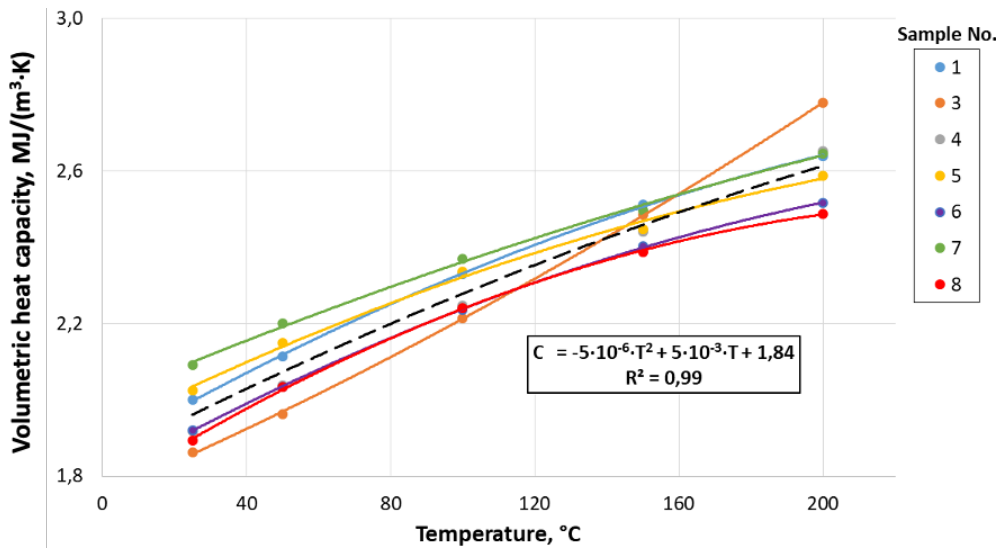


**Figure 40.** The dependence of the volumetric heat capacity on temperature for Bazhenov formation rock samples from oil field 1.

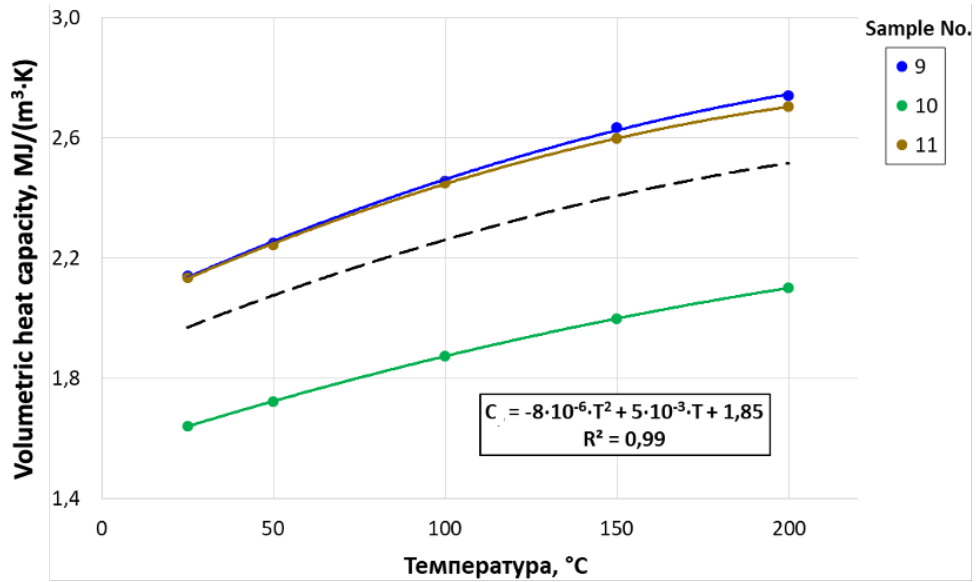


**Figure 41.** The dependence of the volumetric heat capacity on temperature for Abalak formation rock samples from oil field 1.

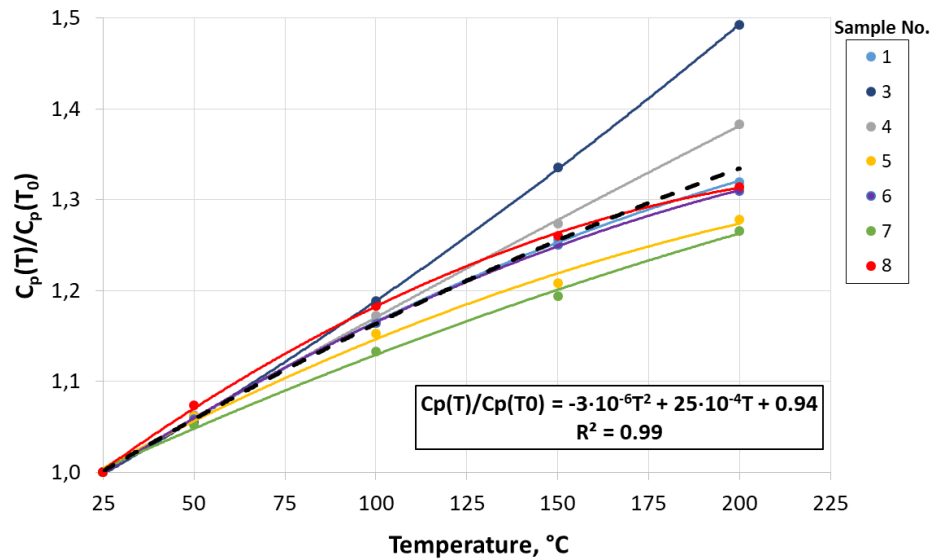


**Figure 42.** The ratio of volumetric heat capacity at elevated temperatures to initial volumetric heat capacity ( $T_0 = 25 \text{ }^{\circ}\text{C}$ ) for Bazhenov formation rocks.

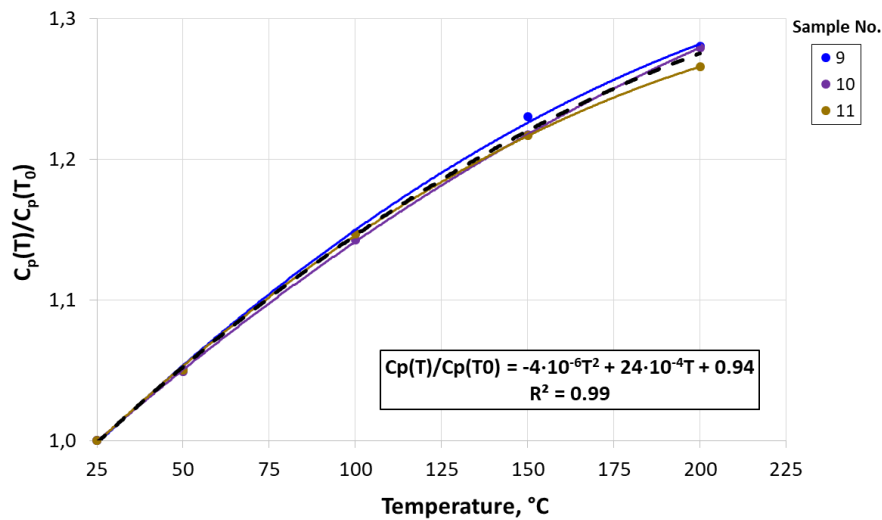


**Figure 43.** The ratio of volumetric heat capacity at elevated temperatures to initial volumetric heat capacity ( $T_0 = 25 \text{ }^{\circ}\text{C}$ ) for Abalak formation rocks.

## Oil field 2

Specific heat measurements were carried out on 8 rock samples of the Golchih and Abalak formations. The measurements were carried out on disc-shaped samples 4.2 mm in diameter, no more than 1 mm thick and weighing 20-40 mg on a NETZSCH-DSC 214 Polyma device in the temperature range 50-300  $^{\circ}\text{C}$ . During measurements, the mass of the samples changed by no more than 0.15%, which indicates the absence of significant possible phase transitions of pore fluids and the reliability of the results obtained. The measurement results are shown in *Figure 44*.

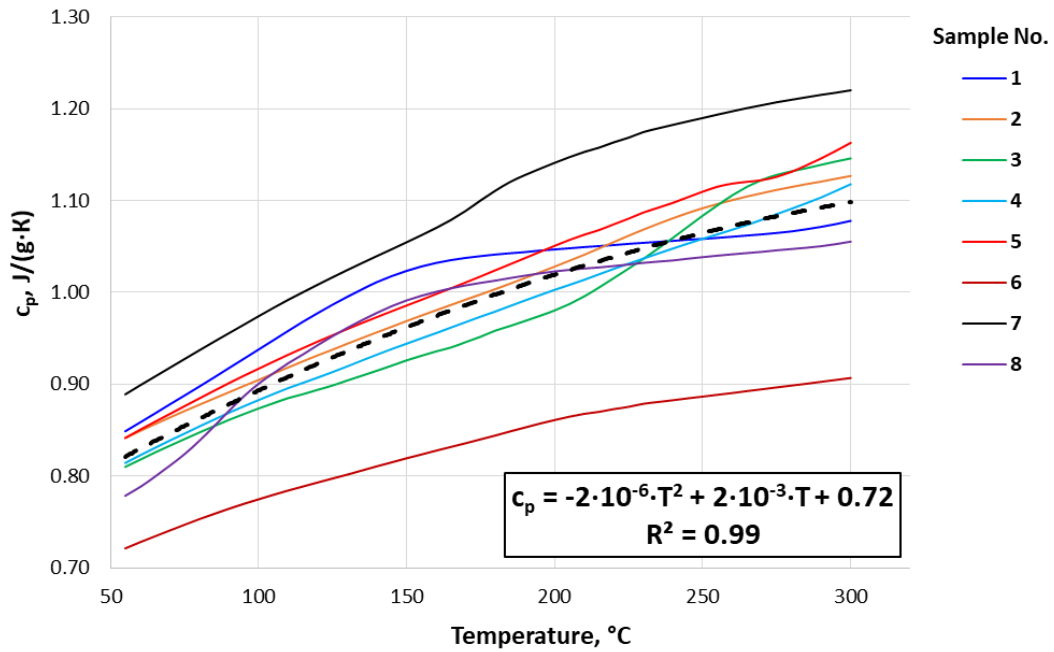


**Figure 44.** Experimental data on the change in the specific heat capacity of rock samples from the Golchih and Abalak formations (Oil field 2) with temperature increasing. The black dotted line is the curve obtained by averaging the specific heat capacity for all samples.

According to the results of the CLTE measurements (*Chapter 4.3*) and the results of density measurements (2.37-2.70 g/cm<sup>3</sup>) (measurements were carried out by the method of hydrostatic weighing (GOST 25281-82, 1982)), it was found that for this collection of rock samples, the density of samples practically does not depend on temperature: the difference in density at 25 °C and 150 °C when calculating by formula (15) is less than 1% (*Figure 45*). In this regard, for this collection of samples, it is quite correct to assume that  $\rho(T) \approx \rho_0$  in the temperature range 25-300 °C. Taking into account this assumption, formula (16) for calculating the volumetric heat capacity takes the form (19).

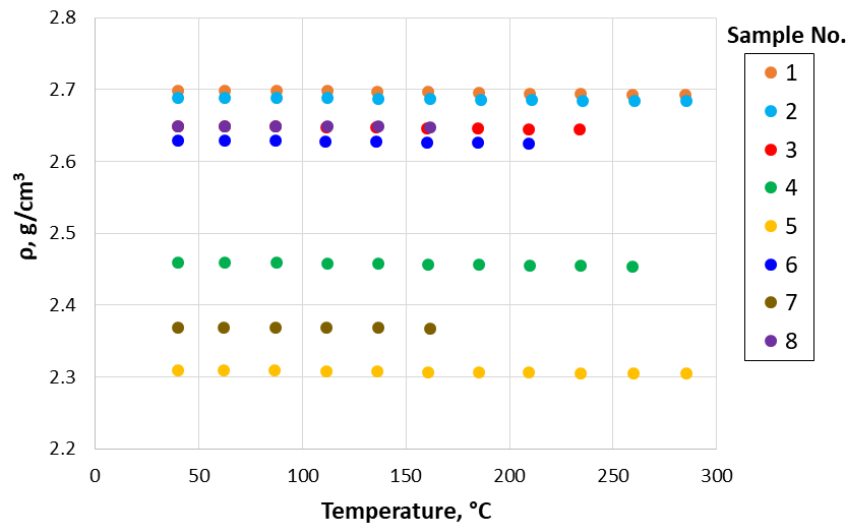


**Figure 45.** Dependence of density on temperature for rock samples of the Golchih and Abalak formations (Oil field 2).

Neglecting the volumetric heat capacity of air in formula (18), we obtain:

$$C^M(T) = (C_p^m(T) \cdot \rho_0) / (1-x) \quad (20)$$

Expression (20) was used to determine the matrix values of the volumetric heat capacity as a function of temperature. *Figure 46* shows the general relationships and equations for VHC vs temperature for the rocks of the Golchih and Abalak formations, constructed from the results of measurements for all studied samples. The specific and volumetric heat capacities of the studied rocks of the Golchih and Abalak formations at 300 °C increase by an average of 35% relative to the specific and volumetric heat capacities at 25 °C.

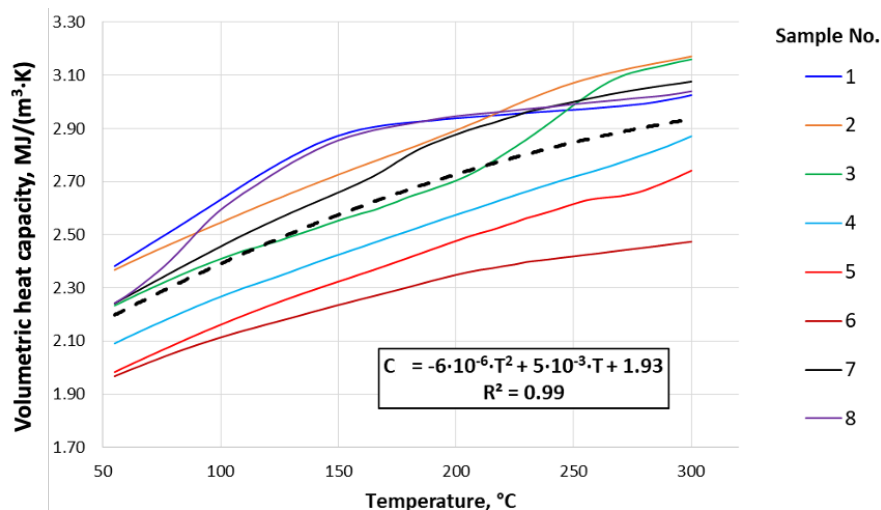


**Figure 46.** The dependence of the volumetric heat capacity of the matrix for all rock samples of the Golchih and Abalak formations (Oil field 2) on temperature. The dashed line is the curve obtained by averaging the volumetric heat capacity of the matrix over all samples.

### Oil field 3

Specific heat measurements were carried out on 12 rock samples of the Bazhenov formation. Measurements were carried out on disk-shaped samples 4.2 mm in diameter, no more than 1 mm thick and weighing 20-40 mg on a NETZSCH-DSC 214 Polyma device in the temperature range 25-200 ° C. During measurements, the mass of the samples changed by no more than 0.15%, which indicates the absence of significant possible phase transitions of pore fluids and the reliability of the results obtained. The measurement results are shown in *Figure 47*.

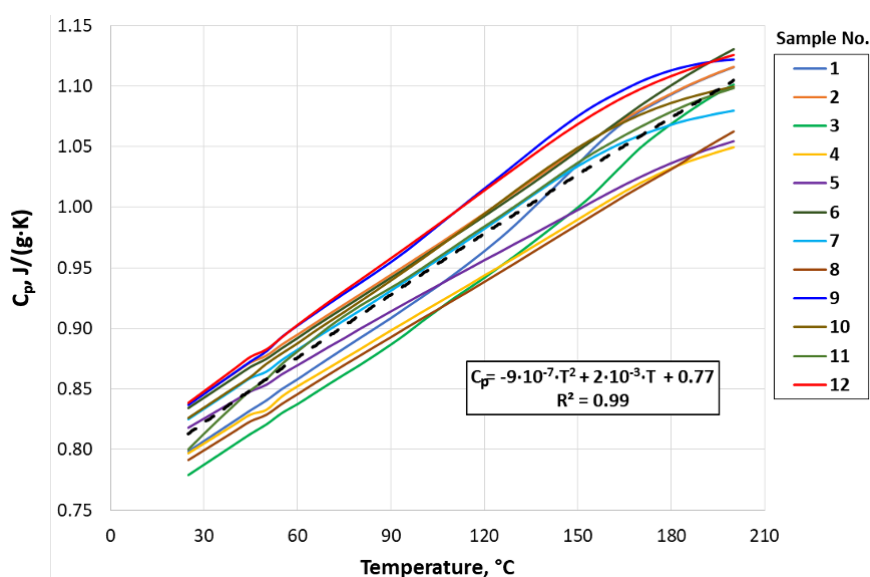


**Figure 47.** Experimental data on the change in the specific heat capacity of rock samples of the Bazhenov formation with an increase in temperature. The black dotted line is the curve obtained by averaging the specific heat capacity for all samples.

According to the results of the measurements of the CLTE (*Chapter 4.3*) and the results of density measurements (2.34-2.47  $g/cm^3$ ) (the density was determined on the basis of measurements of sample volumes obtained using a PIK-PP porosimeter (Geologika) and measurements of sample masses, it was found that for this collection of rock samples, the density of the samples is practically independent of temperature: the difference in density at 25 °C and 200 °C when calculating by formula (15) is less than 1%. In this regard, for this collection of samples, it is permissible to assume that  $\rho(T) \approx \rho_0$  in the temperature range 25-200 °C. Formula (16) for calculating the volumetric heat capacity takes the form (19).

*Figure 48* shows the general relationships and equations for the rocks of the Bazhenov Formation, constructed from the results of measurements for all studied samples. The specific and volumetric heat capacities of the studied rocks of the Bazhenov formation at 200 °C increase

by an average of 34% relative to the specific and volumetric heat capacities at 25 °C. The range of volumetric heat capacity values is 1.87-2.71 MJ/(m<sup>3</sup>·K).

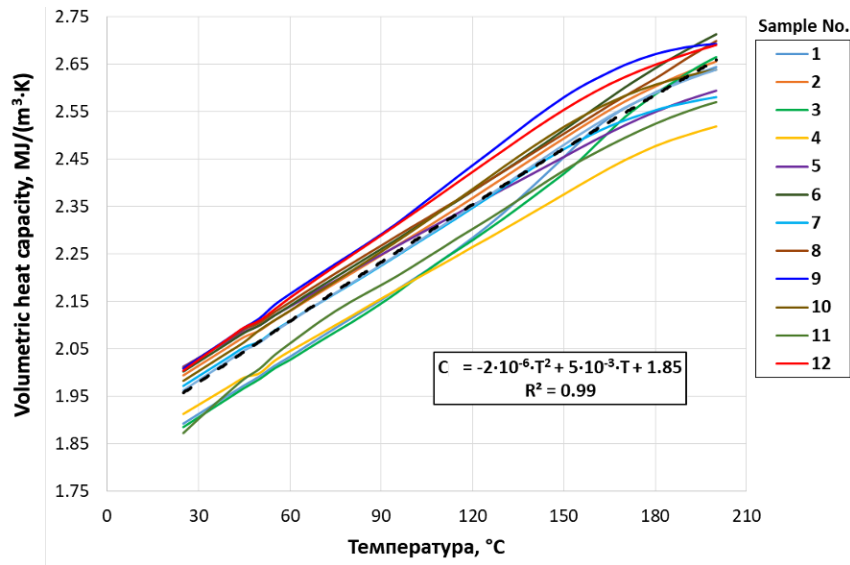


**Figure 48.** The dependence of the volumetric heat capacity, averaged over all rock samples of the Bazhenov formation (Oil field 4), on temperature. The dashed line is the curve obtained by averaging the volumetric heat capacity of all samples.

#### 4.4.3 Equations that relate volumetric heat capacity to temperature for unconventional reservoir rocks

The developed methodology of volumetric heat capacity measurements allows us to establish new equations of VHC vs temperature for unconventional reservoir rocks in the temperature range 25-300 °C (Table 32). Volumetric heat capacity range 1.64-3.16 MJ/(m<sup>3</sup>·K). The average percentage of volumetric heat capacity increasing is 27-34%.

**Table 32.** Equations of VHC vs temperature for studied unconventional reservoir rocks

Oil field	Formation	Number of samples	Temperature range, °C	VHC range, MJ/(m <sup>3</sup> ·K)	Equations	Average percentage of VHC increasing, %
1	Bazhenov	7	25-200	1.86-2.78	$C = -5 \cdot 10^{-6} \cdot T^2 + 5 \cdot 10^{-3} \cdot T + 1.84$	34
	Abalak	3	25-200	1.64-2.74	$C = -8 \cdot 10^{-6} \cdot T^2 + 5 \cdot 10^{-3} \cdot T + 1.85$	27
2	Golchih	7	50-300	1.97-3.16	$C = -6 \cdot 10^{-6} \cdot T^2 + 5 \cdot 10^{-3} \cdot T + 1.93$	35
	Abalak	1				
3	Bazhenov	12	25-200	1.87-2.71	$C = -2 \cdot 10^{-6} \cdot T^2 + 5 \cdot 10^{-3} \cdot T + 1.85$	34

#### 4.4.4 Analysis of volumetric heat capacity with temperature characteristic of unconventional reservoir rocks in comparison with other sedimentary rocks

Figure 49 shows the percentage of volumetric heat capacity increasing relatively to initial volumetric heat capacity ( $T = 25\text{ }^{\circ}\text{C}$ ) for Bazhenov formation and other sedimentary rocks. The percentage of volumetric heat capacity increasing for unconventional reservoir rocks with temperature is higher (1.5-1.7 times) than for other sedimentary rocks (limestones, sandstones).

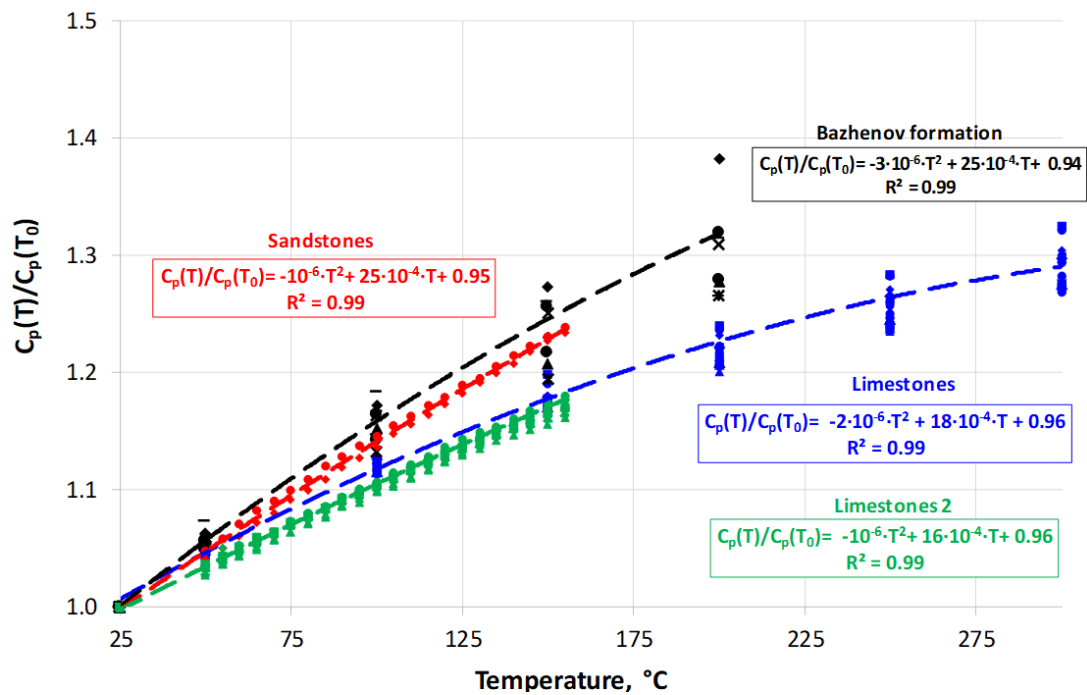


Figure 49. The volumetric heat capacity increasing relatively to initial volumetric heat capacity ( $T_0 = 25\text{ }^{\circ}\text{C}$ ) for Bazhenov formation and other sedimentary rocks.

#### 4.5 Experimental investigations of thermal conductivity on rock cuttings and non-consolidated rocks at elevated temperatures

Developed methodology of thermal conductivity measurements on rock cuttings and non-consolidated rocks (Chapter 3.2) at elevated temperatures allows us to obtain thermal conductivity of matrix for rock cuttings. Table 33 shows the results of determining the thermal conductivity and volumetric heat capacity of the matrix for 31 rock-cuttings samples of Domanic formation in the temperature range  $25\text{-}75\text{ }^{\circ}\text{C}$ . Figures 50a, b, c, d show the temperature dependence of the thermal conductivity of the rock matrix for the studied lithotypes.

**Table 33.** The results of determining the thermal conductivity of the matrix (at 25, 50, and 75 °C) and the volumetric heat capacity of the matrix (at 25 °C) based on the results of measurements on rock-cuttings.

Sample №	Lithotype	T, °C	$\lambda_{\text{matrix}}$ , W/(m·K)	$C_{\text{matrix}}$ , MJ/(m <sup>3</sup> ·K) (T = 25°C)
1	limestone	25	2.09	2.22
		50	2.01	
		75	1.92	
2	limestone	25	3.86	2.44
		50	3.75	
		75	3.64	
3	limestone	25	3.48	2.48
		50	3.43	
		75	3.38	
4	dolomitic limestone	25	4.68	2.40
		50	4.56	
		75	4.43	
5	dolomite	25	5.18	2.52
		50	5.07	
		75	4.59	
6	dolomite	25	5.10	2.44
		50	4.94	
		75	4.77	
7	limestone	25	2.55	2.46
		50	2.35	
		75	2.16	
8	argillite	25	2.90	2.33
		50	2.77	
		75	2.64	
9	argillitic limestone	25	2.64	2.20
		50	2.51	
		75	2.39	
10	limestone	25	2.88	2.22
		50	2.72	
		75	2.57	
11	limestone	25	2.46	2.17
		50	2.31	
		75	2.17	
12	argillite	25	2.38	2.01
		50	2.33	
		75	2.28	
13	argillite	25	2.76	2.14
		50	2.64	
		75	2.52	
14	argillitic limestone	25	2.41	2.25
		50	2.28	
		75	2.16	
15	limestone	25	2.24	2.35
		50	2.12	
		75	1.99	
16	limestone	25	2.54	2.26
		50	2.42	
		75	2.29	
17	argillite	25	3.17	2.03
		50	2.91	
		75	2.67	

18	argillite	25	2.10	2.04
		50	1.99	
		75	1.87	
19	argillite	25	2.48	2.03
		50	2.34	
		75	2.20	
20	argillitic limestone	25	2.54	1.81
		50	2.39	
		75	2.25	
21	argillitic limestone	25	1.95	2.68
		50	1.84	
		75	1.73	
22	argillite	25	1.93	2.26
		50	1.85	
		75	1.76	
23	argillite	25	2.00	2.27
		50	1.91	
		75	1.82	
24	argillite	25	1.98	2.42
		50	1.88	
		75	1.79	
25	argillite	25	2.58	2.39
		50	2.45	
		75	2.32	
26	limestone	25	2.23	2.37
		50	2.11	
		75	1.99	
27	limestone	25	2.22	2.46
		50	2.11	
		75	1.99	
28	limestone	25	2.30	2.39
		50	2.17	
		75	2.03	
29	gneiss	25	2.14	2.16
		50	2.01	
		75	1.87	
30	gneiss	25	2.03	2.12
		50	1.97	
		75	1.91	
31	gneiss	25	2.03	2.25
		50	1.97	
		75	1.91	

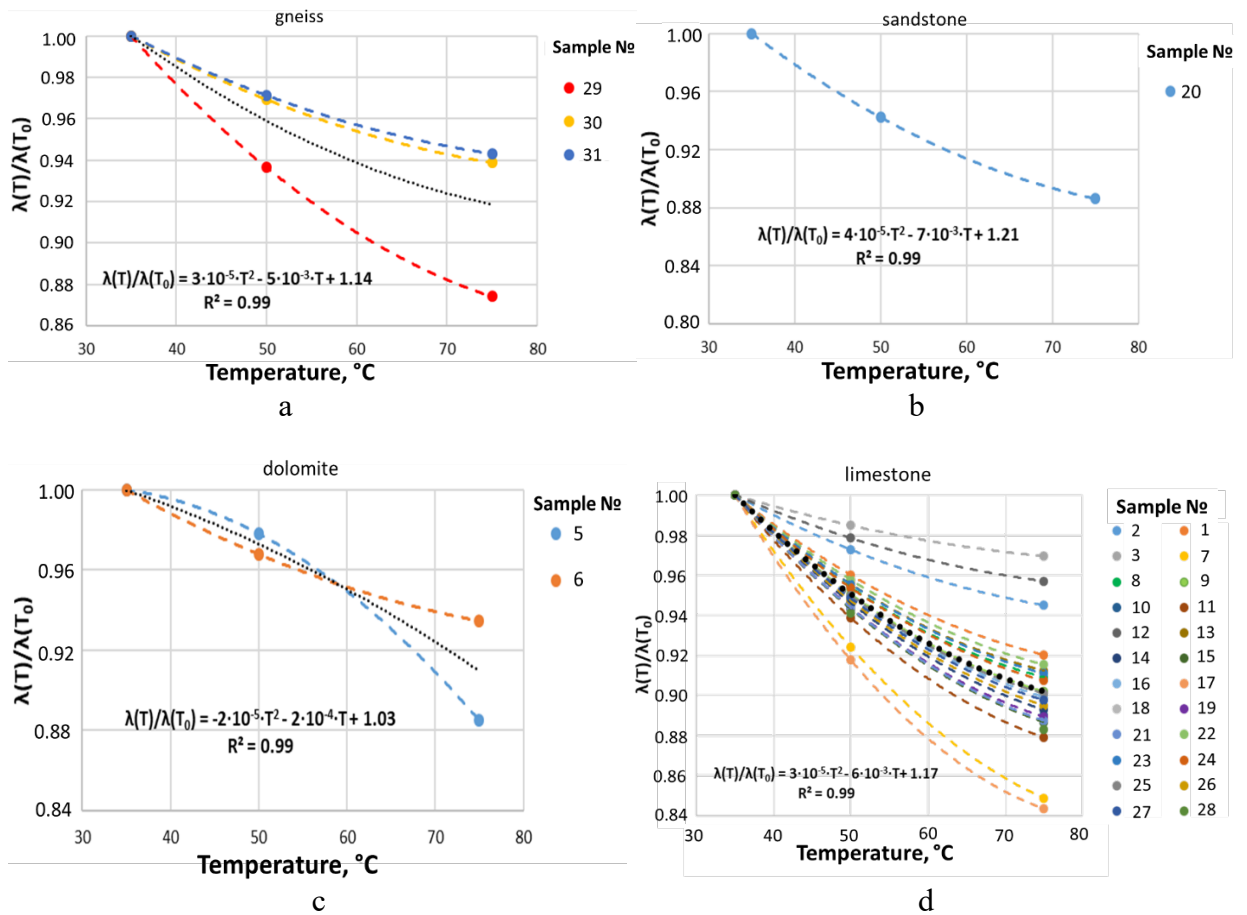


**Figure 50.** The results of determining the dependences of the thermal conductivity of the matrix on temperature from the results of measuring the thermal properties on rock cuttings. The equations show the average decreasing of thermal conductivity for the corresponding lithotype.

*Figure 51* shows the results of comparing the dependences of the relative decrease in the thermal conductivity of rocks on temperature, obtained by measurements on standard rock samples, with the dependences of the relative decrease in the thermal conductivity of the matrix on temperature, obtained by measurements on rock cuttings.

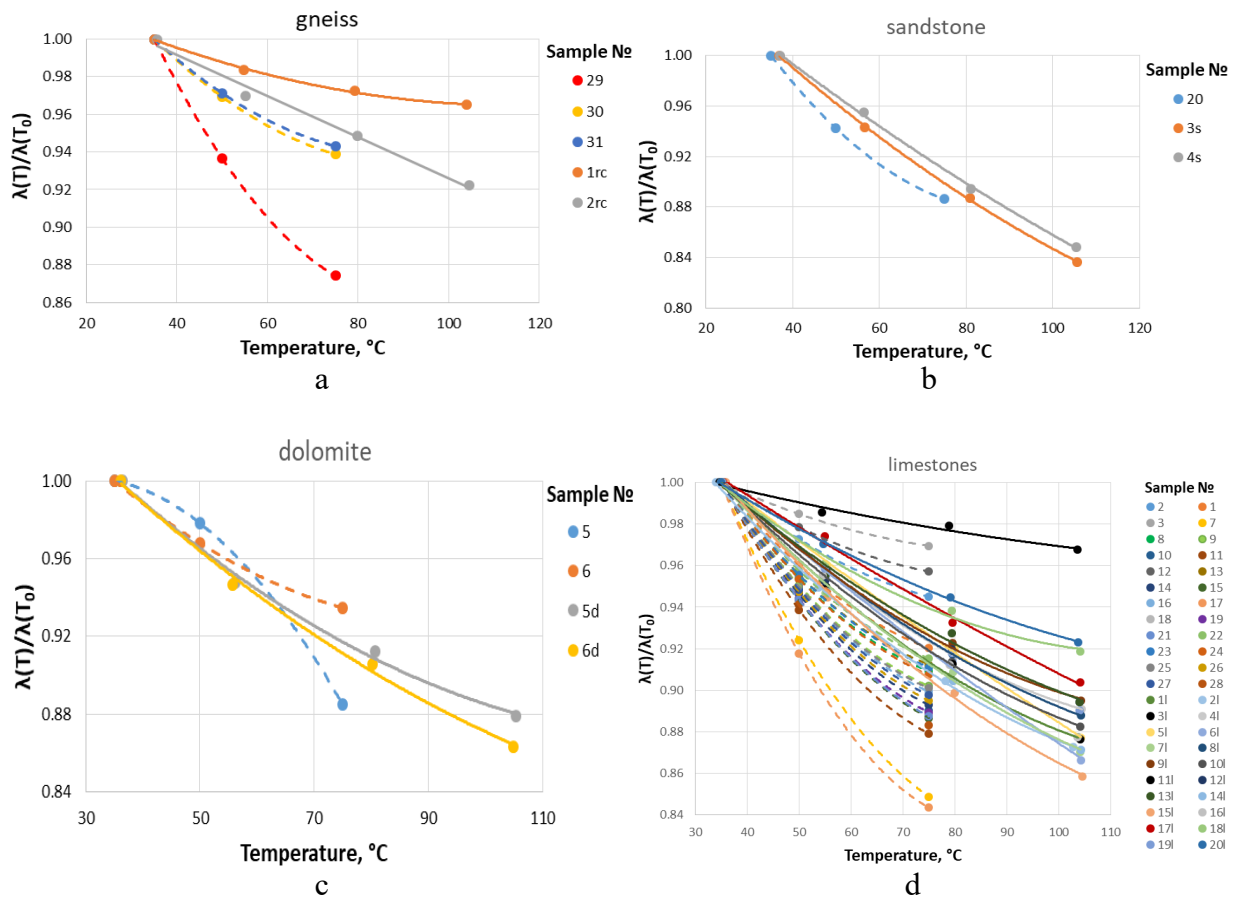


**Figure 51.** Comparison of the results of determining the dependences of the thermal conductivity of the matrix on temperature (according to the results of measurements on rock cuttings) with the results of determining the dependences of the thermal conductivity of rocks on temperature (according to the results of measurements on standard samples). The dashed lines represent the dependences obtained from the results of measurements on rock cuttings, the solid lines represent the dependences obtained from the results of measurements on standard rock samples.

Based on comparison of the dependences of the thermal conductivity of the matrix on temperature (according to the results of measurements on rock cuttings) with the dependences of the thermal conductivity of rocks on temperature (according to the results of measurements on standard core samples) (*Figure 51*), the following conclusions can be drawn:

- The behavior of the relative decrease in the thermal conductivity of rocks with increasing temperature is similar to the behavior of the relative decrease in the thermal conductivity of the rock matrix with increasing temperature.
- The average percentage of decrease in the thermal conductivity of the matrix at 75 °C for the “limestone” lithotype was 10%, for the “dolomite” lithotype - 9%, for the “sandstone” lithotype - 11%, and for the “gneiss” lithotype - 8%.

- For each of the studied lithotypes, averaged equations are obtained (*Table 34*), which show the dependence of the thermal conductivity of the matrix on temperature.

The main difference in dependences obtained for the whole rock samples and cuttings is that for the whole rock sample effective thermal conductivity is determined, for cuttings – the thermal conductivity of the matrix is determined. Also, rock samples and tablets prepared from rock cuttings have different porosity and degree of fracturing.

**Table 34.** Correlation equations of the temperature dependence of measured thermal conductivities of rock cuttings.

Lithotype	Number of samples	Equations
limestone	25	$\lambda(T)/\lambda(T_0) = 3 \cdot 10^{-5} \cdot T^2 - 6 \cdot 10^{-3} \cdot T + 1.17$
dolomite	2	$\lambda(T)/\lambda(T_0) = -2 \cdot 10^{-5} \cdot T^2 - 2 \cdot 10^{-4} \cdot T + 1.03$
sandstone	1	$\lambda(T)/\lambda(T_0) = 4 \cdot 10^{-5} \cdot T^2 - 7 \cdot 10^{-3} \cdot T + 1.21$
gneiss	3	$\lambda(T)/\lambda(T_0) = 3 \cdot 10^{-5} \cdot T^2 - 5 \cdot 10^{-3} \cdot T + 1.14$

## Chapter 5. Conclusion

### 5.1 Summary

The present study reports new experimental thermal conductivity data for 39 rock samples from Bazhenov and Abalak formations in the West-Siberian oil basin and Mendym, Domanic, Sargaev, and Timan formations in the Volga-Ural oil basin over the temperature range from 30 to 300 °C. The new approach to the measurement of rock thermal conductivity at elevated temperatures, combining two methods (divided-bar and optical scanning) was developed. The approach was applied to organic-rich rocks from unconventional reservoirs. It allows us to control changes in the rock samples during their heating to 300 °C, making a separate definition of changes in thermal conductivity components along the bedding plane and perpendicular to it and correcting the experimental data for variations of rock thermal conductivity with temperature increase, which are due to changes in the rock samples (the appearance of cracks) during heating of the samples.

Comparison of thermal conductivity behavior with temperature for two different regions (West Siberia and Volga-Ural) showed different variations of rock thermal conductivity with temperature and equations with different constants. The results demonstrate that the extrapolation of equations for organic-rich samples from different formations can lead to significant uncertainties due to major differences in the minerals and organic matter contained in the samples.

Quartz dilatometer allowed us to obtain CLTE values of Bazhenov and Abalak formations rocks in a temperature range of 25-300 °C. It is important as reliable information on thermal expansion of particular shale formation could not be obtained from literature data and requires experimental investigation of CLTE on particular representative rock samples collection with advanced equipment and methodology, accounting for rock anisotropy. The total amount of studied samples is 44. Integration of quartz dilatometer and TCS gave the possibility to establish relations between CLTE and thermal conductivity of Bazhenov and Abalak formations rocks. Directions of CLTE anisotropy main axes were obtained for each rocks sample by multiple measurements in different directions in a short temperature window with following using the least square method. CLTE profiles along wells of unconventional reservoirs were provided as well.

The new methodology of determining the volumetric heat capacity of rocks at elevated temperatures allowed us to obtain new data on the volumetric heat capacity of unconventional reservoir rocks (31 samples) within a temperature range of 25-300 °C. New equations of VHC vs temperature for Bazhenov and Abalak formations were obtained.

Using original techniques for measuring the thermal properties of rocks on rock cuttings for well intervals drilled without core sampling, the thermal conductivity of the rock matrix was measured and the dependence of thermal conductivity on temperature was obtained for 31 rock cutting samples. Based on the results of measurements on rock cuttings, equations were obtained that characterize the dependence of the thermal conductivity of the matrix on temperature for four lithotypes. For each of the studied lithotypes, averaged equations were obtained, which show the dependence of the thermal conductivity of the matrix of the selected lithotypes on temperature.

## **5.2 Conclusions and recommendations**

Unconventional reservoir rocks require new approaches to experimental investigation of thermal properties at elevated temperatures as their properties are different from other sedimentary rocks due to the presence of fractures, organic matter, etc. Experimental investigation of thermal properties of unconventional reservoir rocks at elevated temperatures provided in this research allowed us to make the following conclusions:

- The new approach to the measurement of rock thermal conductivity at elevated temperatures improves the quality of thermal conductivity measurement: (1) the uncertainty up to 20% in DTC-300 thermal conductivity measurement results caused by

nonparallelism of studied rock samples was removed, and (2) systematic decrease in thermal conductivity up to 12% caused by rock sample fracturing was accounted for;

- After heating runs thermal conductivity components of Bazhenov, Abalak, and Domanic formations rocks decrease up to 20%, a thermal anisotropy coefficient increases up to 13%. The increase of the thermal anisotropy coefficient is caused by the creation of microcracks during heating when the microcracks explain the reduction of thermal conductivity component perpendicular to the bedding plane.
- The effect of temperature on thermal conductivity of the Bazhenov and Abalak formations rocks was found to be much lower (by 2-3 times) than for other sedimentary rocks that is explained by a high content of organic matter in rock samples, which thermal conductivity increases with temperature.
- Bazhenov and Abalak formation rocks have a high degree of CLTE anisotropy. The range of thermal expansion values of the Bazhenov rocks is much higher than values of carbonates, limestones, and clay minerals that is caused by high TOC in studied rock samples (while the thermal expansion of organic matter is much higher than the thermal expansion of rock mineral matrix). Directions of CLTE anisotropy main axes correspond closely to the direction of the main axes of thermal conductivity tensor, that can be used in practice (e.g., for express evaluation of main CLTE directions with optical scanning and correct positioning of a sample before performing time-consuming CLTE measurements).
- New close correlations between CLTE, thermal conductivity, TOC, and density were explained by the high sensitivity of these parameters to the presence of organic matter in studied rock samples. Correlation CLTE vs thermal conductivity showed that core plugs for CLTE investigations should be sampled according to the results of continuous thermal profiling on full-size core samples.
- The temperature behavior of thermal expansion coefficient of the Bazhenov and Abalak formations rocks turned out to have non-monotonic behavior. It agrees with previous observations and differs from the CLTE behavior of other sedimentary rocks (demonstrating a monotonous increase of thermal expansion with temperature). The non-monotonic behavior is, probably, related to bitumen exudation and evaporation of volatile components during heating or non-linear behavior of CLTE of organic matter with temperature. New experimental data showed that the investigation of thermal expansion of organic-rich shales requires an integrated approach to explain observed features like anisotropy and non-monotonic behavior with temperature.

- The average percentage of volumetric heat capacity increase for Bazhenov and Abalak formations rocks is 30%. The results showed that the percentage of volumetric heat capacity increase for unconventional reservoir rocks with temperature is 2 times higher than for other sedimentary rocks.
- The behavior of the relative decrease in the thermal conductivity of the matrix with increasing temperature coincides quite well with the behavior of the relative decrease in the effective thermal conductivity of rocks with increasing temperature. The relative decrease in the thermal conductivity of the matrix and the thermal conductivity of rocks at a temperature of 75 ° C varies from 8 to 11% for the studied four lithotypes.

New results of thermal properties of unconventional reservoir rocks at elevated temperatures can reduce uncertainties during EOR modeling, which are enough high without reliable experimental research (Chekhonin et al., 2021).

The results of this work were used in industrial projects (jointly with Lukoil-Engineering, Rosneft, VNIINEft, Zarubezneft, Gazpromneft, Novatek) on the investigation of thermophysical properties on cores. Experimental data on thermal properties (thermal conductivity, CLTE, VHC) of rocks at elevated temperatures were used for heat flow density determination, basin and petroleum system modeling.

### **Recommendations for future work**

We recommend the following investigations for future research.

1. Investigation of thermal anisotropy changing at elevated temperatures and pressures.
2. Investigation of pressure influence on thermal conductivity, CLTE and VHC of unconventional reservoir rocks behavior.
3. Experimental research and theoretical modeling of thermal conductivity of organic matter behavior at elevated temperatures and pressures.
4. Comparison of data on thermal properties of unconventional reservoir rocks at elevated temperatures and pressures with theoretically based models.
5. Proper research of influence of uncertainties in experimental data on thermal properties of unconventional reservoir rocks on results of basin modeling and modeling thermal methods of EOR.

## Bibliography

1. Abdulagatova, Z.Z., Abdulagatov, I.M., Emirov, V.N., 2009. Effect of temperature and pressure on the thermal conductivity of sandstone. *Int. J. Rock Mech. Min. Sci.* 46: 1055–1071.
2. Abdulagatov, I., Emirov, S., Abdulagatova, Z., Askerov, S., 2006. Effect of pressure and temperature on the thermal conductivity of rocks. *J Chem Eng Data* 51:22–33.
3. Abey, A., Durham, W., Trimmer, D., Dibley, L., 1982. Apparatus for determining the thermal properties of large geologic samples at pressures to 0.2 GPa and temperatures to 750 K. *Review of Scientific Instruments* 53:876. <https://doi.org/10.1063/1.1137073>
4. Alver, B., Gökhan, D., Alver, Ö., 2016. Investigation of the influence of heat treatment on the structural properties of illite-rich clay mineral using FT-IR, <sup>29</sup>SiMAS NMR, TG, and DTA methods. *Anadolu Univ J Sc Tech.* 17(5):823-829. <https://doi.org/10.18038/aubtda.279851>
5. Anderson, D.L. 1989. Theory of the Earth. *Boston, Blackwell Scientific Publications.*
6. Babaev, V., Budymka, V., Dombrovskiy, N., Sergeeva, T., 1987. Thermophysical properties of rocks. Moscow: Nedra.
7. Bauer, S.J., Handin, J., 1983. Thermal expansion and cracking of three confined water-saturated igneous rocks to 800°C. *Rock Mech Rock Eng.* 16:181-198. <https://doi.org/10.1007/BF01033279>
8. Asaad, Y., 1995. A study of the thermal conductivity of fluid-bearing porous rocks. *Ph.D. Dissertation (Univ. of Calif. Berkeley).*
9. ASTM C177-13, 2013. Standard Test Method for Steady-State Heat Flux Measurements and Thermal Transmission Properties by Means of the Guarded-Hot-Plate Apparatus. ASTM International, West Conshohocken, PA. <https://www.astm.org/Standards/C177.htm>
10. ASTM E1530-11, 2016. Standard Test Method for Evaluating the Resistance to Thermal Transmission of Materials by the Guarded Heat Flow Meter Technique, ASTM International, West Conshohocken, PA. <https://www.astm.org/Standards/E1530.htm>
11. ASTM D4535-85, 2000. Standard Test Methods for Measurement of Thermal Expansion of Rock Using a Dilatometer. ASTM International, West Conshohocken, PA [www.astm.org](http://www.astm.org)
12. ASTM E1269-11, 2018. Standard Test Method for Determining Specific Heat Capacity by Differential Scanning Calorimetry. – ASTM International, West Conshohocken, PA. [www.astm.org](http://www.astm.org).

13. Barry-Macaulay, D., Bouazza, A., Singh, R.M., Wang, B., and Ranjith, P.G., 2013. Thermal conductivity of soils and rocks from the Melbourne (Australia) region. *Engineering Geology* 164: 131–138.
14. Beck, A., 1957. A steady state method for the rapid measurement of the thermal conductivity of rocks. *J. Sci. Instrum.* 34: 186. doi:10.1088/0950-7671/34/5/304.
15. Beck, A., 1988. Methods for determining thermal conductivity and thermal diffusivity. In: Haenel R, Rybach L, Stegena L (eds) *Handbook on terrestrial heat flow density determination*. Kluwer, Dordrecht, pp 87–124.
16. Birch, F., Scherer, J., Spicer, G., 1949. Handbook for geologists on physical constants. Moscow: Foreign Literature Publishing House.
17. Chekhonin, E., Popov, E., Popov, Y., Gabova, A., Romushkevich, R., Spasennykh, M., Zaganovskaya, D., 2018. High-resolution evaluation of elastic properties and anisotropy of unconventional reservoir rocks via thermal core logging. *Rock Mech. Rock Eng.* 51: 2747-2759. <https://doi.org/10.1007/s00603-018-1496-z>
18. Chekhonin, E., Parshin, A., Pissarenko, D., Popov, Y., Romushkevich, R., Safonov, S., Spasennykh, M., Chertenkov, M., Stenin, V., 2012. When rocks get hot: thermal properties of reservoir rocks. *Oilfield Review* 24(3):20-37. <https://www.slb.com/-/media/files/oilfield-review/2-rocks-hot-2-english>
19. Chekhonin, E., Romushkevich, R., Popov, E., Popov, Y., Goncharov, A., Pchela, K., Bagryantsev, M., Terentiev, A., Kireev, I., Demin, S., 2021. Advanced Methods of Thermal Petrophysics as a Means to Reduce Uncertainties during Thermal EOR Modeling of Unconventional Reservoirs. *Geosciences* 11(5): 203. <https://doi.org/10.3390/geosciences11050203>
20. Chudnovsky, A., 1962. Thermophysical characteristics of dispersive materials, *first ed.* *Physmatgiz*, Moscow (in Russian).
21. Clauser, C., 2006. Types of geothermal energy use, in: Heinloth, K. (Ed.), *Renewable Energy*, Springer-Verlag Berlin Heidelberg. pp. 551-565. <https://doi.org/10.1007/b83039>
22. Clauser, C., Huenges, E., 1995. Thermal conductivity of rocks and minerals, in: Ahrens, T. J. (Ed.), *Rock Physics & Phase Relations: A Handbook of Physical Constants*, AGU Ref. Shelf, pp. 105-126. <http://dx.doi.org/10.1029/RF003p0105>
23. Cooper, H.W., Simmons, G., 1977. The effect of cracks on the thermal expansion of rocks. *Earth Planet Sc Lett.* 36:404-412. [https://doi.org/10.1016/0012-821X\(77\)90065-6](https://doi.org/10.1016/0012-821X(77)90065-6)
24. Dmitriev, A., Goncharov, S., 1990. Thermodynamic processes in rocks. Moscow: Nedra.

25. Dobrynin, V.M., Vendelstein, B.Yu., Kozhevnikov, D.A., 2004. Petrophysics (Physics of rocks). *Moscow: Oil and Gas, Russian State University of Oil and Gas.*
26. DuBow, J., Nottenburg, R., Collins, G. (1976). Thermal and electrical conductivities of Green River oil shales. *J. Am. Chem. Soc.* 21: 77-86.
27. DTC-300 instrument. <https://www.tainstruments.com/dtc-300/>
28. Duvall, F., Sohn H.Y., Pitt, C.H., Bronson, M.C., 1983. Physical behavior of oil shale at various temperatures and compressive loads: 1. Free thermal expansion. *Fuel* 62:1455-1461. [https://doi.org/10.1016/0016-2361\(83\)90114-X](https://doi.org/10.1016/0016-2361(83)90114-X)
29. Dyakonov, D., Yakovlev, B., 1969. Determination and use of thermal properties of rocks and reservoir fluids of oil fields. Moscow: Nedra.
30. Edvabnik, V.G., 2015. Modern problems of science and education. On the theory of generalized conductivity of mixtures. *Issue 1 (Part 2).*
31. Findikakis, A., Bean, J., Sinks, D., Howard, C., Hardi, 2004. Heat Capacity Analysis Report. U.S. Department of Energy.
32. Gabova, A., Chekhonin, E., Popov, Yu., Savelev, E., Romushkevich, R., Popov, E., Kozlova, E., 2020. Experimental Investigation of Thermal Expansion of Organic-Rich Shales. *International Journal of Rock Mechanics and Mining Sciences.*
33. Garitte, B., Gens, A., Vaunat J., Armand G., 2014. Thermal conductivity of argillaceous rocks: determination methodology using in situ heating tests. *Rock Mech. Rock Eng.* 47: 111-129. <https://doi.org/10.1007/s00603-012-0335-x>
34. Gens, A., Vaunat, J., Garitte, B., Wileveau, Y., 2007. In situ behavior of a stiff layered clay subject to thermal loading: observations and interpretation. *Géotechnique* 57(2): 207–228.
35. Gilliam, T., Morgan, I., 1987. Shale: Measurement of thermal properties. *Technical Report, Oak Ridge National Laboratory, United States.* <https://doi.org/10.2172/6163318>
36. GOST 25281-82. 1982. Powder metallurgy. Method for determining the density of moldings.
37. Grebowicz, J., 2014. Understanding thermal properties of oil shales at high temperature toward the application of nuclear energy in the extraction of natural hydrocarbons. *J. Therm. Anal. Calorim.* 116: 1481–1490. <https://doi.org/10.1007/s10973-014-3822-3>
38. Childs G.E., Ericks L.J., Powell R.L., 1973. Thermal conductivity of solids at room temperature and below. A review and compilation of the literature. *National Bureau of Standards, Department of commerce.* Washington, D.C. 20234.

39. Hammerschmidt, U., 2002. Guarded Hot-Plate (GHP) Method: Uncertainty Assessment. *International Journal of Thermophysics* 23: 1551–1570.
40. Hantschel, T., Kauerauf, A.I., 2009. Fundamentals of basin and petroleum systems modeling. *Springer-Verlag Berlin Heidelberg*. <https://doi.org/10.1007/978-3-540-72318-9>
41. Harvey, R.D., 1967. Thermal expansion of certain Illinois limestones and dolomites. *Illinois State Geol Surv* 415:1-33. <https://core.ac.uk/download/pdf/17355277.pdf>
42. Heard, H.C., Page, L., 1982. Elastic Moduli, Thermal Expansion, and Inferred Permeability of Two Granites to 350°C and 55 Megapascals. *J Geophys Res* 87:9340–9348. <https://doi.org/10.1029/JB087iB11p09340>
43. Hillel, D., 1980. *Fundamentals of Soil Physics*.
44. Horai, K., Susaki, G., 1989. The effect of pressure on the thermal conductivity of silicate rocks up to 12 kbar. *Phys. Earth Planet. Inter.* 55: 292-305. [https://doi.org/10.1016/0031-9201\(89\)90077-0](https://doi.org/10.1016/0031-9201(89)90077-0)
45. Huotari, T., Kukkonen, I., 2004. Thermal expansion properties of rocks: literature survey and estimation of thermal expansion coefficient for Olkiluoto mica gneiss. *Working Report, Geological Survey of Finland, Finland*. [http://www.posiva.fi/files/2259/POSIVA-2004-04\\_Working-report\\_web.pdf](http://www.posiva.fi/files/2259/POSIVA-2004-04_Working-report_web.pdf)
46. Ilozobhie, A., George, A., Asuquo, O., Yahaya, I., 2016. Determination of thermal conductivity of some shale samples in Awi formation and its geophysical implications, Cross River State, Nigeria. *Journal of Environment and Earth Science. Environ Earth Sci.* 6(8): 102-111.
47. Irani, M., Cokar, M., 2016. Discussion on the effects of temperature on thermal properties in the steam-assisted-gravity-drainage (SAGD) process. *Part 1: Thermal Conductivity*. 21, SPE 178426. <https://doi.org/10.2118/178426-PA>
48. Jha, M., Verma, A., Maheshwar, S., Chauhan, A., 2016. Study of temperature effect on thermal conductivity of Jhiri shale from Upper Vindhyan, India. *Bull Eng Geol Environ.* 75: 1657–1668. <https://doi.org/10.1007/s10064-015-0829-3>
49. HAWK Pyrolysis Instrument. <http://www.wildcattechnologies.com>
50. Hofmeister A., Branlund J., Pertermann M., 2007. Properties of Rocks and Minerals– Thermal Conductivity of the Earth. Editor(s): Gerald Schubert. *Treatise on Geophysics*. Elsevier, Pages 543-577.
51. Kaevand, T., Lille, U., 2005. Atomistic molecular simulation of thermal volume expansion of Estonian kukersite kerogen. *Oil Shale* 22(3): 291–303.

52. Kasyanov, B.K., Ermagambet, Bekturganov, N.S., Nabiev, M.A., Kasenova, Sh.B., Sagintaeva, Zh.I., Kuanyshbekov, E.E., Seisenova, A.A., 2016. Chemical composition and Heat Capacity of Shale from the Kendyrlyk and Shubarkol Deposits. *Solid Fuel Chemistry* 50(3): 149-151.
53. Khan, L., Maqsood, A., 2007. Prediction of effective thermal conductivity of porous consolidated media as a function of temperature: a test example of limestones. *J. Phys. D: Appl. Phys.* 40: 4953–4958. <https://doi.org/10.1088/0022-3727/40/16/030>
54. Kukkonen, I., Suppala I., 1999. Measurement of thermal conductivity and diffusivity in-situ: Literature survey and theoretical modeling of measurements. *Report POSIVA 99-1, Geological Survey of Finland, Helsinki.*
55. Kurbanov A., 2007. Regularities of changes in the thermophysical properties of fluid-containing reservoirs with a change in temperature and pore pressure. *Ph.D. dissertation.*
56. Lemenager, A., O'Neill, C., Zhang, S., Evans, M., 2018. The effect of temperature-dependent thermal conductivity on the geothermal structure of the Sydney Basin., *Geothermal Energy* 6: 1-27.
57. Lipaev, A.A., 2013. Development of deposits of heavy oils and natural bitumen: [textbook. manual] / A.A. Lipaev .— Moscow: Institute of Computer Research,- 484 p.
58. Luque, A., Leiss, B., Álvarez-Lloret, P., Cultrone, G., Siegesmund, S., Sebastian, E., Cardell, C., 2011. Potential thermal expansion of calcitic and dolomitic marbles from Andalusia (Spain). *J Appl Cryst.* 44: 1227-1237. <https://doi.org/10.1107/S0021889811036910>
59. MacGillivray, D.A., Dusseault, M.B., 1998. Thermal conduction and expansion of saturated quartz-illitic and smectitic shales as a function of stress, temperature, and bedding anisotropy. *Int J Rock Mech Min Sci.* 35:613. [https://doi.org/10.1016/S0148-9062\(98\)00051-5](https://doi.org/10.1016/S0148-9062(98)00051-5)
60. McKinstrey, H.A., 1965. Thermal expansion of clay minerals. *American Mineralogist* 50(1-2): 212-222.
61. Merriman, J., Whittington, A., Hofmeister, A., 2017. Re-evaluating thermal conductivity from the top down: thermal transport properties of crustal rocks as a function of temperature, mineralogy, and texture. *Proceedings of 42nd Workshop on Geothermal Reservoir Engineering, Stanford University, Stanford, California* 1: 1180-1191.
62. Merriman, J., Whittington, A., Hofmeister, A., Nabelek P., Benn K., 2013. Thermal transport properties of major Archean rock types to high temperature and implications for cratonic geotherms. *Precambrian Research* 233: 358–372.

63. Miklashevsky, D., 2007. Development and application of an instrumental and methodological complex for measuring the thermal properties of rocks at elevated temperature and pressure conditions. *Ph.D. dissertation*.
64. Miklashevsky, D., Popov, Yu., Vertogradsky, V., Bayuk, I., 2006. Measurements of components of thermal conductivity and thermal diffusivity tensors of rocks at reservoir thermobaric conditions. *Geology and Exploration* 6: 38-42 (in Russian).
65. Milner, H.B., 1962. Sedimentary petrography, *volume II, Principles and Applications*. MacMillan Company, NY, 715 pp.
66. Nottenburg, R., Rajeshwar, K., Rosenvold, R., DuBow, J., 1978. Measurement of thermal conductivity of Green River oil shales by a thermal comparator technique. *Fuel* 57(12): 789-795. [https://doi.org/10.1016/0016-2361\(78\)90141-2](https://doi.org/10.1016/0016-2361(78)90141-2)
67. Novikov, S.V., Popov, Yu.A., Tertychnyi, V.V., Shako, V.V., Pimenov, V.P., 2008. The potentialities and problems of modern thermal logging. *Geology and Exploration* 3: 54–57 (in Russian).
68. Pasquale, V., Verdoya, M., Chiozzi, P., 2015. Measurements of rock thermal conductivity with a Transient Divided Bar. *Geothermics* 53: 183–189.
69. Petrunin, G., Popov, V., 2011. Thermophysical properties of the Earth's substance. Part 1.M., Moscow State University.
70. Pitts, M., 2017. Thermal properties of the Cobourg limestone. *Master Thesis*. Queen's University, Kingston, Ontario, Canada. <https://qspace.library.queensu.ca/handle/1974/15339>
71. Popov, E., Chekhonin, E., Popov, Y., Romushkevich, R., Gabova, A., Zhukov, V., 2016a. Novel approach of Bazhenov formation investigation through thermal core profiling. *Nedropolzovanie XXI vek* 6: 52-61 (in Russian).
72. Popov, E., Popov, Y., Romushkevich, R., Spasennykh, M., Kozlova, E., 2019. Detailed Profiling Organic Carbon Content of Oil Shales with Thermal Core Logging Technique. *Proceedings of the Sixth EAGE Shale Workshop, Bordeaux, France*. <https://doi.org/10.3997/2214-4609.201900305>
73. Popov, E., Romushkevich, R., Popov, Y., 2017. Measurement of thermal properties on standard core samples as necessary step for thermophysical investigation of hydrocarbon reservoirs. *Geol Explor.* 2: 56-70.
74. Popov, E., Trofimov, A., Goncharov A., Abaimov S., Chekhonin E., Popov Yu., Sevostianov I., 2018. Technique of rock thermal conductivity evaluation on core cuttings

- and nonconsolidated rocks. *International Journal of Rock Mechanics and Mining Sciences* 108: 15–22.
75. Popov, Yu., Beardsmore, G., Clauser, C., Roy, S., 2016b. ISRM Suggested methods for determining thermal properties of rocks from laboratory tests at atmospheric pressure. *Rock Mech. Rock Eng.* 49(10): 4179-4207. <https://doi.org/10.1007/s00603-016-1070-5>
  76. Popov, Yu., Berezin, V., Solov'ev, G., Romushkevich, R., Korostelev, V., Kosturin, A., 1987. Thermal conductivity of minerals. *Izvestiya, Physics of the Solid Earth* 3: 83-92 (in Russian).
  77. Popov, Yu., Chekhonin, E., Parshin, A., Law, D.H.-S., Pissarenko, D., Miklashevskiy, D., Popov, E., Spasennykh, M., Safonov, S., Romushkevich, R., Bayuk, I., Danilenko, A., Gerasimov, I., Ursegov, S., Konoplev, Yu., Taraskin, E., 2013. Experimental investigations of spatial and temporal variations in rock thermal properties as necessary stage in thermal EOR. *SPE Heavy Oil Conference, Calgary, Alberta, Canada*, SPE-165474-MS. <https://doi.org/10.2118/165474-MS>.
  78. Popov, Y.A., Miklashevsky, D.Y., Vertogradsky, V.A., Shuvalov, V.I., Korobkov, D.A., Lazarenko, A.P., 2008. Improvement of instrumental and methodical base for measuring the coefficient of linear thermal expansion of rocks and minerals. *Geol Explor.* 6: 63-68.
  79. Popov, Yu., Parshin, A., Al-Hinai, S., Miklashevskiy, D., Popov, E., Dyshlyuk, E., Chekhonin, E., Safonov, S., Khan, R., 2014. Experimental investigations of reservoir thermal properties for heavy oil field in Oman with new methods and equipment. *World Heavy Oil Congress, New Orleans, Louisiana, USA*, WHOC14 – 258.
  80. Popov, Y., Parshin, A., Miklashevskiy, D., Abashkin, V., 2012. Instrument for Measurements of Linear Thermal Expansion Coefficient of Rocks. *Proceedings of 46th US Rock Mechanics/Geomechanics Symposium, Chicago, IL, USA*. ARMA-2012-510.
  81. Popov, Yu.A., Popov, E.Yu., Chekhonin, E.M., Gabova, A.V., Romushkevich, R.A., Spasennykh, M.Yu., Zagranovskaya, D.E., 2017. Investigation of Bazhenov formation using thermal core logging technique. *Oil Industry* 3: 23-27. <https://doi.org/10.24887/0028-2448-2017-3-22-27>
  82. Popov, Y., Pribnow, D., Sass, J., Williams, C., Burkhardt, H., 1999. Characterization of rock thermal conductivity by high-resolution optical scanning. *Geothermics* 28: 253–276.
  83. Popov, Yu., Tertychnyi, V., Romushkevich, R., Korobkov, D., Pohl, J., 2003. Interrelations between thermal conductivity and other physical properties of rocks: experimental data. *Pure Appl. Geophys.* 160: 1137–1161. <https://doi.org/10.1007/PL00012565>

84. Powell, R.W., Ho, C.Y., and Liley P. E., 1966. Thermal Conductivity of Selected Materials, National Standard Reference Data Series –NBS, Vol 8, 25 November.
85. Prats, M., O'Brien, S., 1975. Thermal conductivity and diffusivity of Green River Oil Shale, *J. Pet. Technol.* 27: 97-106. <https://doi.org/10.2118/4884-PA>
86. Pribnow, D., Sass, J.H., 1995. Determination of thermal conductivity from deep boreholes, *Journal of Geophysical Research* 100: 9981–9994.
87. Ramazanov, A., Magdiev, A., 2014. Influence of pressure and temperature on thermal conductivity of limestone. *Izvestiya MGTU "MAMP"* 1(19):91-95 (in Russian).
88. Rajeshwar, K., Nottenburg, J., Dubow, J., 1979. Thermophysical properties of oil shales. *J. Mater. Sci.* 14(9): 2025–2052. <https://doi.org/10.1007/BF00688409>
89. Rajeshwar, K., DuBow, J., 1980. Thermophysical properties of Devonian shales. *Fuel.* 59(11): 790-794. [https://doi.org/10.1016/0016-2361\(80\)90257-4](https://doi.org/10.1016/0016-2361(80)90257-4)
90. Rajeshwar, K., DuBow, J., Rosenvold, R., 1980. Dependence of thermal conductivity on organic content for Green River oil shales. *Ind. Eng. Chem. Prod. Res. Dev.* 19(4): 629–632. <https://doi.org/10.1021/i360076a029>
91. Sass, J. H., Stone, C., and Munroe, R. J., 1984. Thermal conductivity determinations on solid rock. A comparison between a steady-state divided-bar apparatus and a commercial transient line-source device. *Journal of Volcanology and Geothermal Research* 20: 145-153.
92. Savest, N., Oja, V., 2013. Heat capacity of kukersite oil shale: literature overview. *Oil Shale* 30(2): 184–192.
93. Seipold, U., 1998. Temperature dependence of thermal transport properties of crystalline rocks - a general law. *Tectonophysics* 291: 161-171. [https://doi.org/10.1016/S0040-1951\(98\)00037-7](https://doi.org/10.1016/S0040-1951(98)00037-7)
94. Sekiguchi, K., 1984. A method for determining terrestrial heat flow in oil basinal areas. *Tectonophysics* 103: 67–79. [https://doi.org/10.1016/0040-1951\(84\)90075-1](https://doi.org/10.1016/0040-1951(84)90075-1)
95. Sergeev, O., Shashkov, A., 1983. Thermal physics of optical medium. *Science and Technology, Moscow*, 230 pp (in Russian).
96. Siegesmund, S., Ullemeyer, K., Weiss, T., Tschegg E.K., 2000. *Int J Earth Sci.* 89:170. <https://doi.org/10.1007/s005310050324>
97. Sratovich, P.A., Aulock, F.W., Lavallée, Y., Cole, J.W., Kennedy, B.M., Villeneuve, M.C., 2015. Thermoelastic properties of the Rotokawa andesite: a geothermal reservoir constraint. *J Volcanol Geotherm Res.* 301:1-13. <https://doi.org/10.1016/j.jvolgeores.2015.05.003>

98. Sokolova, L.S., Duchkov, A.D., Yurchenko, N.V., 1986. Thermal conductivity of bituminous argillites from the Bazhenov formation. *Russ Geol. Geophys.* 10: 42-46 (in Russian).
99. Somerton, W.H., 1992. Thermal properties and temperature related behavior of rock/fluid systems. *Elsevier, New York*. [https://doi.org/10.1016/S0376-7361\(09\)70024-X](https://doi.org/10.1016/S0376-7361(09)70024-X)
100. Somerton, W., Boozer, G., 1960. Thermal characteristics of porous rocks at elevated temperatures. *J. Pet. Tech.*, 12(6): 77–81. doi: 10.2118/1372-G
101. Smith, D., 1978. Thermophysical Properties of Conasauga Shale. *Master Thesis. Oak Ridge Y-12 Plant, TN*. <https://www.osti.gov/servlets/purl/6431483>
102. Smith, J.W., Johnson, D.R., 1976. Mechanisms helping to heat oil shale blocks. *Am Chem Soc Prepr, Fuel Chem Div.* 21(6): 25-33.
103. Sun, Q., Lü, C., Cao, L., Li, W., Geng, J., Zhang, W., 2016. Thermal properties of sandstone after treatment at high temperature. *Int. J. Rock Mech. Min. Sci.* 85: 60–66. <https://doi.org/10.1016/j.ijrmms.2016.03.006>
104. Tarelko, N., 2011. Study of the thermal properties of heavy oil reservoirs and host rocks applied to thermal recovery methods. *Ph.D. dissertation*.
105. Vosteen, H.-D., Schellschmidt, R., 2003. Influence of temperature on thermal conductivity, thermal capacity and thermal diffusivity for different types of rock. *Phys. Chem. Earth.* 28: 499–509. [https://doi.org/10.1016/S1474-7065\(03\)00069-X](https://doi.org/10.1016/S1474-7065(03)00069-X)
106. Wang, G., Yang, D., Kang, Z., Zhao, J., 2018. Anisotropy in Thermal Recovery of Oil Shale-Part 1: Thermal Conductivity, Wave Velocity, and Crack Propagation. *Energies* 11(77). <https://doi.org/10.3390/en11010077>
107. Weaver, C.E., 1976. Thermal properties of clays and shales. *Technical Report, Oak Ridge, US*.
108. Wong, T.F., Brace, W.F., 1979. Thermal expansion of rocks: some measurements at high pressure. *Tectonophys.* 57:95-117. [https://doi.org/10.1016/0040-1951\(79\)90143-4](https://doi.org/10.1016/0040-1951(79)90143-4)
109. Yanchenko, G.A., 2009. Information value rising for the rocks expansion temperature coefficients determination experiments. *Min Inf Anal Bull.* 2: 110-115. <https://cyberleninka.ru/article/n/o-povyshenii-tochnosti-i-informativnosti-eksperimentov-po-opredeleniyu-temperaturnyh-koeffitsientov-lineynogo-rasshireniya-gornyh>
110. Yarzev, V.P, Erofeev, A.V., 2004. Operating properties and durability of bitumen-polymer composites. *FGBOU VPO, TGTU, Tambov*. <http://www.tstu.ru/book/elib/pdf/2014/yarcev.pdf>

111. Yu, Y. J., Liang, W. G., Bi, J. L., Geng, Y. D., Zhang, C. D., Zhao, Y. S., 2015. Thermophysical experiment and numerical simulation of thermal cracking and heat transfer for oil shale. *Proceedings of 13th ISRM International Congress of Rock Mechanics, Montreal, Canada, ISRM-13CONGRESS-2015-178.*
112. Yudin, V., Korolev, A., Afanaskin, I., Volpin S., 2015. Heat capacity and thermal conductivity of rocks and fluids of Bazhenov formation rocks – input data for numerical modeling of thermal methods development. *FGU FNC NIISI RAN, Moscow.* ISBN 978-5-93838-059-2 (in Russian). <https://www.niisi.ru/n3.pdf>
113. Zhdanov, L.S., Zhdanov, G.L., 1984. Physics for secondary specialized educational institutions: Textbook. — *4th ed., Revised* — *M.: Science. Main editorial office of physical and mathematical literature.*
114. Zhou, H., Liu, H., Hu, D., Yang, F., Lu, J., Zhang, F., 2016. Anisotropies in Mechanical Behaviour, Thermal Expansion and P-Wave Velocity of Sandstone with Bedding Planes. *Rock Mech Rock Eng.* 49:4497. <https://doi.org/10.1007/s00603-016-1016-y>